THE PHOTORECEPTORS AND NEUROTRANSMITTERS DRIVING SUBCONCOIUS RESPONSES TO LIGHT

by

William Thomas Keenan

A dissertation submitted to Johns Hopkins University in conformity with the requirements for the degree of Doctor of Philosophy

Baltimore, Maryland

October, 2017

Abstract

Our sensory systems allow us to detect and successfully navigate the environment. The visual system translates environmental light into our conscious perception of sight, as well as subconscious physiological responses such as circadian photoentrainment, the pupillary light reflex, and mood modulation among others. The first step in these processes is photon detection by photoreceptors in the neural retina of the eye. In mammals, 3 general classes of photoreceptors exist: rods, cones, and intrinsically photosensitive retinal ganglion cells (ipRGCs). ipRGCs, in addition to being photoreceptors, are the critical relay for light information from rods and cones to brain areas responsible for the subconscious responses to light. In order for this light information to get to the brain, ipRGCs are known to employ 2 distinct neurotransmitters: glutamate and PACAP. However, the contribution of each photoreceptor and neurotransmitter to subconscious behaviors remains unclear. In this thesis, I demonstrate the role each photoreceptor plays in responding to the multitude of potential environmental light conditions. I show, similar to the photoreceptors, the neurotransmitters relay distinct and necessary aspects of the information detected by the photoreceptors. In addition, I identify novel neurotransmitters within subsets of ipRGCs which may be responsible for relaying their own unique aspect of the light environment to the brain.

Thesis advisor: Samer Hattar, Ph.D.

Secondary reader: Haiqing Zhao, Ph.D.

Thesis Committee: Robert Johnston, Ph.D. & Seth Blackshaw, Ph.D.

Table of Contents

Chapter 1: Introduction

I want to start with a general introduction to the system I have worked on for the past 5 years. This chapter is simply to provide a framework for the questions I will be asking in the subsequent chapters. More detailed information can be found in the introductions to each experimental chapter.

Light and animal behavior

All organisms rely on their sensory systems to navigate and interact with the environment. In mammals, vision, smell, hearing, touch, and taste are our most readily recognizable sensory systems. Each sensory system detects and translates a particular aspect of the environment into conscious perception as well as subconscious physiological responses. For instance, the visual system relies on photons to generate the percept of sight and subconsciously regulate activity, pupil size, mood, and sleep among a variety of other physiological processes.

The visual system faces an environment with an incredible range of light conditions. Over the course of a typical day and night, ambient light intensity can vary by more than 100 million-fold (0.001 lux to 200,000 lux by my own measurements). In addition to intensity, the wavelengths of the photons making up light, or spectral composition, in the environment changes. In humans, we can detect photons ranging from ~390nm to ~760nm[1]. Our visual system's ability to discriminate between photons of different wavelengths is the basis of our perception of color.

While conscious visual perception is the most easily appreciated function of the visual system, it also coordinates a multitude of critical processes subconsciously.

Among these, some of the most well studied are circadian photoentrainment, the pupillary light reflex, and mood and sleep modulation[2]. The system supporting subconscious visual responses, namely the pupillary light reflex, has been the focus of my thesis work.

The eye and the retina

The eye is the sensory organ of the visual system. It has three primary components: the pupil, the lens, and the retina. Its construction is remarkably similar to that of a modern man-made camera. First, the pupil is analogous to a camera's aperture, it regulates the amount of light entering the system. The lens of the eye and the camera serve to focus the light into a coherent image on the photodetector. For cameras that photodetector is likely film or a photosensitive chip – the retina serves this purpose in our eyes.

The retina is a neural tissue that lines the back of the eye and consists of 6 general classes of neuron: the classical photoreceptors (rods and cones), horizontal cells, amacrine cells, bipolar cells, and retinal ganglion cells. Most of these classes of neurons have many subtypes within that class making the retina an incredibly diverse and complex tissue.

Importantly, only the photoreceptors sense photons. The other neuronal cell types and subtypes function to modulate, process, and relay the information gathered at the photoreceptors to the brain.

Photoreceptors

The classical photoreceptors make up the outermost layer of the retina (the furthest from the center of the eye)[3]. The two types of photoreceptor, rods and cones, differ considerably in morphology and function. Rods provide the basis for our incredibly high sensitivity low-light vision while cones support vision during daylight as well as color perception in humans.

One reason rods and cones differ functionally is because they express a different cohort of proteins. Most notably, they express different photosensitive proteins called opsins – rods express the opsin named Rhodopsin and cones express one of the cone opsins[3]. These proteins impart photosensitivity onto photoreceptors by activating a signaling cascade in response to being struck by a photon. For rods and cones, opsin activation counterintuitively reduces photoreceptor activity. This photoreceptor activity modulation by light is subsequently relayed to the other retinal cell types and eventually reaches the brain.

Until recently, these classical photoreceptors were thought to be the sole source of light information for all visual responses – conscious perception and subconscious responses. Work in the late 1990s and early 2000s revealed a novel photoreceptor unlike either rods or cones[4–11]. These cells are a subtype of retinal ganglion cell subsequently named intrinsically photosensitive retinal ganglion cell or ipRGC. Retinal ganglion cells, RGCs, reside in the innermost layer of the retina and are the sole output neurons of the retina; they provide the only conduit for retinal information to the brain. Like other RGCs, ipRGCs receive and relay light information from rods and cones to the brain, but unlike other RGCs, ipRGCs are themselves photosensitive by expression of the

photosensitive protein Melanopsin (*Opn4*). Thus, ipRGCs serves both as a light relay and a light sensor and must integrate these two modalities.

Remarkably, it was found that ipRGCs provide exclusive retinal input to many subconscious visual responses. When ipRGCs are killed, you lose circadian photoentrainment, the pupillary light reflex, and activity masking[12,13]. These results really solidified ipRGCs as central and critical components of the subconscious visual response circuitry.

Neurotransmission in the retina

Communication by neurons in the retina is achieved through the release of neurotransmitters. The primary neurotransmitter in the retina is glutamate. Photoreceptors communicate with bipolar cells via glutamate, bipolar cells talk to RGCs via glutamate, and RGCs communicate with the brain with glutamate. However, the modulatory cells in the retina, horizontal and amacrine cells, are known to use a multitude of different neurotransmitters. Glycine, GABA, dopamine, and acetylcholine are just a few examples.

Researchers realized early on that ipRGCs were unique among RGCs in more than their photosensitivity. PACAP, a peptide neurotransmitter, was found to be present in addition to glutamatergic machinery[14–16]. A significant amount of work has gone into understanding the reason ipRGCs need two neurotransmitters, but it still remains an open question. The general consensus so far is that PACAP plays a minor role in supporting glutamatergic neurotransmission.

In this thesis, I have defined the roles of glutamate and PACAP in the ipRGC system, and I have expanded ensemble of ipRGC neurotransmitters to include somatostatin and substance P.

The pupillary light reflex (PLR)

The pupillary light reflex is a critical component of the visual system. It allows the visual system to autoregulate the intensity of sensory input and keep it in an optimal range for function. The primary reason I have focused on the PLR is because of the incredible advantages it provides for research *in vivo*.

For research purposes, the PLR has many features that make it an ideal system of study. First, the input is well defined – ipRGCs are the exclusive source of retinal information. Second, the output, pupil size, is readily observable, easily quantifiable, and unambiguous in interpretation. Finally, the light stimulus can be easily controlled and modulated so you know exactly what you are putting into the system.

Using the PLR as an assay for ipRGC sensory function and neurotransmission allows us to make quantitative conclusion about the system *in vivo* which is critical to understanding ipRGCs in the context of the whole organism.

Contents of this thesis

During my thesis work, I have focused on two primary questions regarding the ipRGC system. (1) the role rod, cone, and melanopsin light detection in the ipRGC circuit. (2) the contribution of glutamatergic and PACAPergic neurotransmission toward

ipRGC-elicited behavioral responses. chapter 2 is based on now published work which answers several aspects of both questions and forms the basis for chapters 3 and 4. These chapters follow up on questions that arose as a result of the experiments presented in chapter 2 with respect to (2). chapter 5 is a simple and straightforward method that I devised on a walk home from lab and I hope will be useful for neuroscience moving forward. chapter 5 is based on a manuscript currently in review.

As a note, chapters 2 and 5 are completed manuscripts and are written as such. Chapters 3 and 4 are not yet complete stories with satisfying answers. However, they highlight interesting and unstudied aspects of the ipRGC system and provide a starting point for future work in the field.

Chapter 2 lays the groundwork for all subsequent work in this thesis. I highly recommend reading it before proceeding to chapters 3 and 4.

Chapter 2: Mechanisms supporting rapid and sustained phases of ipRGC signaling

This chapter is based on a published manuscript:

William T Keenan*, Alan C Rupp*, Rachel A Ross, Preethi Somasundaram, Suja Hiriyanna, Zhijian Wu, Tudor C Badea, Phyllis R Robinson, Bradford B Lowell, and Samer Hattar. A visual circuit uses complementary mechanisms to support transient and sustained pupil constriction. *eLife* (2016).

*equal contribution

Abstract

Rapid and stable control of pupil size in response to light is critical for vision, but the neural coding mechanisms remain unclear. Here, we investigated the neural basis of pupil control by monitoring pupil size across time while manipulating each photoreceptor input or neurotransmitter output of intrinsically photosensitive retinal ganglion cells (ipRGCs), a critical relay in the control of pupil size. We show that transient and sustained pupil responses are mediated by distinct photoreceptors and neurotransmitters. Transient responses utilize input from rod photoreceptors and output by the classical neurotransmitter glutamate, but adapt within minutes. In contrast, sustained responses are dominated by non-conventional signaling mechanisms: melanopsin phototransduction in ipRGCs and output by the neuropeptide PACAP, which provide stable pupil maintenance across the day. These results highlight a temporal switch in the coding mechanisms of a neural circuit to support proper behavioral dynamics.

Introduction

Environmental light influences a variety of subconscious physiological functions, including circadian photoentrainment, light modulation of sleep/mood, and the pupillary light response (PLR). These diverse effects of light are all mediated by a small subpopulation of retinal output neurons called intrinsically photosensitive retinal ganglion cells (ipRGCs) [12,13,17–21]. Even in the vast array of environmental light conditions, subconscious visual behaviors are remarkable for their rapid induction and stable maintenance throughout the day. However, how the ipRGC circuit achieves rapid and stable control of visual behaviors remains uncertain.

Multiple photoreceptive systems participate in the ipRGC circuit, including their endogenous melanopsin-based phototransduction and indirect synaptic input from the classical rod and cone photoreceptors [22,23]. Each photoreceptive system presumably encodes a unique aspect of the light environment, but to date no consensus exists on the photoreceptive mechanisms supporting ipRGC-dependent behaviors. Several studies using a variety of methods have proposed competing models arguing for the predominance of cone-based [24–27] or rod-based [28,29] synaptic input to ipRGCs and their behavioral responses. Additionally, it has been suggested that melanopsin mediates persistent light detection in ipRGCs [17,20,30–32] because melanopsin phototransduction is relatively slow to initiate but stable for minutes to hours [31,33,34]. However, animals lacking melanopsin still retain sustained light responses in ipRGCs and their central targets [34–36] and relatively normal circadian photoentrainment [37,38] and PLR [39,40]. In total, it remains unclear how ipRGCs utilize each distinct photoreceptive input, especially across the environmental range of light intensities and durations.

ipRGCs must faithfully relay information about the light environment to the brain. Many neurons, including ipRGCs, release multiple neurotransmitters, a classical neurotransmitter and one or more neuropeptides [41]. However, systems to evaluate mammalian cotransmitter systems *in vivo* in real time are lacking. ipRGCs contain the principal excitatory neurotransmitter glutamate and the neuropeptide PACAP (pituitary adenylyl cyclase-activating polypeptide) [14,42]. Recent studies have suggested that glutamate is the predominant regulator of ipRGC-dependent behaviors, including circadian photoentrainment and the PLR [43–45]. By comparison, animals lacking PACAP or its receptors show at best minor deficits in circadian photoentrainment and the PLR [46–

[50]. This difference in outcomes between glutamate and PACAP has led to the conclusion that PACAP is dispensable and serves primarily as a modulator of glutamatergic signaling [51]. It remains puzzling why ipRGCs, like many other neuronal cell types, would possess two distinct neurotransmitters.

To date, the precise behavioral contributions of rod, cone, and melanopsin input or their output neurotransmitters glutamate and PACAP to visual behaviors across time are essentially unknown. Here, we have systematically addressed the behavioral contributions of all three photoreceptive inputs and both neurotransmitter outputs of ipRGCs, and how these change with time. To do so, we have silenced each individual photoreceptor or neurotransmitter component of ipRGCs, and in multiple combinations, while measuring pupil size across environmental light intensities and time domains. We have taken advantage of the fact that the PLR provides the unique opportunity to dissect the precise temporal dynamics of inputs and outputs of the ipRGC circuit in a behaving animal. This study reveals how ipRGC circuit dynamics *in vivo* support pupil regulation across time and provides insights into ipRGC regulation of other subconscious visual behaviors.

Results

ipRGC behavioral responses are composed of both transient and sustained phases

To measure ipRGC responses in real time, we measured the pupillary light response (PLR). Importantly, we used a novel experimental setup that mimics environmental light using overhead light with spectral composition similar to daylight in

an unanesthetized mouse (**Figure 1A** and **Figure 1—figure supplement 1**), unlike previous studies that used monochromatic light delivered to a single eye [13,25,31,39,45,47].

Following light onset, we observed rapid pupil constriction that is maintained for the duration of the 30-second recording (**Figure 1B**), with greater constriction under higher light intensities (**Figure 1D**). Previous studies have noted a PLR decay during a sustained light stimulus lasting minutes [28,31,52], prompting us to systematically monitor the pupil across a range of times and light intensities. We observed a decay in pupil constriction over time that reached a new steady state (**Figure 1C**), resulting in two phases in the PLR: transient and sustained (mean intensity to reach 50% constriction (EC_{50}) for transient PLR = 0.53 lux, sustained PLR = 7.9 lux)(**Figure 1D,E**). Because pupil constriction itself lowers the amount of light reaching the retina and therefore limits the drive to continued pupil constriction, the PLR is a form of negative feedback. To test if PLR decay is a consequence of negative feedback, we measured the effect of negative feedback both computationally and experimentally, and found that it has little role in PLR decay (**Figure 1—figure supplement 2**). Furthermore, we observed full PLR decay at dim light intensities (≤1 lux) within the first 5 minutes of light stimulation (**Figure 1C,F**), but full maintenance of pupil constriction at high light intensities (≥1000 lux), with apparently slower decay rates at higher light intensities (half-life: ~2–5 minutes, **Figure 1F**). These results suggest that ipRGCs possess temporally distinct inputs and/or outputs for transient and sustained signaling.

Transient input to ipRGCs is mediated by rods

To identify the photoreceptor(s) inputs that contribute to transient ipRGC responses (**Figure 2A**), we tested the PLR in mutant mouse lines that lack the function of a single photoreceptor type, leaving the function of the other photoreceptors intact (**Table 1**, for references on production and initial characterization of each line); we refer to these lines as cone knockout, rod knockout, and melanopsin knockout mice. To corroborate our findings, we tested a variety of mutant mouse lines that silence each photoreceptor type in unique ways (**Table 1**).

Importantly, these mutant mouse lines have been extensively tested for visual function [29,53–59]. Rod sensitivity and function is unchanged in cone mutant animals and cone sensitivity and function is unchanged in rod mutant animals [29,53–58]. Electrophysiological recordings of ipRGCs show functional rod input in cone mutants and functional cone input in rod mutants [59]. Additionally, all of the photoreceptor mutant lines we used have similar pupil sizes in darkness (**Figure 2—figure supplement 1**). Therefore, these mouse lines allow precise separation of rod, cone, and melanopsin activation while leaving the function of the other photoreceptors intact.

When we tested the transient PLR of rod, cone, and melanopsin mutant mice, we found that both cone and melanopsin knockout mice were identical to wildtype in both sensitivity and kinetics (**Figure 2B** and **Figure 2—figure supplement 2B**). Despite previous reports of melanopsin requirement for the transient PLR [39], we find that melanopsin is dispensable for the PLR when using more environmentally relevant stimuli (**Figure 2—figure supplement 3**). In contrast, rod knockout mice displayed no pupil constriction until the light intensity becomes relatively bright (i.e. >10 lux, **Figure 2B**),

despite the normal spatial vision in rod knockout mice at these moderate light intensities [53]. To corroborate these results, we tested three different cone mutant lines and two different rod mutant lines with distinct mutations and observed virtually identical results: cone mutants are similar to wildtype and rod mutants have severe transient sensitivity deficits (**Figure 2—figure supplement 2C,D**).

These results are surprising given previous proposals that cones are important for transient ipRGC responses, including acute changes in pupil size [24–26,31,60–65]. Therefore, we sought to acutely modulate cone activity using a previously characterized mouse line that expresses the human 'red' opsin (*OPN1LW*) in place of the mouse 'green' opsin (*Opn1mw*) (Red cone KI), making cones the only photoreceptors with enhanced sensitivity to red light [25] (**Figure 2C**). We found that these mice have identical transient PLR in response to red light as wildtype (**Figure 2D**), indicating that acute cone modulation does not affect the overall magnitude of the PLR. Furthermore, crossing this line to a rod knockout line abolishes the PLR in response to red light (**Figure 2E**). These results show that rods are the predominant photoreceptor inputs for transient PLR at low to moderate light intensities, even in a mouse line with sensitized cones.

To evaluate the inputs contributed by each photoreceptor in isolation to the PLR, we generated double mutants lacking the function of two photoreceptor types, resulting in mice with only rods (Rods alone), only cones (Cones alone) or only melanopsin (Melanopsin alone) (**Table 1**). We found that the only photoreceptors capable of recapitulating the wildtype PLR are rods. Mice with only rod function had identical light sensitivity as wildtype and a similar rapid induction of pupil constriction (**Figure 2F,G**), though their ability to maintain stable pupil sizes in bright light was slightly diminished

(**Figure 2G**). We corroborated the sufficiency of rods using three different mouse lines (**Figure 2—figure supplement 4**). Interestingly, while two of the lines were nearly identical to wildtype, one line had similar sensitivity, but altered kinetics, suggesting that cones might regulate rod signaling dynamics.

In marked contrast to rod input, cone and melanopsin inputs were severely deficient in mediating the transient PLR (**Figure 2F,G**). Animals with melanopsin alone retained a normal PLR at bright light intensities (**Figure 2F)**, as seen previously [31,40,66], with sensitivity that is indistinguishable from rod knockouts (**Figure 2—figure supplement 5**), though they had relatively sluggish kinetics (**Figure 2G**). In contrast, cone-only animals had minimal PLR (**Figure 2F**), resulting in a further sensitivity deficit compared to rod knockout and melanopsin-only animals (**Figure 2—figure supplement 5**). Additionally, cone input decayed rapidly (**Figure 2G**), presumably due their robust light adaptation properties.

Collectively, these results show that rods serve as the primary input to ipRGCs for transient PLR responses, especially at low to moderate light intensities. At bright light intensities, additional input originates predominantly from melanopsin phototransduction.

Glutamaterigic output provides precise and rapid transient signaling

To investigate how ipRGCs relay transient light detection to the brain, we tested the transient PLR in mice lacking glutamatergic neurotransmission in ipRGCs (*Opn4*$^{Cre/+}$; *Slc17a6*$^{fl/fl}$, also known as *Vglut2*$^{fl/fl}$) or mice lacking PACAP in ipRGCs (*Opn4*$^{Cre/+}$;

Adcyap1$^{fl/-}$) (**Figure 3A** and **Table 2**). See **Figure 3—figure supplement 2** for details on design of the conditional PACAP allele (*Adcyap1*^{fl}).

Though ipRGC glutamate knockout mice (*Opn4*$^{Cre/+}$; *Slc17a6*$^{fl/fl}$) exhibited a small decrease in resting pupil size (**Figure 3—figure supplement 1**) [45], we observed that they had minimal transient PLR at all light intensities (**Figure 3B-E**), with more robust PLR at very bright light intensities (**Figure 3—figure supplement 3**), in agreement with previous studies [44,45]. This indicates that ipRGC glutamatergic neurotransmission is a critical transient signal for the PLR. Presumably, the residual transient response is PACAPergic.

In contrast to ipRGC glutamate knockout mice, ipRGC PACAP knockout mice had no deficits in transient PLR sensitivity or kinetics (**Figure 3B-E**), as observed previously [47], suggesting that glutamate is sufficient for the entirety of the transient PLR. Additionally, these results show that any potential modulation of glutamatergic signaling by PACAP [51,67] is dispensable for the transient PLR. Together, these data derived from retinal mutants for photoreceptors and neurotransmitters identify rods as the principal input and glutamate as the principal output of ipRGC-mediated transient PLR signaling.

Melanopsin/rod synergy supports PLR under sustained conditions

Since wildtype responses decay over time (**Figure 1**), we next asked how ipRGC inputs and outputs drive the PLR across longer times (**Figure 4A**). Strikingly, when we measured the sustained PLR in melanopsin knockout mice, which have a normal transient PLR (**Figure 2B**), there was virtually no pupil constriction (**Figure 4B**), even at bright

light intensities (up to 10,000 lux, **Figure 4—figure supplement 1A**). We observed that melanopsin knockout mice lose pupil constriction in minutes (half-life: ~4 minutes, **Figure 4C**), similar to the wildtype PLR decay rate at lower light intensities (WT half-life range: ~2–4 minutes at 1–100 lux, **Fig. 1F**). This suggests that melanopsin phototransduction maintains robust light input in ipRGCs during the day (**Figure 4—figure supplement 1B**), after rods adapt to background light.

The severe deficits we observed in the sustained PLR in melanopsin knockout mice raised the possibility that these animals may have developmental deficits that affect their signaling [68,69]. To directly address this issue, we rescued ipRGC function in adult melanopsin knockout mice using either chemogenetics or restoration of melanopsin expression. Using our mouse line with Cre introduced into the melanopsin locus (*Opn4*$^{Cre/Cre}$) and a Cre-dependent chemogenetic DREADD virus (AAV2-hSyn-DIO-hM3D(G_q)-mCherry) (**Figure 4—figure supplement 2**), we administered the selective DREADD agonist CNO [70] and observed robust and sustained pupil constriction for at least one hour (**Figure 4D**). This result demonstrates that ipRGCs and their downstream circuits remain competent for sustained signaling in melanopsin knockout mice. Furthermore, we acutely restored melanopsin in the majority of ipRGCs of melanopsin-Cre knockout mice (*Opn4*$^{Cre/Cre}$) using a virus that expresses melanopsin in a Cre-dependent manner (**Figure 4E** and **Figure 4—figure supplement 2C-E**, AAV2-CMV-DIO-mRuby-P2A-Melanopsin-FLAG). Following melanopsin restoration, we observed a rescue of the sustained PLR (**Figure 4F**). These results demonstrate for the first time that the effect of melanopsin loss can be rescued in adulthood, indicating that melanopsin-based light detection is directly required for ipRGCs to signal sustained PLR.

Surprisingly, although melanopsin is required for sustained signaling, we found that melanopsin signaling could not fully recapitulate the sustained PLR. Despite the observation that the sustained PLR is normal at bright light intensities in melanopsin-only mice, these mice had a sensitivity deficit compared to wildtype (**Figure 4G**). Notably, we observed that rod knockout mice display an identical sensitivity deficit as melanopsin-only (**Figure 4G** and **Figure 4—figure supplement 3**), indicating that rods contribute to sustained ipRGC signaling. This indicates that at intermediate intensities, both rod and melanopsin signaling cooperate to sustain the PLR.

As with the transient PLR, we found that cone knockout mice had no deficit in sustained PLR (**Figure 4G**). Again, multiple independent mouse lines corroborate these conclusions (**Figure 4—figure supplement 3**). Furthermore, we found that rods alone could drive the remainder of the sustained PLR in melanopsin knockout mice (**Figure 4—figure supplement 4A**), whereas cone-only mice had no sustained PLR (**Figure 4—figure supplement 4B**).

These results show that melanopsin signaling dominates sustained light input to ipRGCs, but rods, which are thought to be nonfunctional under continuous bright light, are intimately involved in supporting the sustained PLR. Notably, rod contributions to the sustained PLR occur predominantly at light intensities above their presumed saturation (~40 lux), showing that rods are indeed capable of contributing to visual function above previously defined limits [29,53,57]. Therefore, sustained ipRGC responses are not a simple consequence of a single photoreceptive system, but instead require rod/melanopsin synergy for highest sensitivity.

PACAP is essential for the sustained PLR

Studies of ipRGC neurotransmitters, in combination with our transient PLR results presented here, suggest that glutamate is the primary ipRGC neurotransmitter, and that PACAP plays a minor, or modulatory, role [44,45,47–50,71]. However, when we tested the sustained PLR in ipRGC glutamate knockout mice, we found that their pupil constriction improved over time compared to their transient PLR sensitivity (**Figure 5B,C**). In contrast, PLR sensitivity either stays the same or declines in all other mutant lines, suggesting that the remaining signal in glutamate knockout mice, presumably PACAP, becomes more effective with longer stimulus duration. Intriguingly, ipRGC glutamate knockout mice showed pulsatile or periodic pupil constriction over time, potentially due to waves of neuropeptide vesicle delivery and release from ipRGC axons (**Video 1**).

Neuropeptides have been shown to require high frequency neuronal activity for release and have relatively slow signaling kinetics compared to classical neurotransmitters [41], suggesting that PACAP may be involved in sustained ipRGC signaling at bright light intensities. In support of a role for PACAP in sustained PLR signaling, we find that even though ipRGC PACAP knockout mice show normal transient PLR, they have an attenuated sustained PLR (**Figure 5B-E**). This deficit in ipRGC PACAP knockout mice occurs even at moderate light intensities (10 and 100 lux). ipRGC PACAP KO mice display decaying constriction over time at 1000 lux as opposed to maintained constriction in wildtype mice and enhanced constriction in ipRGC glutamate KOs (**Figure 5D**). At the brightest light intensity tested, 5000 lux, ipRGC PACAP KO mice display present significantly worse sustained constriction than ipRGC glutamate KO

mice (**Figure 5E**), suggesting that PACAP is more important than glutamate for maintained responses under daylight conditions (1,000-100,000+ lux).

Additionally, we observed similar yet more pronounced deficits in full body PACAP KO mice (*Adcyap1*$^{-/-}$; **Figure 5—figure supplement 1**). They display wildtype transient responses (**Figure 5—figure supplement 1A,B**) and severely attenuated sustained responses (**Figure 5—figure supplement 1C-E**). Interestingly, these PACAP knockout mice exhibit PLR decay on a similar timescale as melanopsin knockout mice (half-life: ~5 minutes, **Figure 4C** and **Figure 5—figure supplement 1F**). These results provide evidence that PACAP allows ipRGCs to communicate sustained input to downstream neurons. As observed with the photoreceptor contributions, the highest sensitivity of sustained PLR requires PACAP/glutamate synergy.

Model of ipRGC circuit transitions

Based on our results, we generated a quantitative representation of the distinct roles played by each photoreceptor input and neurotransmitter output of ipRGCs for the PLR over a range of light intensities and light stimulus durations (**Figure 6,** see Methods for detailed explanation). We integrated individual necessity (i.e. from knockout lines) and sufficiency (i.e. from '–only' lines) of rods, cones, and melanopsin in driving the PLR (**Figure 6—figure supplement 1**) to generate a merged heat map representing each photoreceptor's input to the PLR (**Figure 6A,B**). We then performed the same technique to represent the neurotransmitter outputs of ipRGCs for the PLR (**Figure 6C,D** and **Figure 6—figure supplement 1**) using only the necessity heat maps because we cannot rule out the possibility that other neurotransmitters contribute to ipRGC function. These

heat maps provide a comprehensive visualization of the contribution made by each photoreceptor's input and each neurotransmitter's output for ipRGC signaling at any particular time or environmental light intensity. ipRGC transient signaling for the PLR is dominated by input from rods (**Figure 6A**, red) and output by glutamate (**Figure 6C**, green). In contrast, sustained PLR signaling is dominated by melanopsin (**Figure 6B**, blue) and PACAP (**Figure 6D**, blue). Together, these experiments and our model highlight a mechanistic transition in the ipRGC circuit supporting transient and sustained behavioral outputs.

Discussion

We show here how inputs and outputs for a specific circuit change across time to support a behavioral response. Remarkably, the mechanisms supporting transient and sustained responses are distinct, suggesting stimulus duration as a critical determinant of circuit state. Transient PLR responses predominantly utilize classical, well-characterized visual system synaptic mechanisms: rod phototransduction and signal relay to ipRGCs, followed by ipRGC glutamatergic output. However, as conventional signaling mechanisms adapt, non-conventional mechanisms are recruited to maintain persistent signaling, including endogenous melanopsin phototransduction and peptidergic neurotransmission through PACAP. Our findings highlight fundamental circuit changes in the light-adapted retina that are relatively unexplored [72].

Our results reveal the roles of distinct photoreceptors and neurotransmitters in the PLR and probably other ipRGC-dependent behaviors. We show how ipRGC inputs and outputs can contribute to the PLR through changes in their relative contribution across

stimulus intensity and duration. Our ability to decipher these elaborate dynamic changes stems from the fact that we used a large array of environmental light intensities and durations, coupled with genetic means to silence individual circuit components. Ultimately, our quantitative model makes testable predictions about the role of each photoreceptor and neurotransmitter for other ipRGC-dependent behaviors.

We show that in contrast to many proposed models, rods provide the exclusive transient input to ipRGCs for the PLR at dim (scotopic) and moderate (mesopic) light intensities. That rods are capable of rapid and sensitive input to ipRGCs is not surprising given electrophysiological evidence of sensitive rod input to ipRGCs [59,73] and the fact that rods are widely appreciated as the mediators of dim light vision. However, their exclusive input at mesopic light intensities suggests that cone input to ipRGCs is relatively weak, consistent with the inability of cones to drive circadian photoentrainment [25,74]. Furthermore, we report here that in addition to their role in high-sensitivity transient signaling, rods are capable of driving sustained signaling at bright light intensities well above their saturation level (~40 lux, **Figure 4—figure supplement 4**). This agrees with previous findings that rods are capable of supporting circadian photoentrainment at bright light intensities [29] but also provides more precise temporal kinetics of rod input to subconscious behaviors. It has been proposed that rods never fully saturate [75], and here we provide a physiological role for rod activity at daylight intensities.

In contrast to previous data that melanopsin is largely dispensable for the PLR [39], we find that it is the dominant determinant of pupil size during the day. This is likely due to the fact that rod and cone inputs adapt to background light, while we find no evidence of behavioral light adaptation in melanopsin phototransduction (i.e. identical sensitivity

of melanopsin-only mice in transient and sustained PLR). While melanopsin phototransduction adapts *in vitro* [76,77], it has been proposed that only the adapted state is able to influence downstream behaviors [77]. We predict that melanopsin will be required in other visual functions throughout the day, for example as in more natural photoentrainment conditions that need to precisely measure changing light intensity under bright conditions or measuring day length [32,65,78]. This requirement for melanopsin in sustained light detection is likely the main reason melanopsin has been conserved in vertebrates.

To date, glutamatergic neurotransmission is the only retina-brain signaling mechanism that has been robustly characterized. We confirm previous data that ipRGCs predominantly rely on glutamatergic output for the transient PLR [43–45]. However, we show that the stimulus durations in which glutamate predominates over PACAP is relatively restricted (<5 min), revealing the first critical role for a neuropeptide in retinal signaling to the brain. Further, we find that PACAP appears sufficient to drive the PLR independent of its potential to modulate glutamate. There have been discrepancies in the literature about the role of PACAP in the PLR [46,47], which we believe is likely due to differences in light stimulus duration. Intriguingly, PACAPergic neurotransmission appears to be pulsatile, potentially reflecting the imprecision of slow vesicle delivery from the soma and suggesting why ipRGCs also require a fast and reliable glutamatergic signal. Glutamate and PACAP are the only known ipRGC neurotransmitters, but it remains possible there are neurotransmitters which remain undiscovered. An ipRGC-specific glutamate/PACAP double knockout is a crucial next step in understanding ipRGC neurotransmission. Given the expression of other neuropeptides in many RGCs,

including ipRGCs [79–82], it remains possible that neuropeptides have a broader role in visual function than previously appreciated.

The complementary arrangement of inputs and outputs for the PLR we describe here demonstrates how the visual system accomplishes high sensitivity, transient responses as well as integrative, long-term responses. Many other signaling systems may employ discrete methods for signaling robustly through time. While melanopsin is specific to the ipRGC circuit, PACAP and other neuropeptides may play similar roles in long-term signaling in other circuits, such as hypothalamic feeding circuits [83]. Expanding the timescales over which we investigate these systems is likely to reveal entirely new aspects of cell signaling.

Materials and Methods

Animal husbandry

C57Bl/6 × Sv129 hybrid mice were used in all experiments except PACAP KO mice which were C57Bl/6. All mice were housed according to guidelines from the Animal Care and Use Committee of Johns Hopkins University. Male and female mice age 2–8 months were housed in plastic translucent cages with steel-lined lids in an open room. Ambient room temperature and humidity were monitored daily and tightly controlled. Food and water were available *ad libitum.* All mice were maintained in a 12hr:12hr light-dark cycle with light intensity around 100 lux for the entirety of their lives.

Pupillometry

All mice were dark-adapted for at least 30 minutes prior to any experiments and all PLR experiments were performed between Zeitgeber times (ZT) 2 and 10. For all experiments, mice were unanesthetized and restrained by hand. Because stress can affect pupil size, we ensured that the mice were not stressed during these experiments. To do so, we handled the mice for several days prior to the experiments to get them accustomed to the researchers and to being scruffed. Any mice that showed signs of stress, including vocalizations and wriggling during the experiments, were not used and were subjected to more handling sessions before use in experiments.

Mice were restrained manually under a 10-, 13-, or 23-Watt compact fluorescent light bulb (GE Daylight FLE10HT3/2/D or Sylvania Daylight CF13EL and CF23EL) with a color temperature of 6500 K to simulate natural sunlight. The light intensity was measured using a light meter (EXTECH Foot Candle/Lux Light Meter, 401025) at the surface on which the mouse was held. The light meter was initially calibrated by EXTECH using a Tungsten 2856 K light source; because our experiments used a fluorescent bulb of 6500 K, all measured light intensities reported here may vary by 0.92–1.12 times the actual light intensity. Light intensity was adjusted by a combination of altering the distance of the light bulb(s) from the mouse and/or applying neutral density filters (Roscolux). The light meter is incapable of detecting light intensities below 1 lux, so one neutral density filter cutting the light intensity by 12.5% was applied to the bulb to estimate 1-log unit decreases in illumination below 1 lux. Light intensities above 500 lux required the use of multiple light bulbs.

For the monochromatic light PLR experiments, an LED light (SuperBrightLEDs) was housed in a microscope light source with fiber optic gooseneck arms to direct the light source to the mouse eye. For the experiments involving the *Opn1mw*^{red} mice, we used a 626-nm LED in this setup and directed light to both eyes simultaneously or to just one eye and measured the PLR in the illuminated eye (see figure legends). The photon flux was measured using a luminometer (SolarLight) and converted from W/m^2 to photons/cm^2/sec. The light intensity was decreased by 12.5% using neutral density filters (Rosco).

Videos of the eye were taken using a Sony Handycam (DCR-HC96) mounted on a tripod a fixed distance from the mouse. Manual focus was maintained on the camera to ensure that only one focal plane existed for each mouse and that therefore variable distance from the camera should not contribute to differences in relative pupil area throughout the video. Pupil size was first recorded under dim red light and the endogenous infrared light source of the camera to capture the dark-adapted pupil size. Following at least 5 seconds of recording in dark, the pupil was continuously recorded for at least 30 seconds of a light step stimulus. For all sustained PLR, animals were kept in a cage for 60 minutes under the light stimulus. Animals were removed from the cage after 60 minutes and held in front of the camera for 30 seconds as for the transient PLR. All pupil images presented in the paper were cropped to a fixed square area (generally 100 × 100 pixels) surrounding the eye using GNU Image Manipulation Program (GIMP). The images were made grayscale and then brightness and contrast were adjusted to enhance visibility of the pupil and exported as PNG files.

Data analysis

Videos were transferred from the camera to a computer as Audio Video Interleave (AVI) files and individual frames were taken using VLC media player (www.videolan.org/vlc/) and saved in portable network graphics format (PNG). Images were taken in the dark, at 5 seconds, and 30 seconds following stimulus onset. Pupil area was then quantified manually in ImageJ (http://rsbweb.nih.gov/ij/) software. The pupil area was measured in pixels using the oval tool in which the 4 cardinal points of the oval were touching their respective edges of the pupil. The relative pupil area was calculated using LibreOffice Calc or Microsoft Excel in which the area during the light stimulus was divided by the area prior to lights onset. For the transient PLR, the minimum relative pupil size of either 5 seconds or 30 seconds after stimulus was used for all genotypes.

The intensity-response curve was fit using a variable slope sigmoidal dose-response curve in Graphpad Prism 6. The top and bottom of the fit were constrained to 1.0 and between 0 and 0.10, respectively, to ensure the EC_{50} for each genotype was represented by similar curves. For genotypes that never showed evidence of reaching between 0 and 0.10 relative pupil size, the bottom was not constrained. The sensitivity for each genotype was calculated using the same process of fitting each individual animal's data points with a sigmoidal dose-response curve to generate EC_{50}.

Conditional PACAP allele

The lox-modified *PACAP* (*Adcyap1*) targeting construct was made by recombineering technology. To engineer the targeting vector, 5' homology arm, 3' homology arm and CKO region were amplified from mouse Sv129 BAC genomic DNA

and confirmed by end sequencing (Cyagen biosciences, Santa Clara, CA). The two *loxP* sites flank the second exon and when recombined, create a frameshift mutation and truncated protein. The plasmid was electroporated into W4 ES cells and cells expanded from targeted ES clones were injected into C57BL6 blastocysts. Germline transmitting chimeric animals were obtained and then mated with flpE mice to delete the *frt*-site flanked neomycin selection cassette. The resulting heterozygous offspring were crossed to generate homozygous $PACAP^{lox/lox}$ study subjects. All mice are thus on a mixed C57Bl6/J and 129Sv background. Offspring were genotyped by PCR using 2 primers (F: CCGATTGATTGACTACAGGCTCC and R: GTGTTAAACACCAGTTAGCCACGC) which detect the presence or absence of the 5' loxP site and a 3rd primer was used in conjunction with the forward primer (CKO-R GGGCTTTGATCTGGGAACTGAAG) to detect the recombination event. By generating mice homozygous for a germline deleted cre-deleted allele, we have established that the cre-deleted allele does not express intact *PACAP* mRNA (by PCR and by ISH). A more detailed description of the generation and use of the allele will appear in a manuscript that is in preparation (Ross RA…Lowell BB *in preparation*).

Viral infection

Mice were anesthetized by intraperitoneal injection of avertin (2, 2, 2-Tribromoethanol) and placed under a stereo microscope. 1 µl of AAV2-hSyn-DIO-$hM3DG_q$-mCherry (4.6×10^{12} viral particles/ml, Roth lab, UNC Vector Core) or AAV2-CMV-DIO-mRuby-P2A-Melanopsin-FLAG (Robinson lab, UMBC) was placed on a piece of Parafilm and drawn into a 10-µl microcapillary tube (Sigma P0674) that had

been pulled to a needle (Sutter Instruments, Model P-2000). The loaded needle was then placed in the holster of a pico-injector (Harvard Apparatus PLI-90). The needle punctured the eye posterior to the ora serrata and air pressure was used to drive the viral solution into the vitreous chamber of the eye to ensure delivery specifically to the retina. Mice recovered from surgery on a heating pad until they woke from anesthesia. All PLR experiments and confocal imaging were done at least 3 weeks following viral injection.

Immunofluorescence and confocal microscopy

Mice that had been infected with the AAVs were anesthetized with avertin and then euthanized using cervical dislocation. The eyes were removed and the retinas were dissected in PBS and then fixed in 4% paraformaldehyde for 1–2 hours on ice. The retinas were then washed in PBS at least three times before mounting on a microscope slide (Fisher) in Fluoromount (Sigma) with DAPI (2-(4-amidinophenyl)-1H -indole-6-carboxamidine). Some retinas were co-stained for melanopsin using rabbit anti-OPN4 (Advanced Targeting Systems, AB-N38, 1:1000) in 4% goat serum with secondary antibody Alexa Fluor 488 goat anti-rabbit (Life Technologies A11008, 1:1000). Images were taken on a Zeiss LSM 710 confocal microscope using a 20× objective. After imaging, images were made grayscale, background subtracted, and brightness and contrast were adjusted in FIJI (http://fiji.sc) for the image presented in the paper.

Statistical analysis

All statistical tests were performed in Graphpad Prism 6. Specific statistical comparisons are listed in the figure captions. Because the EC_{50} data appears to be a

normal distribution on a log scale (log-normal distribution), all statistical tests and data analysis involving EC_{50} were performed on the log transformed data set.

Heat map generation

The photoreceptor contribution heat map was generated by first creating estimated pupil size matrices for the both the rapid and sustained PLR at every light intensity and time for wildtype mice (x axis = time, y axis = intensity). To do so, we applied the equation for a one-phase association:

$$(1)\quad Y = Y0 + (Plataeu - Y0) * (1 - e^{(-K*x)})$$

In our case, Y is the **relative pupil area** generated at **time**, x. For the WT rapid PLR heat map, $Y0_{rapid}$ is set to 1 for every light intensity and the K_{rapid} was extracted from the wildtype rapid constriction kinetics curve at 100 lux. The $Plateau_{rapid}$ value at each light intensity is the rapid PLR value extracted from the WT rapid intensity-response curve fit. This allows us to generate a full matrix of WT pupil sizes at every intensity and time by knowing the final pupil size (Plateau) and the rate of constriction (K). This then generates a full matrix of values for every time and intensity for WT mice.

The same method was applied to make the sustained PLR heat map. However, in this case, $Y0_{sustained}$ was set to the value of the rapid PLR at each light intensity (e.g. the same value as $Plateau_{rapid}$). The $Plateau_{sustained}$ value is extracted from the sustained intensity-response curve fit at each intensity. The $K_{sustained}$ was extracted from our wildtype sustained time courses (**Fig. 1c**). Because the decay rate for sustained constriction appeared to change with intensity (**Fig. 1f**) we used a sigmoidal curve fit to

our experimentally determined decay rates (1, 10, 100 lux) to generate decay rates for a range of light intensities. We constrained the top and bottom of this curve to the decay rates determined for 1 and 100 lux respectively.

This process was used to generate two matrices of relative pupil areas with the y-axis being light intensity varying logarithmically (0.001-100,000 lux) and the x-axis being time varying linearly from 0 to 30 seconds for the rapid and 30 seconds to 60 minutes for the sustained. This was done using a custom MATLAB script.

The matrices generated for the wildtype mice were also done to the photoreceptor mutants. In order to determine necessity of a photoreceptor we subtracted rod (average of *Gnat1*$^{-/-}$ and Rod-DTA), cone (average of *Cnga3*$^{-/-}$, *Gnat2*$^{-/-}$ and Cone-DTA), or melanopsin (*Opn4*$^{-/-}$) knockout matrices from the wildtype matrix. This yields larger values for genotypes that are more required and also normalizes for the overall constriction in wildtype mice at that intensity (i.e. because rods are fully necessary at some dim intensities at which WT mice have minimal constriction, the necessity value attributed to rods is small despite their absolute necessity at that intensity). To determine sufficiency we used 'rod-only' (*Cnga3*$^{-/-}$; *Opn4*$^{-/-}$), 'cone-only' (*Gnat1*$^{-/-}$;*Opn4*$^{-/-}$) and 'melanopsin-only' (average of *Gnat1*$^{-/-}$;*Gnat2*$^{-/-}$, *Gnat1*$^{-/-}$; *Cnga3*$^{-/-}$ and Rod-DTA;Cone-DTA) matrices. Additionally, we applied the decay rate of pupil constriction from the 'cone-only' mouse line transient PLR at 100 lux for all light intensities.

Finally, matrices generated above were exported as heat map images with MATLAB.

Negative feedback modeling

In order to isolate negative feedback's impact on the PLR, we generated a computational model. Computational modeling was performed with MATLAB using two experimentally determined parameters. First, the relative pupil area (RPA) values for the wildtype intensity-response curve (**Fig. 1d**). These values give us the response driven when the pupil starts fully open. We will later multiply the environmental intensity by the new relative pupil area to determine the new retinal intensity. We will use this new retinal intensity to extract the pupil size from the rapid intensity-response curve to find the constriction driven by that new intensity under baseline conditions. The model does this recalculation of retinal intensity and the PLR driven by it every second for 956 seconds.

The second experiment integrated into the model is a 1s light pulse-chase experiment. Here, we dark-adapted the mouse, gave a single second of light and then followed subsequent constriction for 30 sec. These constriction values were normalized to the maximum constriction achieved, in this case the 6-sec time point. This gives us the ability to weight the contribution of light at a particular time to constriction at subsequent times. As you can see, light does not instantly constrict the pupil. It takes several seconds for the signal to maximally impact pupil size, which is then followed by signal decay. Importantly, this temporal weighting, while not required for the model, does give us a rough estimate of the potential kinetics of feedback's impact on PLR decay.

With these pieces of experimental data in hand, the model does the following at every light intensity (0.0001-100,000 lux): (1) it extracts the RPA in response to a particular light intensity from the wildtype intensity-response curve. (2) The model uses

the temporal weighting values from the pulse-chase experiment to weight that RPA across subsequent times (0-30s). This gives us a 30-sec constriction time course for the light detected at time zero. (3) The model next moves to time 1 sec. Now it takes into account the maximum constriction caused by light at previous times (time 0 in this case). The model uses that constriction to reduce the light intensity and calculate a new retinal light intensity: RPA * Light intensity = Retinal intensity. (4) Next, it determines the RPA driven by this new retinal intensity using the DRC once again. (5) Repeats step (2) for this RPA giving another time course of constriction (1-31s). (6) The model repeats steps (3-5) moving up in 1s increments each time. Importantly, at each new time point it finds the maximum constriction value in response to all previous time points in order to calculate the new retinal intensity. (7) Finally, it finds the maximum constriction at each time point in order to produce a negative feedback PLR decay time course. See graphical representation of the negative feedback model (**Figure 1—figure supplement 2A**)

*The primary assumption the model makes is that the PLR system has zero summation of signal. This is probably unlikely. However, this assumption was made to maximize the impact of feedback on pupil constriction. This model provides us with an upper bound on negative feedback's contribution to PLR decay.

*Source code and materials used are available on Github (https://github.com/keenanw27/PLR-Decay-Model).

Mathematical description of the negative-feedback model of PLR decay

At a given environmental light intensity: $\boldsymbol{lux_o}$. The effect of pupillary negative-feedback during a 956s stimulation is modeled as follows:

$$\boldsymbol{for}\ time\ \boldsymbol{t} = 1, 2, 3 \ldots 956$$
$$max\left(\overrightarrow{RPA}(:, t)\right) \times lux_o = lux_t \qquad (1)$$

In equation (1) above, we determine the retinal light intensity, $\boldsymbol{lux_t}$, that is, the intensity of light after modulation by pupil size at time $\boldsymbol{t}$. At t = 1 there is no pupil constriction and therefore no light intensity modulation ($lux_o = lux_t$). $\overrightarrow{\boldsymbol{RPA}}$ is a 956×956 matrix which stores subsequent pupil constriction values. With lux_t we determine the constriction driven by light sensed at time, $\boldsymbol{t}$ **:**

$$\vec{\alpha}(lux_t) \times \vec{\omega} = \overrightarrow{RPA}(t, t{:}\, t + 30) \qquad (2)$$

In equation (2), we calculate the amount of constriction driven by lux_t , $\vec{\boldsymbol{\alpha}}(\boldsymbol{lux_t})$, and approximate the temporal characteristics of that constriction with $\vec{\boldsymbol{\omega}}$. $\vec{\boldsymbol{\omega}}$ is based on a 1s light pulse-chase experiment where we followed the constriction driven by 1s of light for 30s. Again, we store calculated constriction values: $\overrightarrow{\boldsymbol{RPA}}(\boldsymbol{t}, \boldsymbol{t}{:}\, \boldsymbol{t} + \boldsymbol{30})$. Finally, we extract the highest constriction value at t :

$$\overrightarrow{max\left(\overrightarrow{RPA}(:, t)\right)} = \overrightarrow{Model}_{lux_o}(1, t) \qquad (3)$$

After completing $t = 956$, $\overrightarrow{\boldsymbol{Model}}_{\boldsymbol{lux_o}}$ is a vector containing the model-predicted timecourse of pupil constriction when negative-feedback is the only source of PLR decay.

Acknowledgments

We would like to thank Rejji Kuruvilla, Haiqing Zhao, and other members of the JHU Mouse Tri-Lab for their helpful comments on this project in general and the manuscript in particular. We would like to thank Alex Kolodkin for comments on an earlier version of the manuscript. We would also like to thank Lee E. Eiden for providing PACAP KO mice in addition to experimental insight and comments on the manuscript. This work was supported by National Institutes of Health grants GM076430 and EY024452.

Author Contributions

W.T.K., A.C.R., and S.H. conceived of the study and prepared the manuscript. W.T.K. designed and performed sustained PLR experiments and all neurotransmitter experiments, designed computational model, analyzed data, and wrote the manuscript. A.C.R. designed and performed transient photoreceptor PLR experiments, performed viral injection, analyzed data, and wrote the manuscript. R.A.R and B.B.L. conceived of, designed, and created the conditional PACAP allele and edited the manuscript. S.H. designed experiments and edited the manuscript. P.S. and P.R.R. generated the AAV-Melanopsin construct and S.H., Z.W., T.C.B. packaged the virus. P.S., P.R.R, S.H., Z.W., T.C.B. also read and edited the manuscript.

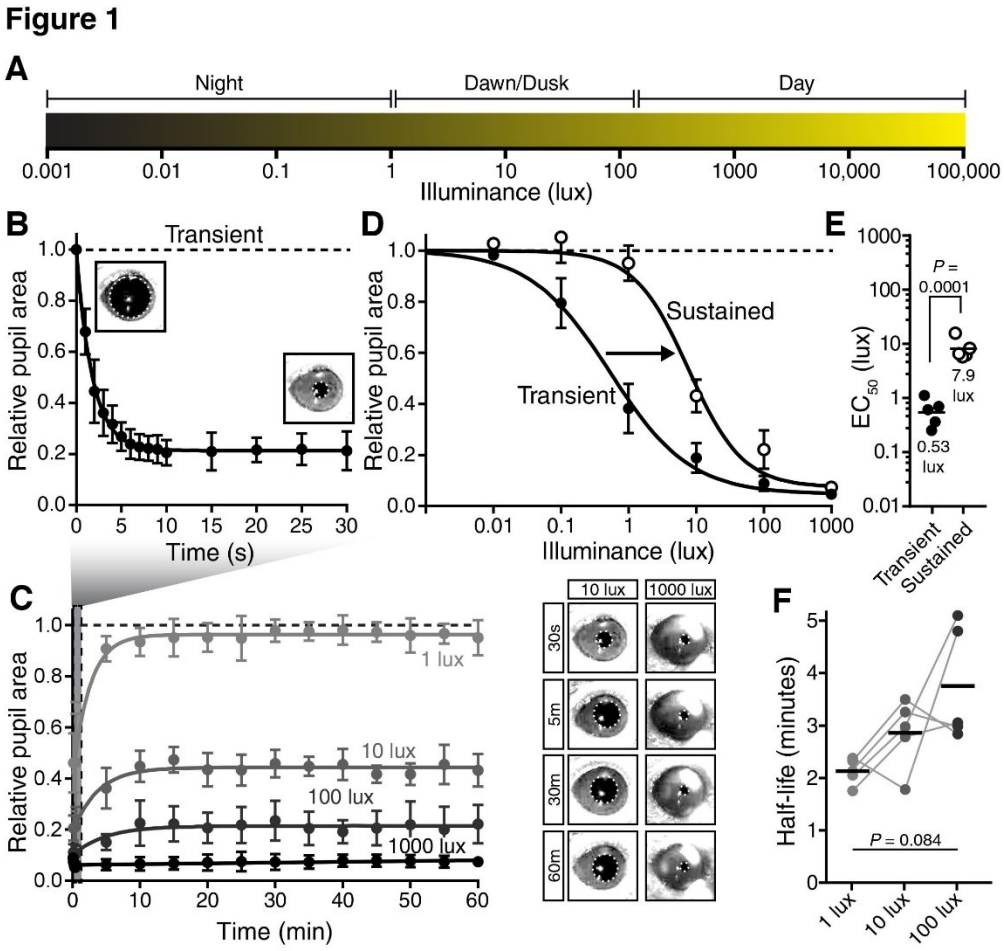

Figure 1: The pupillary light response contains two phases: transient and sustained. (**A**) Approximate light intensity ranges (lux) at different times of day. (**B**) Transient constriction in response to a 10 lux overhead stimulus (mean ± SD). Boxes contain representative pupil images at time 0 and 30 seconds. (**C**) Continued monitoring of pupil constriction from **b** for 60 minutes of continuous light at 5 minute intervals with representative images. (**D**) Intensity-response curve for transient and sustained constriction (30 sec and 60 min, respectively). Data fit with a sigmoidal curve (n = 5, mean ± SD). (**E**) Light intensity required for half-maximal constriction (EC_{50}) determined for both transient and sustained phases of the PLR. EC_{50} extracted from the sigmoidal

curve fits for each mouse (points are individual mice, line is mean). Statistical significance determined with a student's *t* test. (**F**) Half-life of PLR decay at 1, 10, and 100 lux. Statistical significance determined by main effect of light intensity from one-way ANOVA. See also **Figure 1—figure supplement 1**, **Figure 1—figure supplement 2**.

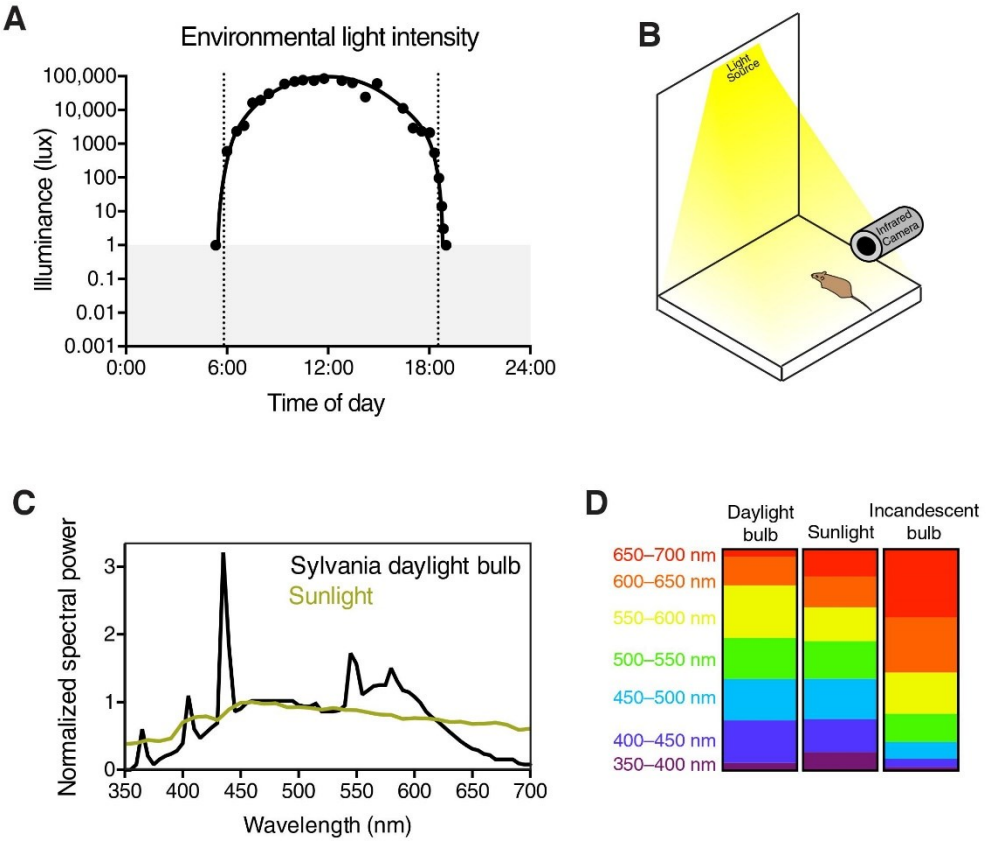

Figure 1—figure supplement 1: Experimental setup and light stimulus details.

(**A**) Environmental light intensity measured in lux across one day (April 2, 2015) in Baltimore, Maryland, USA. The light meter used is unable to measure light intensities below 1 lux, indicated with the gray box. Dotted lines refer to the meteorological sunrise and sunset. Data is fit with a hand-drawn curve for ease of visualization. (**B**) Mice are unanesthetized and restrained by hand under a light bulb with a broad spectrum similar to sunlight (**C**). Spectral power is normalized to the most highly represented wavelength in sunlight. Breaking down the fraction of light into 50 nm bins for each light source, the daylight bulbs are very similar to sunlight across all wavelengths (**D**), while incandescent

bulbs lack short wavelengths and are enriched in long wavelengths. Pupils are continuously recorded in darkness and light using an infrared video camera.

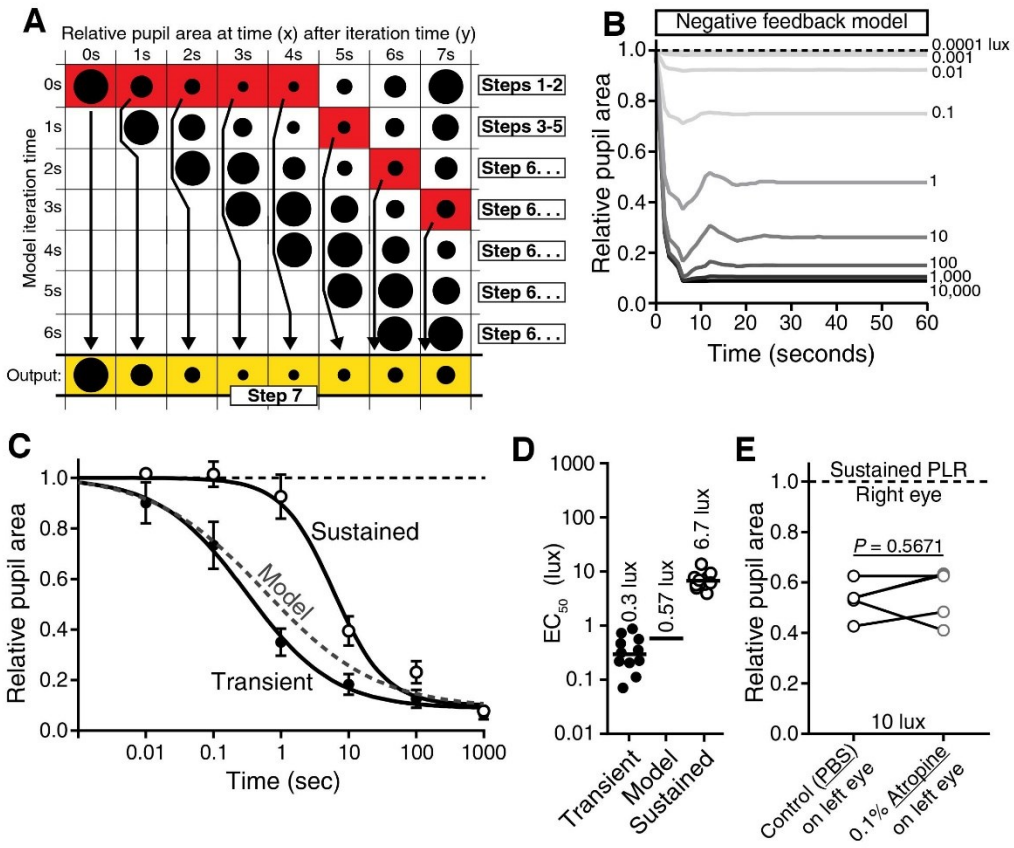

Figure 1—figure supplement 2: Negative-feedback model of PLR decay.

(**A**) Diagram displaying how the negative feedback model works (7s light in example) (See Online Methods for step-by-step explanation). The model assumes that packets of light information are discrete and are relayed to the PLR circuit to result in pupil constriction at later timepoints. We determined the kinetics of light information relay using a 1-second light pulse-chase. Then, we simply modulate the relative light intensity reaching the retina based on assuming continuous 1-second packets of information. At each new 1-second interval, the model samples the assumed pupil sizes currently driven by each previous packet of light information, uses the maximum value as the current pupil size, and then reduces the stimulus intensity using that pupil size. We then use this

new intensity to determine constriction caused at that time. This iterates every second. (**B**) Putative kinetics of feedback's impact on PLR at several light intensities (0.0001, 0.001, 0.01, 0.1, 1, 10, 100, 1000, and 10,000 lux). (**C**) Magnitude of PLR decay caused by feedback as modeled with (**D**) EC_{50}. Note that our model predicts minor PLR decay as a result of PLR feedback. (**E**) Experimental investigation of feedback's role in PLR decay. Atropine was applied to the left eye to inhibit pupil constriction and thus feedback. No enhancement of sustained PLR of the right eye was observed (paired two-tailed t-test).

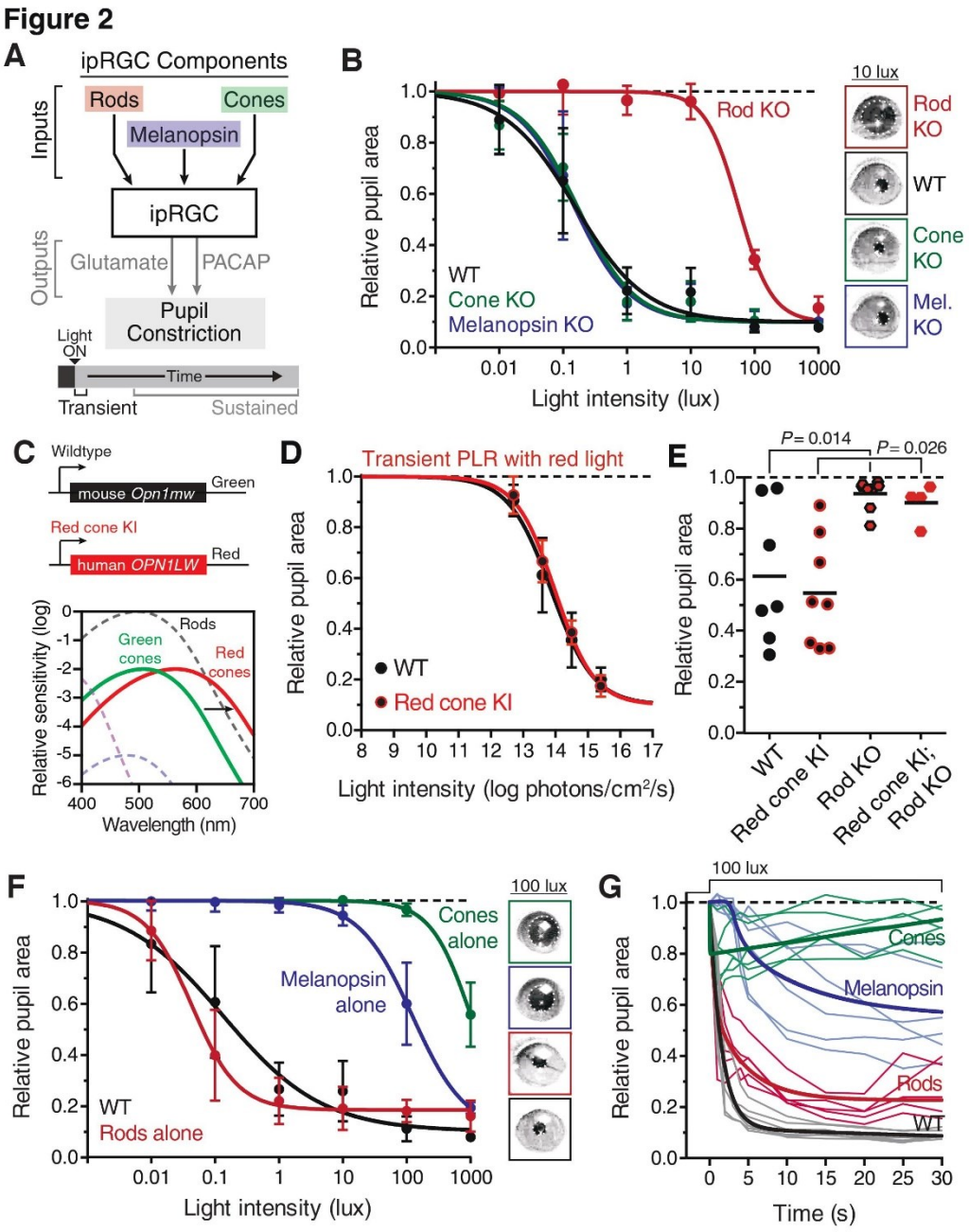

Figure 2: Transient input to ipRGCs is mediated by rods.

(**A**) Diagram of ipRGC behavioral circuit. (**B**) Intensity-response curves of the PLR in each of the photoreceptor mutant mouse lines (mean ± SD): wildtype (n = 6), Rod KO (*Gnat1*$^{-/-}$ n = 6), Melanopsin KO (*Opn4*$^{-/-}$ n = 8), and Cone KO (*Gnat2*$^{-/-}$ n = 7). Representative pupil images for each mouse line at 10 lux. (**C**) Gene schematic

comparison of endogenous mouse M-cone allele and human red cone knock-in allele as well as the spectral sensitivity shift observed. Notice that cones are more sensitive to red light in Red cone KI line. (**D**) The PLR to red light (626-nm LED) is identical in mice with cones that are more sensitive to red light (Red cone KI, $n = 6$) compared to littermate WT ($n = 5$), mean ± SD. (**E**) Removing rod function abolishes the PLR in response to red light (626-nm LED), even in mice with cones with enhanced sensitivity to red light. WT $n = 7$, Red cone KI (*Opn1mw*^{red}) $n = 8$, Rod KO (*Gnat1*$^{-/-}$)$^{-}$ $n = 8$, Red cone KI; Rod KO (*Gnat1*$^{-/-}$; *Opn1mw*^{red}) $n = 4$. Light intensity is 14.3 log photons/cm^2/s. (**F**) Intensity-response curves in mutant mice with each photoreceptor isolated (Rod-only: *Cnga3*$^{-/-}$; *Opn4*$^{-/-}$ $n = 6$)(Cone-only: (*Gnat1*$^{-/-}$; *Opn4*$^{-/-}$ $n = 6$)(Mel.-only: *Gnat1*$^{-/-}$; *Gnat2*$^{-/-}$ $n = 7$) Data is mean ± SD, statistical significance determined using a one-way ANOVA with Sidak's post-test. (right) Representative pupil images at 100 lux. (**G**) Kinetics of transient pupil constriction (100 lux) in mice with only rod, cone, or melanopsin function, same genotypes and number of animals as in **F**. Traces of individual mice are shown behind curve-fits. One-phase decays were fit to all except cone-only which was fit with a two-phase decay due to its rapid pupil decay within 30s. Melanopsin-only kinetic fit was offset from 0 by 3 sec to account for delay in constriction. See also **Figure 2—figure supplement 1**, **Figure 2—figure supplement 2**, **Figure 2—figure supplement 3**, **Figure 2—figure supplement 4**, **Figure 2—figure supplement 5**.

Figure 2—figure supplement 1

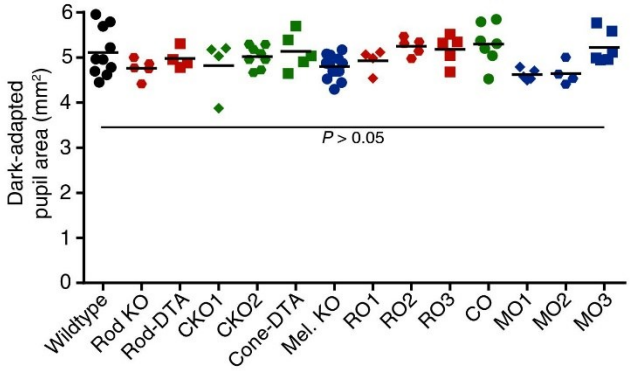

Figure 2—figure supplement 1: Dark-adapted pupil sizes of photoreceptor mutant mouse lines used.

Dark-adapted pupil sizes of all mouse lines used for photoreceptor investigation. Pupil size was recorded before light onset and pupil area (mm^2) is reported. No statistical difference was found for any genotype compared to wildtype ($P > 0.05$ for all comparisons). Statistical significance was determined by one-way ANOVA followed by Sidak's post-test.

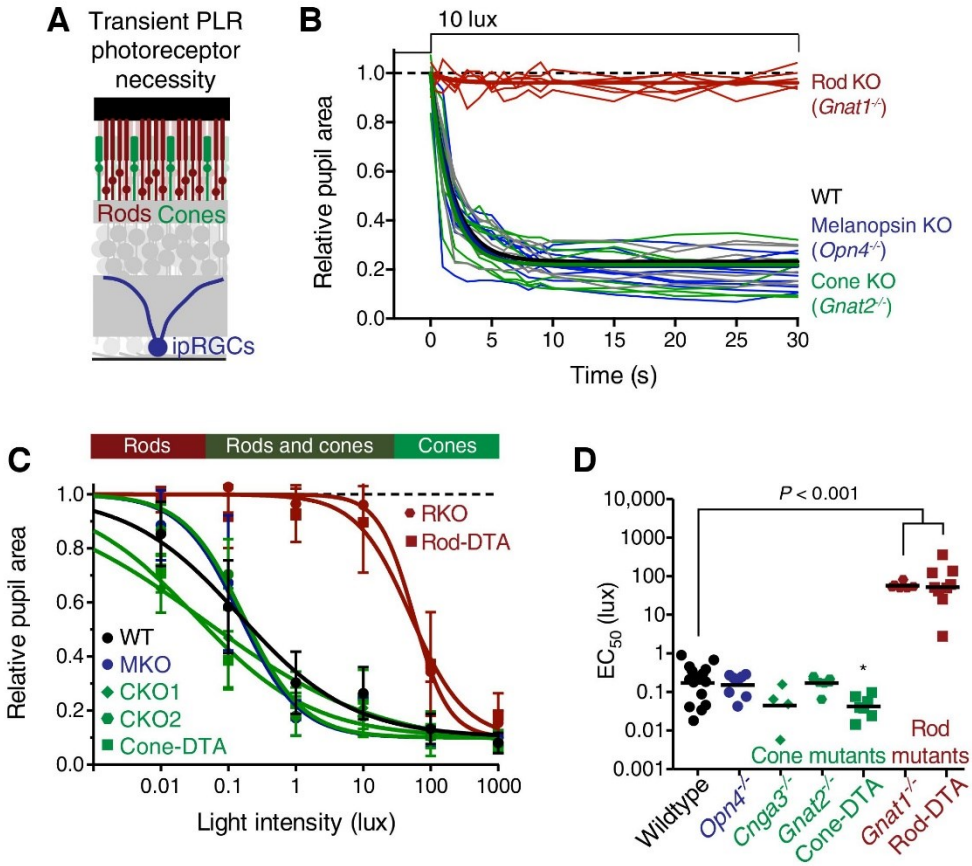

Figure 2—figure supplement 2: Rods are required for the transient phase of the PLR.

(**A**) Diagram of the retina labeling the photoreceptors. For experiments in **B–D**, WT n = 14, *Opn4*$^{-/-}$ n = 8, *Cnga3*$^{-/-}$ n = 4, *Gnat2*$^{-/-}$ n = 7, Cone-DTA n = 7, *Gnat1*$^{-/-}$ n = 6, Rod-DTA n = 9. (**B**) Kinetics of rapid constriction in response to dim light (10 lux). Rod KO mice are the only photoreceptor mutants to display a deficit. Cone and Mel. KO mice are identical to wildtype. (**C**) Intensity-response curves of the PLR in each of the photoreceptor mutant mouse lines (mean ± SD). The bar on top of the figure denotes the estimated sensitivities of rods and cones. (**D**) Rod mutant animals are the only mutants that display a sensitivity (EC_{50}) deficit compared to WT ($P < 0.0001$). In fact, Cone-DTA

mice are moderately more sensitive than WT (* $P = 0.011$). Points indicate individual mice, line indicates mean. Statistical significance determined using a one-way ANOVA with Sidak's post-test.

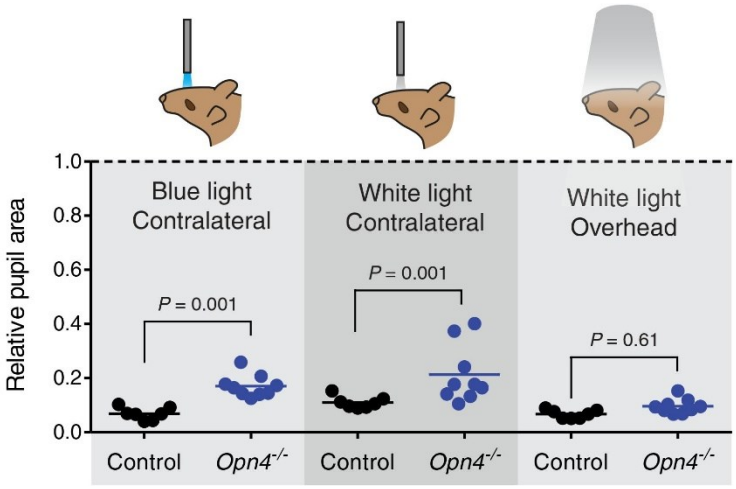

Figure 2—figure supplement 3: Melanopsin is not required for transient PLR in response to environmentally relevant overhead light.

Transient PLR determined under 3 different experimental light conditions. (Left) Blue (474-nm) LED light presented to contralateral eye ($1.9x10^{16}$ photons/cm^2/s). (Middle) White halogen light presented to contralateral eye (27.58 W/m^2). (Right) 1000 lux white compact fluorescent light presented overhead to both eyes (4.4 W/m^2). Line represents mean and points are individual mice. Statistical significance determined by one-way ANOVA followed by Sidak's post-test. No difference observed when light presented overhead. Control (*Opn4*$^{+/-}$) $n = 7$ and *Opn4*$^{-/-}$ $n = 9$.

Figure 2—figure supplement 4

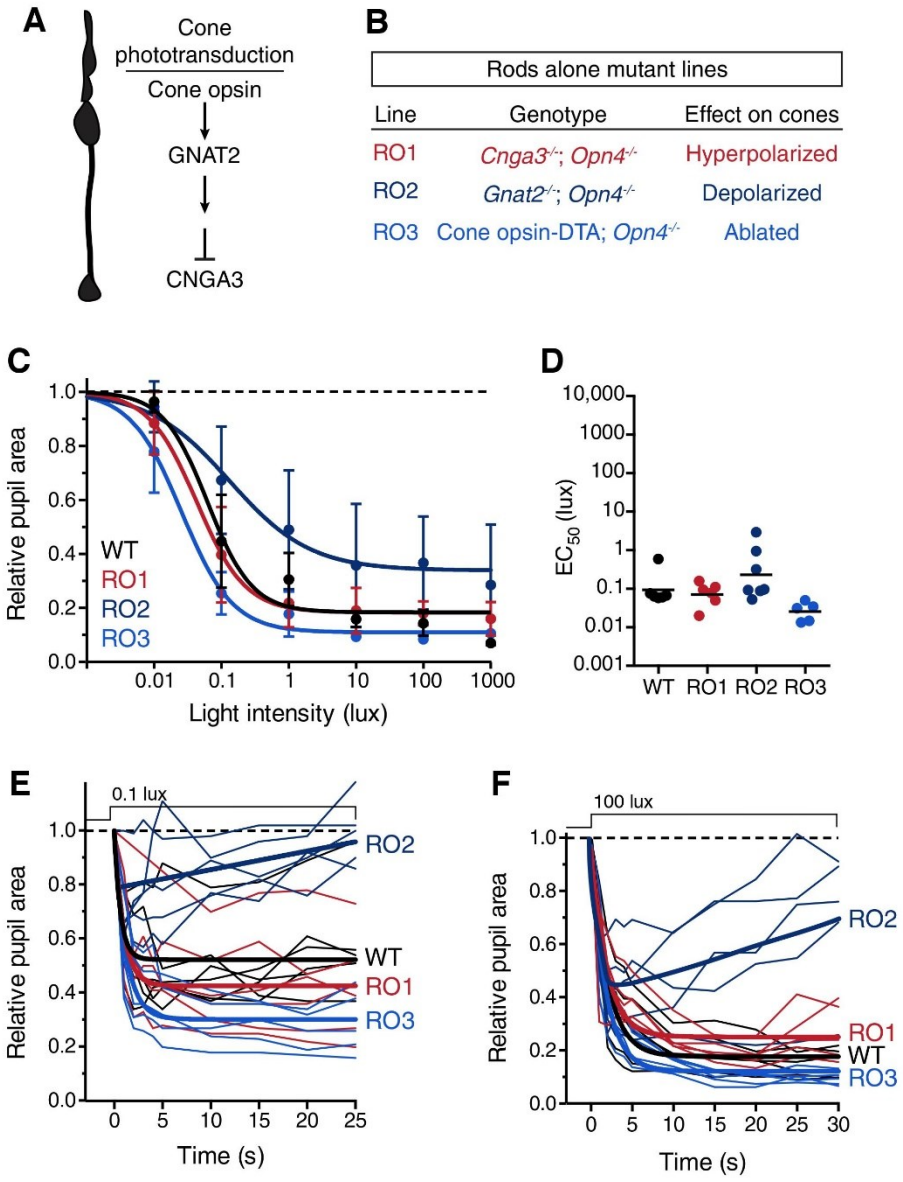

Figure 2—figure supplement 4: Rod input to the transient PLR is influenced by cones.

(**A**) Cartoon representation of a cone and a diagram of its phototransduction cascade. Different aspects of this cascade are disrupted in the various 'rod-only' lines we use. (**B**) Multiple mouse lines with rods as the only functional photoreceptors. For the

experiments in **C** and **D**: WT $n = 6$, Rod-only type 1 (RO1: *Cnga3*$^{-/-}$; *Opn4*$^{-/-}$) $n = 6$, Rod-only type 2 (RO2: *Gnat2*$^{-/-}$; *Opn4*$^{-/-}$) $n = 8$, Rod-only type 3 (RO3: Cone-DTA; *Opn4*$^{-/-}$) $n = 5$. (**C**) Intensity-response curve of the PLR in all of the rod-only lines, which are all similar to wild-type at all light intensities (mean ± SD). At 1000 lux, only RO2s are statistically different from wildtype ($P = 0.006$ by one-way ANOVA with Sidak's post-test). (**D**) Sensitivity (EC_{50}) in each of the mutant lines. No statistical differences were observed between the mouse lines (compared to WT, RO1 $P = 0.956$, RO2 $P = 0.340$, RO3 $P = 0.141$ using a one-way ANOVA with Sidak's post-test), although the RO2 line had more variability and trended toward lower sensitivity. (**E** and **F**) Kinetic comparison of rod-only lines at dim (**E**) and bright (**F**) light intensities. RO1 and RO3 lines are identical to wildtype under both light intensities, however, RO2 mice display PLR decay within 30s. All statistics are one-way ANOVA with Sidak's post-test, line indicates mean.

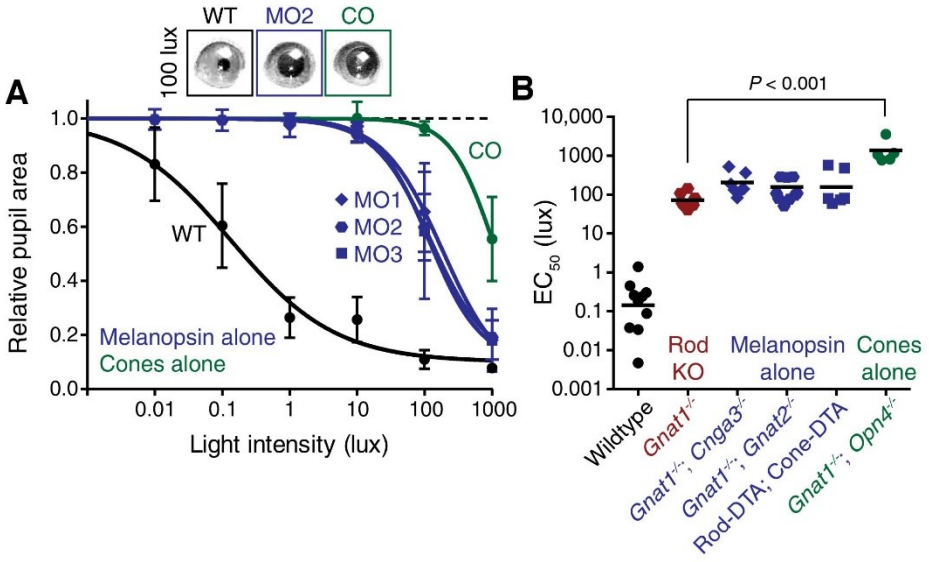

Figure 2—figure supplement 5: Melanopsin can drive rapid constriction at high light intensities.

Multiple mouse lines with ipRGCs as the only functional photoreceptors (melanopsin-only) or a mouse line with cones as the only functional photoreceptors (cone-only) were tested. For the experiments in **A** and **B**: WT $n = 9$, Gnat1$^{-/-}$ $n = 10$, Melanopsin-only type 1 (MO1: *Gnat1*$^{-/-}$*; Cnga3*$^{-/-}$) $n = 7$, Melanopsin-only type 2 (MO2: *Gnat1*$^{-/-}$*; Gnat2*$^{-/-}$) $n = 9$, Melanopsin-only type 3 (MO3: Rod-DTA; Cone-DTA) $n = 6$, Cone-only (*Gnat1*$^{-/-}$*; Opn4*$^{-/-}$) $n = 6$. (**A**) Intensity-response curve of the PLR in all of the melanopsin-only lines and in the cone-only mouse line (mean ± SD). (**B**) EC_{50} in each of the lines. All mutant lines are less sensitive than WT ($P < 0.0001$) by >2 log units. Cone-only mice are additionally less sensitive than Rod KO mice ($P < 0.0001$), but no melanopsin-only line is significantly different from Rod KO (Compared to RKO: MO1 $P = 0.201$, MO2 $P = 0.625$, MO3 $P = 0.591$). All statistics are one-way ANOVA with Sidak's post-test, line indicates mean.

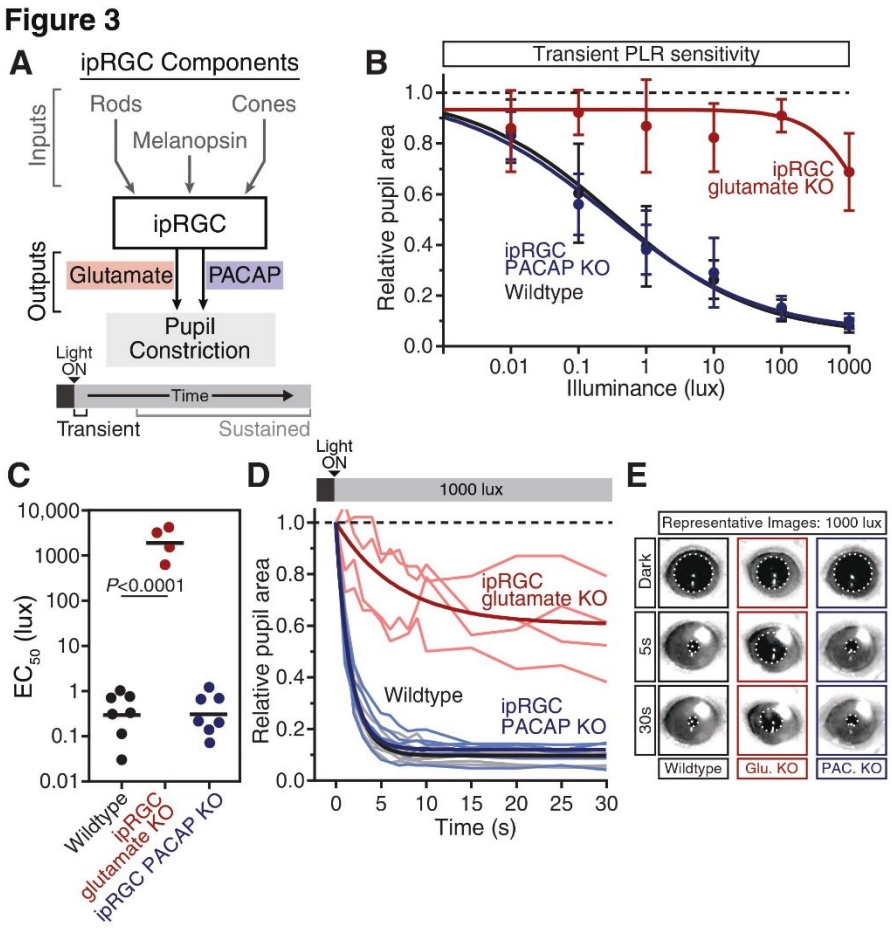

Figure 3: Glutamaterigic output provides precise and rapid transient signaling.

(**A**) Diagram of ipRGC behavioral circuit. (**B**) Intensity-response curves of the PLR in each of the neurotransmitter mutant mouse lines (Wildtype n = 6)(ipRGC glu. KO: *Opn4*$^{Cre/+}$; *Slc17a6*$^{fl/fl}$ n = 4)(ipRGC PACAP KO: *Opn4*$^{Cre/+}$;*Adcyap1*$^{fl/-}$ n = 6)(mean ± SD). (**C**) Sensitivity (EC_{50}) in each of the mutant lines. Statistical significance determined by one-way ANOVA with Sidak's post-test. (**D**) Kinetics of transient pupil constriction (1000 lux) in mice lacking glutamatergic or PACAPergic neurotransmission. Traces of individual mice are shown behind one-phase decay curve-fits. Half-lives: Wildtype (1.1 sec), ipRGC glu. KO (4.8 sec), ipRGC PACAP KO (1.1 sec). (**E**) Representative pupil

images at 5 sec and 30 sec post-illumination (1000 lux). **Figure 3—figure supplement 1**, **Figure 3—figure supplement 2**, **Figure 3—figure supplement 3**.

Figure 3—figure supplement 1

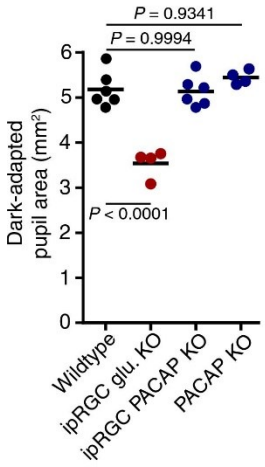

Figure 3—figure supplement 1: Dark-adapted pupil sizes of neurotransmitter mutant lines used.

Dark-adapted pupil sizes of all mouse lines used for neurotransmitter investigation. Pupil size was recorded before light onset and pupil area (mm^2) is reported. ipRGC glutamate KO mice are the only line used which display a significant difference in dark-adapted pupil size suggesting that glutamatergic signaling is important for setting pupil size in darkness ($P = 0.0001$). Statistical significance was determined by one-way ANOVA followed by Sidak's post-test.

Figure 3—figure supplement 2

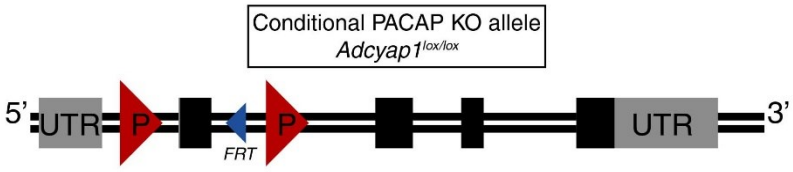

Figure 3—figure supplement 2: Description of conditional PACAP allele.

Schematic of the conditional PACAP allele (*Adcyap1*^{lox}). Boxes indicate exons (1-5). Grey indicates UTR while black indicates protein coding sequence. A single FRT site remains after removal of selection cassette. LoxP sites flank exon 2. Cre-mediated excision results in a frameshift and production of a truncated protein. See **Methods and Materials** for further information of allele generation and confirmation. A more detailed description of the generation and use of the allele will appear in a manuscript that is in preparation (Ross RA…Lowell BB *in preparation*).

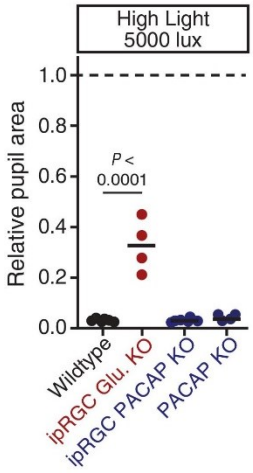

Figure 3—figure supplement 3: PACAP can drive significant constriction within 30s of high light onset.

Transient constriction was monitored in neurotransmitter mutant mice under high light (5000 lux). Data from each mouse is shown with the mean (black bar). ipRGC glutamate KO mice (*Opn4*$^{Cre/+}$*; Slc17a6*$^{fl/fl}$: $n = 4$) display a significant reduction in transient phase pupil constriction compared to wildtype ($n = 6$)($P < 0.0001$) while ipRGC PACAP KO (*Opn4*$^{Cre/+}$*;Adcyap1*$^{fl/-}$: $n = 6$) and PACAP KO ($n = 4$) mice are indistinguishable from wildtype ($P > 0.999$). Statistical signficance determined via one-way ANOVA followed by Sidak's post-test.

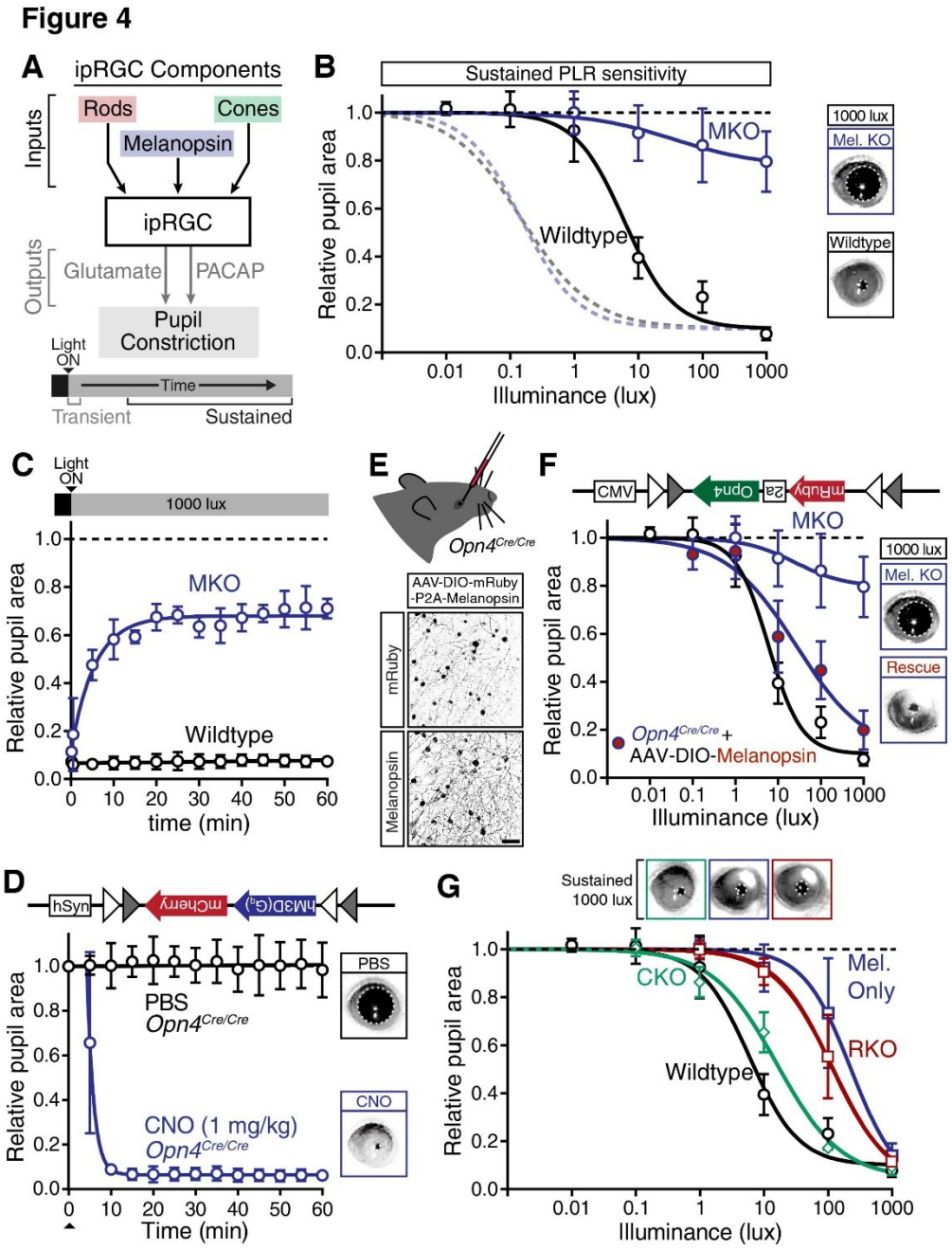

Figure 4: Melanopsin/rod synergy supports PLR under persistent conditions.

(**A**) Diagram of ipRGC behavioral circuit. (**B**) Intensity-response curves for wildtype and melanopsin knockout mice (*Opn4*$^{-/-}$): transient (dotted lines for reference) and sustained (60 minutes: solid lines) (WT $n = 6$, *Opn4*$^{-/-}$ $n = 12$). (right) Representative pupil images

under 1000 lux persistent light. (**C**) 60-min time course of pupil constriction under constant light (1000 lux). Data fit with a one-phase association curve (WT $n = 5$, *Opn4*$^{-/-}$ $n = 7$). (**D**) Sustained pupil constriction monitored every 5 minutes for 1 hour in melanopsin knockout mice (*Opn4*$^{Cre/Cre}$) expressing the G_q-coupled DREADD (hM3D) specifically in ipRGCs (AAV2-hSyn-DIO-hM3D(G_q)-mCherry). CNO injection IP (blue) caused robust constriction within 5–10 minutes that was sustained for 60 minutes, whereas PBS injection (black) did not. CNO data is fit with a one-phase association curve and PBS data is fit with a linear regression ($n = 6$, mean ± SD). (**E**) (top) Diagram showing viral eye injection in only one eye. (bottom) Confocal microscope images of an *Opn4*$^{Cre/Cre}$ retina injected with AAV2-CMV-DIO-mRuby-P2A-Melanopsin-FLAG showing infection and expression (mRuby, top; anti-OPN4, bottom). Scale bar = 50 μm. (**F**) Successful rescue of pupil constriction by virally restored melanopsin expression in a single eye of adult mice (WT $n = 6$, Mel. KO $n = 12$, Mel.-Rescue $n = 4$). (right) Representative pupil images of Mel. KO and Mel.-Rescue mice at 1000 lux. (**G**) PLR intensity-response curves of Wildtype ($n = 6$), Mel.-only (Rod-DTA; Cone-DTA $n = 8$), Cone KO (*Cnga3*$^{-/-}$ $n = 4$), and Rod KO (Rod-DTA $n = 5$) mice (mean ± SD). Melanopsin is sufficient at high light (≥1000 lux), however, rods are required at lower light intensities. Cone KO mice are similar to wildtype. (top) Representative pupil images at 1000 lux. See also **Figure 4—figure supplement 1**, **Figure 4—figure supplement 2**, **Figure 4—figure supplement 3**, **Figure 4—figure supplement 4**.

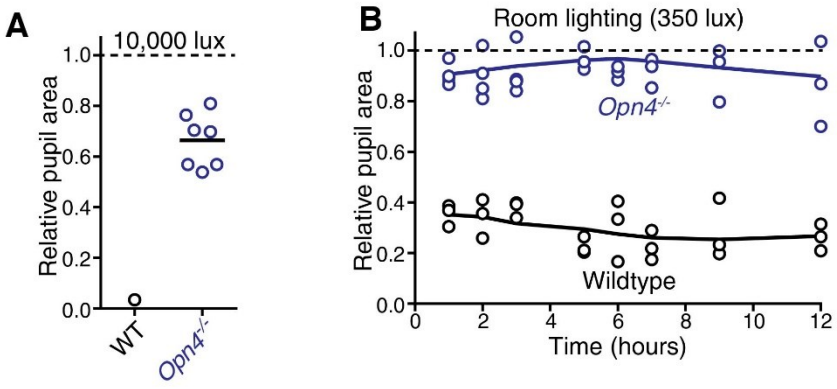

Figure 4—figure supplement 1: Melanopsin is required for sustained constriction across the day.

(**A**) Sustained constriction at 10,000 lux (WT *n* = 6, only 1 is plotted due to inability to see extremely small pupils in very bright light, Mel. KO n = 6). (**B**) Time course of pupil constriction under 12 hours of constant light corresponding to circadian day (room lighting = 350 lux) using wildtype (*n* = 3) and melanopsin knockout mice (*n* = 4) (line is smoothed mean).

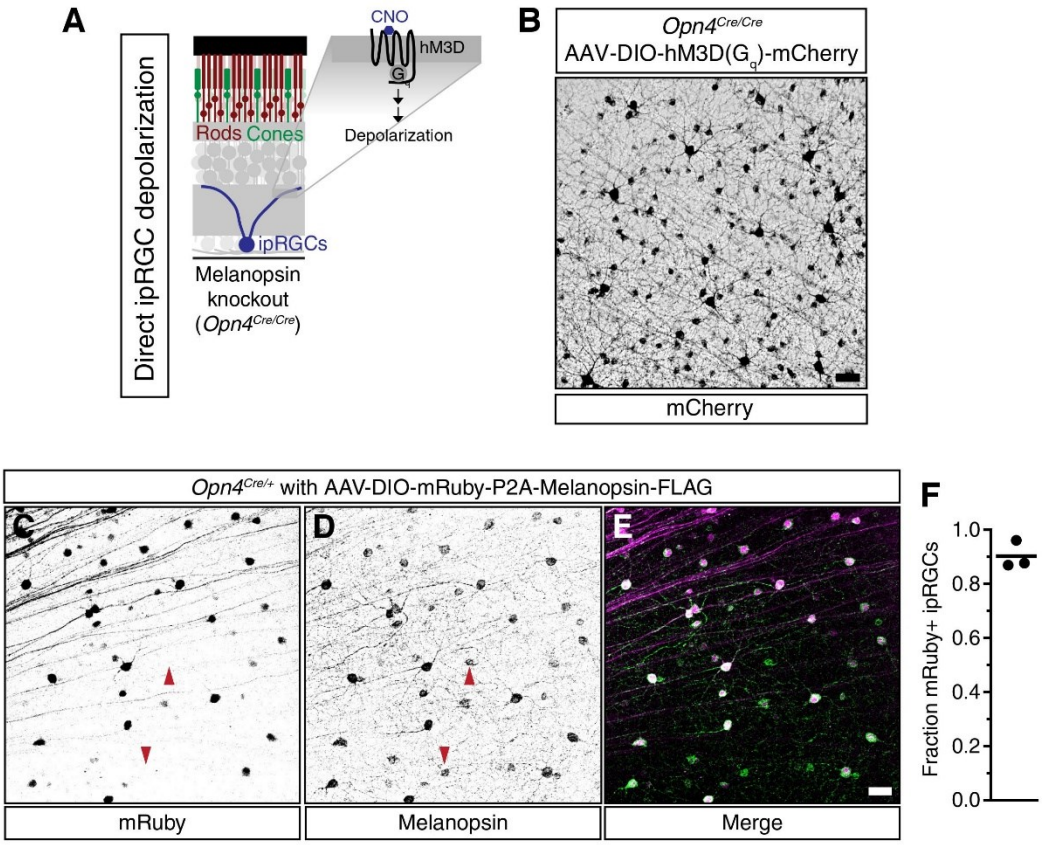

Figure 4—figure supplement 2: Viral infection and expression is specific to ipRGCs. (**A**) Schematic of the method to activate exclusively ipRGCs using an exogenous GPCR (hM3D(G_q)) and its ligand (CNO). (**B**) Confocal microscope image showing infection of ipRGCs observed by mCherry expression following administration of a Cre-dependent AAV injected into the vitreous of melanopsin-Cre knockout mice (*Opn4*$^{Cre/Cre}$). (**C-E**) Confirmation of ipRGC-specific expression of melanopsin from AAV-DIO-mRuby-P2A-Melanopsin-FLAG viral injections. *Opn4*$^{Cre/+}$ mice were used to colocalize viral (**C**) mRuby with (**D**) endogenous and exogenous melanopsin expression. (**E**) We observe specific expression of mRuby in a significant portion of ipRGCs, although some ipRGCs

lack mRuby staining, presumably due to lack of infectivity (arrows show mRuby-negative ipRGCs). Scale bars = 50 μm. (**F**) Quantification of fraction of ipRGCs (melanopsin-antibody) which are mRuby-positive. Quantification shown for three mice (A single 20x field was quantified for each mouse). Approximately 90% of melanopsin-positive cells express mRuby.

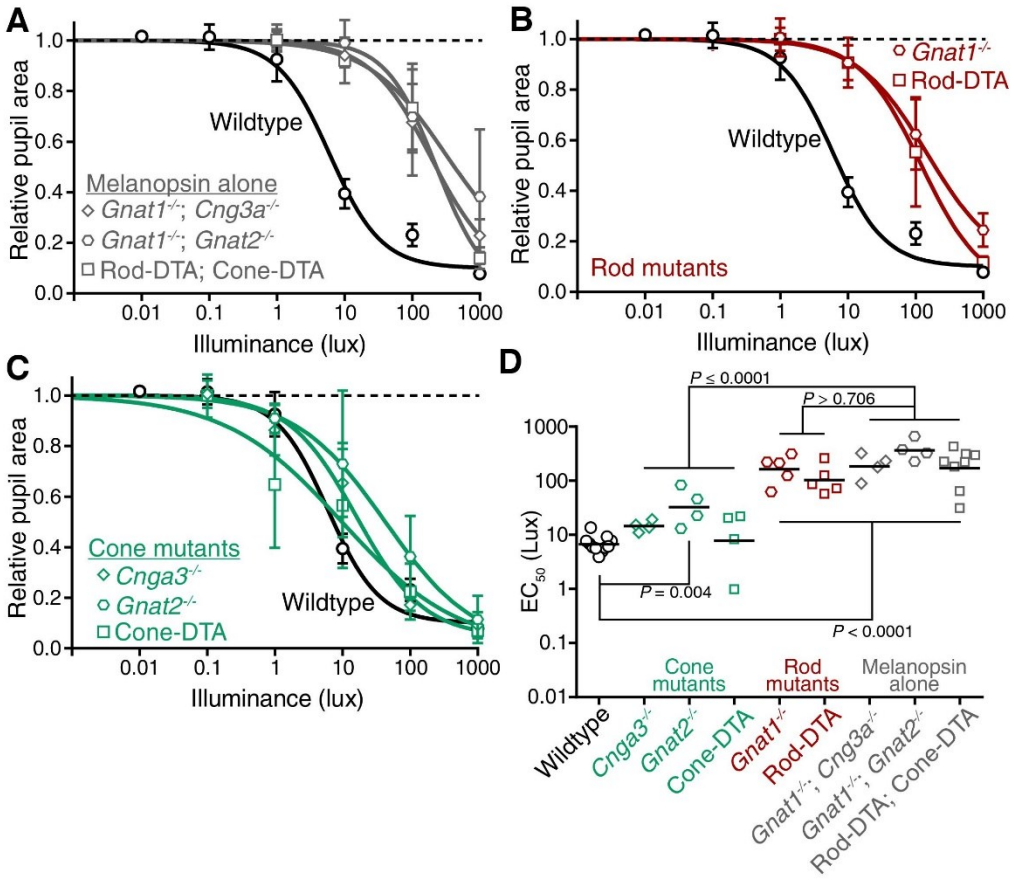

Figure 4—figure supplement 3: Rods, but not cones, contribute to sustained PLR sensitivity.

(**A**) PLR intensity-response curves of wildtype and mice with only melanopsin phototransduction intact ('melanopsin-only': *Gnat1*$^{-/-}$*; Gnat2*$^{-/-}$ *n* = 4, *Gnat1*$^{-/-}$*; Cnga3*$^{-/-}$ *n* = 4, Rod-DTA; Cone-DTA *n* = 8) (mean ± SD). (**B**) Sustained PLR intensity-response curves of wildtype (*n* = 11) and rod mutant mice (*Gnat1*$^{-/-}$ *n* = 5, Rod-DTA *n* = 5) (mean ± SD). (**C**) Sustained PLR intensity-responses of wildtype and cone mutant mice ('cone mutants': *Gnat2*$^{-/-}$ (*n* = 4), *Cnga3*$^{-/-}$ (n = 4), Cone-DTA (*n* = 4)). (**D**) Sustained EC_{50} for

wildtype and cone mutant, rod mutant and melanopsin-only mice (line = mean). All rod mutant and melanopsin-only mouse lines display significnt loss of sensitivity ($P < 0.0001$). Two of three cone mutant mouse lines were not significantly different from wildtype (*Cnga3*$^{-/-}$ $P = 0.57$, Cone-DTA $P > 0.999$), though *Gnat2*$^{-/-}$ displayed a 0.69 log-unit decrease in sustained PLR EC_{50} (*Gnat2*$^{-/-}$ $P = 0.004$). Additionally, all rod mutant lines were similar to their corresponding melanopsin-only line ($P > 0.706$) while all cone mutant lines were significantly more sensitive than their corresponding melanopsin-only line ($P \leq 0.0001$). Statistical significance determined via one-way ANOVA with Sidak's post-test.

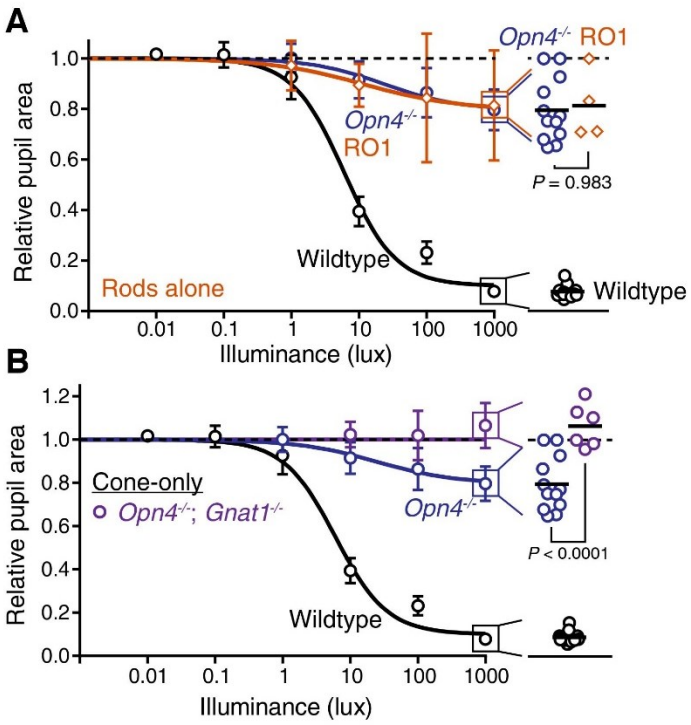

Figure 4—figure supplement 4: Rods drive the residual sustained pupil constriction observed in the absence of melanopsin.

(**A**) Sustained PLR dose-responses for wildtype (n = 11), melanopsin knockout (*Opn4*$^{-/-}$, n = 12) and mice with only rod phototransduction intact ('rod-only': *Cnga3*$^{-/-}$*; Opn4*$^{-/-}$ n = 4) (mean ± SD). (right) Scatter plot of 1000 lux sustained PLR. Melanopsin knockout and 'rod-only' mice not statistically different by one-way ANOVA with Sidak's post-test (P = 0.983) (line indicates mean). (**B**) Sustained PLR intensity-responses for wildtype (n = 11), melanopsin knockout (*Opn4*$^{-/-}$ n = 12) and mice with only cone phototransduction intact ('cone-only': *Opn4*$^{-/-}$*; Gnat1*$^{-/-}$, n = 6, mean ± SD). (right) Scatter plot of 1000 lux sustained PLR. Melanopsin knockout and 'cone-only' mice are statistically different by one-way ANOVA followed by Sidak's post-test.

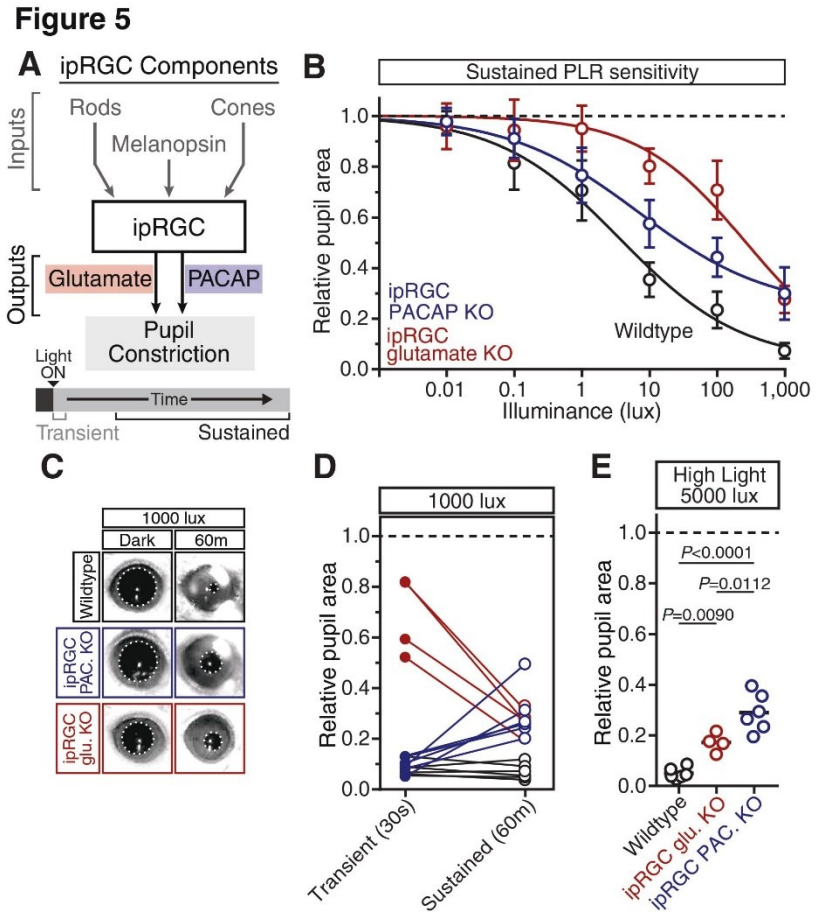

Figure 5: PACAP is essential for the sustained PLR.

(**A**) Diagram of ipRGC behavioral circuit. (**B**) PLR intensity-response curves of sustained constriction in mice lacking glutamatergic or PACAPergic neurotransmission (WT $n = 6$, ipRGC glu. KO $n = 4$, ipRGC PACAP KO $n = 6$)(mean ± SD). Both mutants display deficits at 10, 100, and 1000 lux as compared to wildtype (wildtype v. ipRGC Glu. KO: 10 and 100 lux $P < 0.0001$, 1000 lux $P = 0.0004$ by two-way ANOVA with Sidak's post-test)(wildtype v. ipRGC PACAP KO: 10, 100, and 1000 lux $P < 0.0001$ by two-way ANOVA with Sidak's post-test). (**C**) Representative pupil images of sustained constriction at 1000 lux. (**D**) Comparison of transient and sustained constriction under high light (1000 lux). ipRGC glu. KO mice (red) show an increase in pupil constriction

with time whereas ipRGC PACAP KOs (blue) display a significant loss of constriction over time (ipRGC glu. KO transient v. sustained $P < 0.0001$, ipRGC PACAP KO transient v. sustained $P = 0.0003$, wildtype transient v. sustained $P = 0.9921$ by one-way ANOVA with Sidak's post-test). (**E**) Pupil constriction of neurotransmitter mutant mice after sustained 5000 lux light. Data from individual mice shown with mean (black bar). Statistical significance determined by one-way ANOVA with Sidak's post-test. See also **Figure 5—figure supplement 1**.

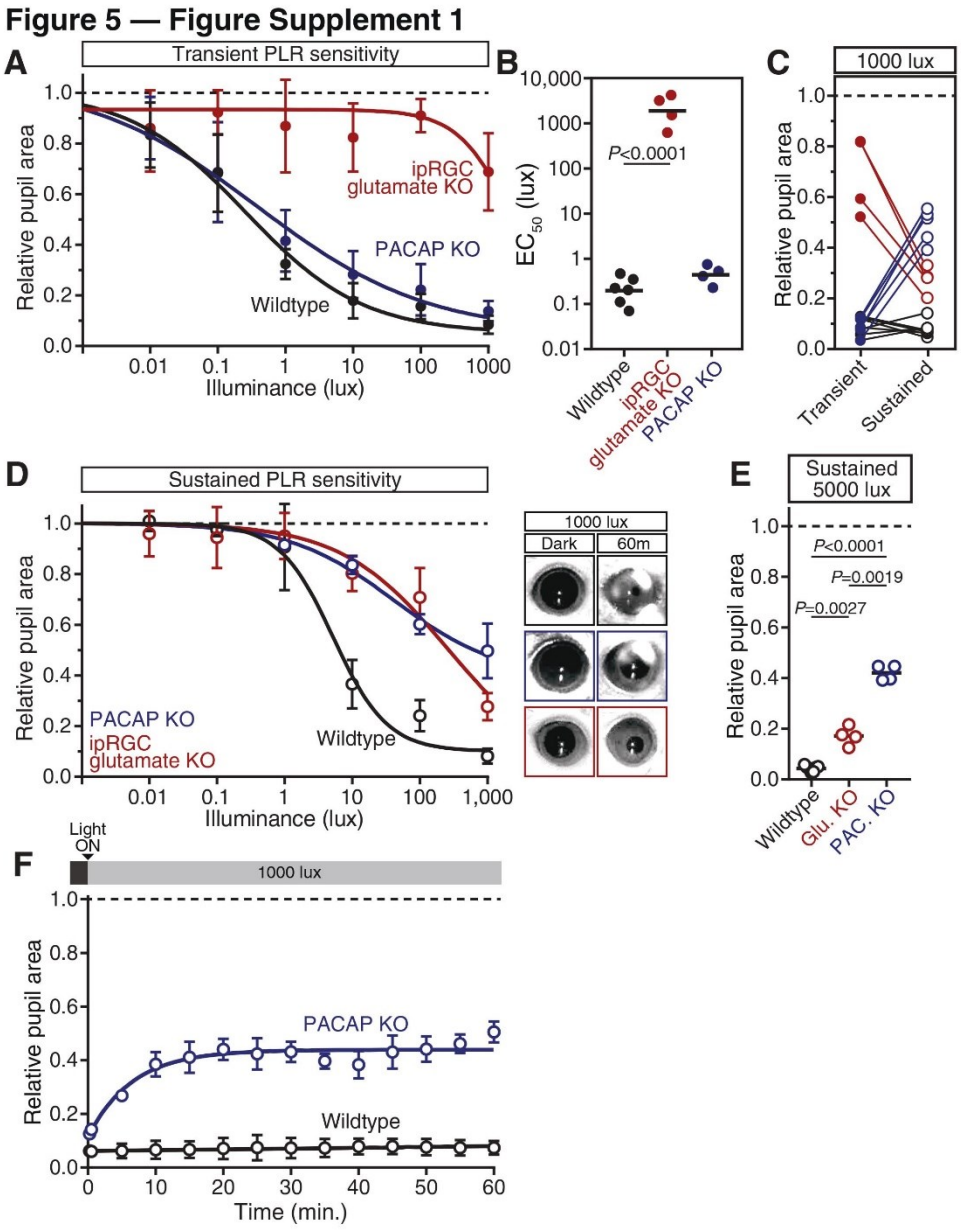

Figure 5—figure supplement 1: PACAP KO mice display similar PLR phenotypes to ipRGC-specific PACAP KO mice.

(**A**) Intensity-response curves of the transient PLR (30s light) in each of the neurotransmitter mutant mouse lines (Wildtype n = 6)(ipRGC glu. KO: *Opn4*$^{Cre/+}$;

Slc17a6$^{fl/fl}$ n = 4)(PACAP KO: *Adcyap1*$^{-/-}$ n = 4)(mean ± SD). (**B**) Sensitivity (EC_{50}) in each of the mutant lines. Statistical significance determined by one-way ANOVA with Sidak's post-test. (**C**) Comparison of transient and sustained (60 min. light) constriction under high light (1000 lux). ipRGC glu. KO mice (red) show an increase in pupil constriction with time whereas PACAP KOs (blue) display a significant loss of constriction over time. (**D**) PLR intensity-response curves of sustained constriction in mice lacking glutamatergic or PACAPergic neurotransmission (WT n = 6, ipRGC glu. KO n = 4, PACAP KO n = 4)(mean ± SD). Both mutants display similar deficits until 1000 lux where PACAP KO mice show a further deficit (PACAP KO v. ipRGC Glu. KO: P = 0.0019 by one-way ANOVA with Sidak's post-test). (right) Representative pupil images of sustained constriction at 1000 lux. (**E**) Pupil constriction of neurotransmitter mutant mice after sustained 5000 lux light. Data from individual mice shown with mean (black bar). Statistical significance determined by one-way ANOVA with Sidak's post-test. (**F**) 60-min. time course of pupil constriction under constant light (1000 lux). Data fit with a one-phase association curve (WT n = 5, PACAP KO n = 4). (mean ± SD).

Figure 6

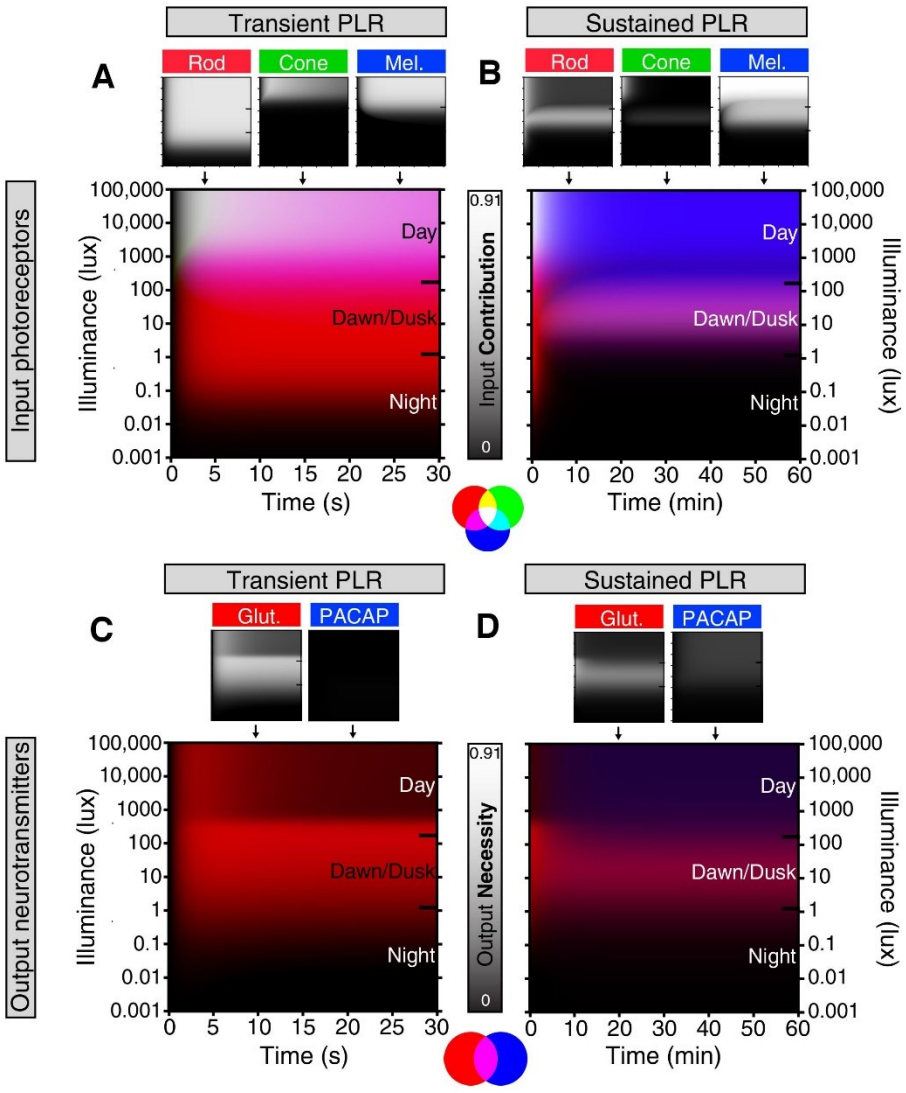

Figure 6: Model of ipRGC circuit transitions.

(**A** and **B**) Heat maps of (**A**) transient and (**B**) sustained PLR as duration and intensity vary. Night, dawn/dusk, and daytime light intensities indicated by ticks on right side of plot. (top) Heat maps of individual photoreceptor contributions (grayscale). Black represents no contribution and degree of white represents increasing contribution. Each photoreceptor contribution heat map is a combination of necessity (individual

photoreceptor transduction knockouts) and sufficiency ('photoreceptor-only') heat maps (for example: Input $Contribution_{rod} = Max(Necessity_{rod}, Sufficiency_{rod})$). (middle) Rod (red), cone (green), melanopsin (blue) contributions are combined into a single heat map. (bottom) Color combination guide for reference when viewing heat map. (**C** and **D**) Same as above for neurotransmitter contributions to transient (**C**) and sustained (**D**) ipRGC signaling. Glutamatergic contribution is in green and PACAPergic contribution is in blue. See the Materials and Methods section for details on heat map generation. Note that the axes are the same for the individual and combined heatmaps. See also **Figure 6—figure supplement 1**.

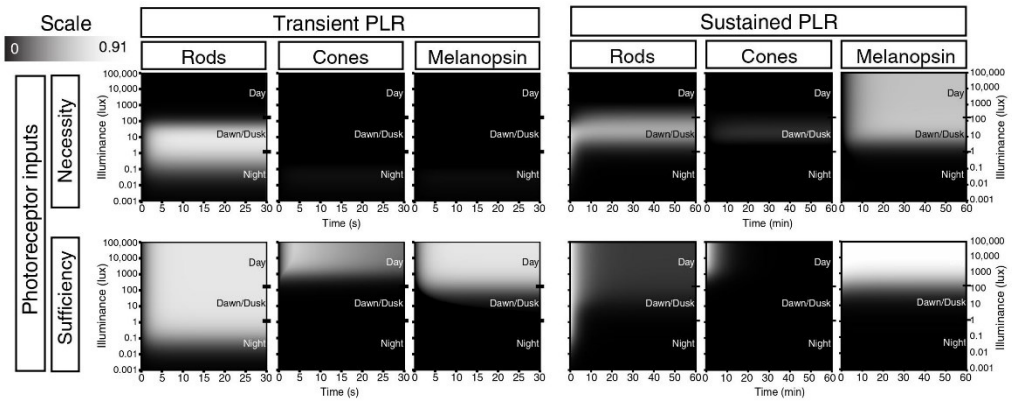

Figure 6—figure supplement 1: Necessity/Sufficiency heat maps for photoreceptor input to pupil constriction.

Heat maps of necessity and sufficiency of each input (top: rods, cones, melanopsin) as stimulus duration and intensity vary. The necessity/sufficiency heat maps for a particular component were subsequently used to generate a photoreceptor contribution heat map (See **Figure 6**). Black indicates no necessity/sufficiency and white indicates full necessity/sufficiency.

Mouse line	Genotype	Effect on retinal function	Citations
Rod KO	*Gnat1*$^{-/-}$	No rod phototransduction	[84]
Rod-DTA	rdta	No rod cell bodies; cones present early in life	
Cone KO1	*Cnga3*$^{-/-}$	No cone phototransduction	[54]
Cone KO2	*Gnat2*$^{cpfl3/cpfl3}$	No cone phototransduction	[85]
Cone-DTA	h.red DT-A	Ablation of all M cones; >95% loss of S cones	[86]
Melanopsin KO	*Opn4*$^{-/-}$	No melanopsin phototransduction	[39]
Cone-only	*Gnat1*$^{-/-}$*; Opn4*$^{-/-}$	No rod/melanopsin phototransduction	
Rod-only 1	*Cnga3*$^{-/-}$*; Opn4*$^{-/-}$	No cone/melanopsin phototransduction	
Rod-only 2	*Gnat2*$^{-/-}$*; Opn4*$^{-/-}$	No cone/melanopsin phototransduction	
Rod-only 3	h.red DT-A; *Opn4*$^{-/-}$	No cone cells nor melanopsin phototransduction	
Melanopsin-only 1	*Gnat1*$^{-/-}$*; Cnga3*$^{-/-}$	No rod/cone phototransduction	
Melanopsin-only 2	*Gnat1*$^{-/-}$*; Gnat2*$^{-/-}$	No rod/cone phototransduction	
Melanopsin-only 3	rdta; h.red DT-A	No rod or cone cell bodies	
Red cone KI	*Opn1mw*^{red}	Cones have shifted sensitivity to red	[87]
Red cone KI; Rod KO	*Opn1mw*^{red}*;Gnat1*$^{-/-}$	Cones have shifted sensitivity to red, no rod phototransduction	

Table 1: Description of photoreceptor mutant mouse lines used.

Mouse line	Genotype	Effect on retinal function	Citations
Melanopsin-Cre	*Opn4*$^{Cre/+}$	Cre expression in ipRGCs	[88]
Slc17a6-flox	*Slc17a6*$^{fl/fl}$	Exon 2 flanked by loxP sites	[89]
ipRGC glutamate KO	*Opn4*$^{Cre/+}$; *Slc17a6*$^{fl/fl}$	Silences ipRGC glutamatergic release	
PACAP KO	*Adcyap1*$^{-/-}$	Whole animal PACAP removal	[90]
PACAP-flox	*Adcyap1*$^{fl/fl}$	Exon 2 flanked by loxP sites	See figure supplement 2
ipRGC PACAP KO	*Opn4*$^{Cre/+}$; *Adcyap1*$^{fl/-}$	Silences ipRGC PACAP release	

Table 2: Description of neurotransmitter mutant mouse lines used.

Chapter 3: Glutamatergic ipRGC signaling is required for active pupil dilation

Abstract

Constriction and dilation of the pupil provides the visual system with a way to regulate the amount of light entering it. The neural circuits responsible for pupil constriction in response to light increments have seen extensive research and insight, however, little work has been done to understand pupil dilation in response to light decrements. IpRGCs relay light information from the retina to areas controlling pupil size and have been shown to be critical relays for light information to drive pupil constriction. In this chapter, we investigate the role of ipRGCs in **pupil dilation**. Using mice lacking ipRGC-glutamatergic or PACAPergic neurotransmission, we asked whether pupil dilation is an active process and which neurotransmitters support it. In this study, we show that pupil dilation in response to dimming light is, in fact, an active process which requires glutamatergic neurotransmission from ipRGCs.

Introduction

Pupil constriction and dilation are equally important aspects of pupillary control. While the mechanisms underlying pupil constriction have been the topic of a significant amount of research (including our own – See Chapter 2), pupil dilation has received remarkably little attention. In fact, I am unaware of a single study on the mechanisms underlying dilation since the dawn of modern genetic tools in mice.

The iris consists of two components: the inner sphincter muscle (constrictor) and the outer radial muscle (dilator). The constrictor is innervated by parasympathetic fibers and the dilator by sympathetic fibers. The pupil constricts as a result of parasympathetic constrictor activation and concomitant relaxation of the dilator. The fundamental cause of

pupil dilation in response to dimming light is less clear. Whether it is caused by passive relaxation of the constrictor or activation of the dilator is an open question even after hundreds of years of pupil research [52,91].

I became interested in pupil dilation after an observation made while asking questions about pupil constriction (Chapter 2). As a control experiment, I measured the resting pupil size (dark-adapted for 1 hour) of all the mouse lines I had used. 16 of the 17 lines had indistinguishable baseline pupil sizes, however, 1 of them, ipRGC glutamate KOs (*Opn4*^{Cre} ; *Vglut2*$^{fl/fl}$), had a significantly smaller pupil (~30%)(see **Chapter 2: Figure 2—figure supplement 1, Figure 3—figure supplement 3**). In fact, a previous study noticed a similar trend when they tested this mouse line[92], although it was not statistically significant.

The first and most obvious explanation for the small resting pupil size is defective dilation. One would expect that decreased dilation drive in response to darkness would lead to an overall smaller pupil size. To answer this question, I performed similar experiments to those described in chapter 2 with a focus on the offset of light stimulus and subsequent pupil dilation.

Results

Mice lacking ipRGC-glutamatergic signaling have massively reduced pupil dilation kinetics

Given the smaller dark-adapted pupil size of mice lacking glutamatergic signaling from ipRGCs (**Chapter 2: Figure3—figure supplement 3**), we asked whether these

mice have deficits in pupil dilation after light dimming. To do so, we submitted wildtype and ipRGC-glu. KO mice to 30 seconds of light (6500K, 1000 lux) followed by 10 seconds of darkness. During the 30 second light stimulus, we observed constriction in both wildtype and ipRGC-glu. KO mice, albeit reduced in amplitude (See Chapter 2 for initial characterization of these mice). While wildtype mice displayed a significant amount of dilation within the 10 seconds after light offset, ipRGC-glu. KO mice showed little to no change in pupil size (**Figure 1**). This suggests that glutamatergic neurotransmission from ipRGCs is critical for dilation in response to darkness, at least over short timescales.

To determine whether glutamate is required for dilation over longer timescales as the reduced resting pupil size suggests, we sought to observe dilation for a more extended duration. We are limited in our continuous pupil observation by the duration a mouse will tolerate scruffing. This tends to be somewhere between 1 and 3 minutes. To maximize the amount of dilation we can observe, we first light-adapted mice for 60 minutes under bright light (6500K, 1000 lux). We then began our observation with 5 seconds of light to determine the extent of constriction achieved during light adaptation followed by a 60 second window of darkness/dilation (**Figure 2**). Wildtype mice's pupils dilated extensively over the 60 seconds of darkness – from 10% to 78% of resting pupil size. IpRGC-glu. KO mice, however, displayed little to no response to light offset – mean pupil size moved from 28% at light offset to 32% given 60 seconds of darkness (**Figure 2**). We also tested PACAP KO mice (*Adcyap1*$^{-/-}$) and observed marked dilation – 45% to 84% of resting pupil size. Note that PACAP KO mice started with less constriction due to their sustained pupil constriction deficit (See Chapter 2 for initial characterization of

these mice). These results highlight and strengthen the specific role glutamatergic neurotransmission plays in pupil dilation even more so than pupil constriction (Chapter 2).

Given the drastic pupil dilation deficit we observed over the 60 second dilation time course and the fact that these mice do eventually reach a more dilated resting pupil size, we performed a long-term pupil dilation time course spanning several hours (**Figure 3**). In this experiment, we light-adapted mice as before and then tracked dilation with 30 second discontinuous observations at 1, 5, 10, 60, 90, 120, and 180 minutes post light offset. Wildtype mice returned to their resting pupil size within the first 10 minutes of observation, however, ipRGC glu. KO displayed an incoherent pattern of pupil size fluctuation (**Figure 3**). Even during the 30 second observations, fairly rapid fluctuations were observed (data not shown). It appears that glutamate is required for coherent dilation of the pupil at short and long timescales. Further observation with more mice and over even longer timescales will be required to determine the extent of this dilation deficit.

Discussion

The results presented in this chapter highlight how little we know about the process of pupil dilation. We have shown that dilation must be an active process which depends on ipRGCs' glutamatergic neurotransmission.

There are many fundamental questions to answer before we can begin to understand dilation to the extent of constriction. First and most important is discovering

the brain nucleus responsible for receiving darkness information and driving pupil dilation. The only lead derives from a 1985 study by R. J. Clarke and H. Ikeda which demonstrates the presence of cells activated by darkness in the posterior pretectal nucleus (PPN)[93]. Fittingly, this study also revealed luminance detectors in the nearby OPN known to control pupil constriction. However, no further investigation of the PPN has been done to confirm its role in pupil dilation.

Once we have the target neuronal population, we can begin to investigate the molecular mechanisms underlying their response to glutamate. Because ipRGCs are known to increase activity in light and decrease activity in darkness, these central target neurons must somehow invert the glutamatergic signal they are receiving. Strong basal activity coupled with expression of an inhibitory glutamate receptor could achieve this goal. Strong inhibition would reduce dilator activation in the presence of light and allow for robust pupil constriction. Darkness would lift inhibition of these neurons subsequently driving dilator activation and robust pupil dilation.

Methods

Animal husbandry

C57Bl/6 × Sv129 hybrid mice were used in all experiments except PACAP KO mice which were C57Bl/6. All mice were housed according to guidelines from the Animal Care and Use Committee of Johns Hopkins University. Male and female mice age 4-8 months were housed in plastic translucent cages with steel-lined lids in an open room. Ambient room temperature and humidity were monitored daily and tightly controlled. Food and water were available *ad libitum.* All mice were maintained in a

12hr:12hr light-dark cycle with light intensity around 100 lux for the entirety of their lives.

Pupillometry

All mice were dark-adapted for at least 12 hours prior to any experiments and all PLR experiments were performed between Zeitgeber times (ZT) 2 and 10. For all experiments, mice were unanesthetized and restrained by hand. Because stress can affect pupil size, we ensured that the mice were not stressed during these experiments. To do so, we handled the mice for several days prior to the experiments to get them accustomed to the researchers and to being scruffed. Any mice that showed signs of stress, including vocalizations and wriggling during the experiments, were not used and were subjected to more handling sessions before use in experiments.

Mice were restrained manually under a 23-Watt compact fluorescent light bulb (GE Daylight FLE10HT3/2/D or Sylvania Daylight CF13EL and CF23EL) with a color temperature of 6500 K to simulate natural sunlight. The light intensity was measured using a light meter (EXTECH Foot Candle/Lux Light Meter, 401025) at the surface on which the mouse was held. The light meter was initially calibrated by EXTECH using a Tungsten 2856 K light source; because our experiments used a fluorescent bulb of 6500 K, all measured light intensities reported here may vary by 0.92–1.12 times the actual light intensity.

Videos of the eye were taken using a Sony Handycam (DCR-HC96) mounted on a tripod a fixed distance from the mouse. Manual focus was maintained on the camera to

ensure that only one focal plane existed for each mouse and that therefore variable distance from the camera should not contribute to differences in relative pupil area throughout the video. Pupil size was first recorded under dim red light and the endogenous infrared light source of the camera to capture the dark-adapted pupil size. Pupils were recorded either at the initial onset of light and offset 30 seconds later or mice were adapted to 1000 lux light for 1 hour followed by pupil monitoring at light offset. All pupil images were cropped to a fixed square area surrounding the eye using GNU Image Manipulation Program (GIMP). The images were made grayscale and then brightness and contrast were adjusted to enhance visibility of the pupil and exported as PNG files.

Data analysis

Videos were transferred from the camera to a computer as Audio Video Interleave (AVI) files and individual frames were taken using VLC media player (www.videolan.org/vlc/) and saved in portable network graphics format (PNG). Images were taken in the dark, at 5 seconds, and 30 seconds following stimulus onset. Pupil area was then quantified manually in ImageJ (http://rsbweb.nih.gov/ij/) software. The pupil area was measured in pixels using the oval tool in which the 4 cardinal points of the oval were touching their respective edges of the pupil. The relative pupil area was calculated using LibreOffice Calc or Microsoft Excel in which the area during the light stimulus was divided by the area prior to lights onset.

Acknowledgements

I would like to thank the entire mouse tri-lab for feedback over the course of many lab meetings. I would also like to thank my thesis committee for the useful suggestions on this project.

Figure 1

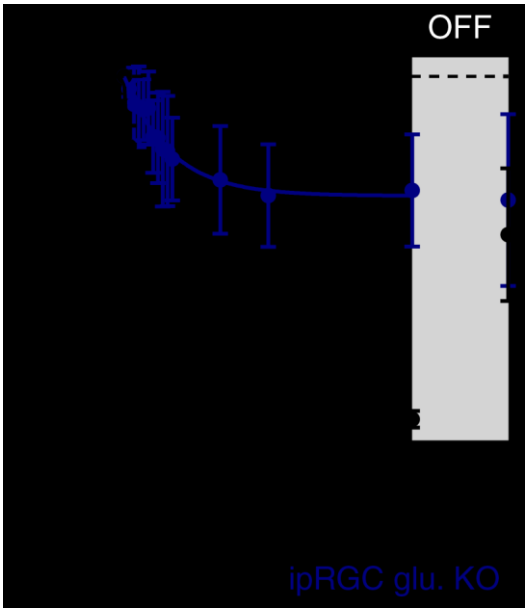

Figure 1: Glutamatergic signaling is required for rapid pupil dilation.

30 seconds of 1000 lux overhead light (6500K) followed by 10 seconds of darkness was performed on wildtype and ipRGC-glu. KO mice (Wildtype $n = 8$, ipRGC glu. KO: $Opn4^{Cre/+}; Slc17a6^{fl/fl}$ $n = 4$)(mean ± SD). The shaded region indicates darkness. Little change is observed in mutant mice after 10 seconds of darkness.

Figure 2

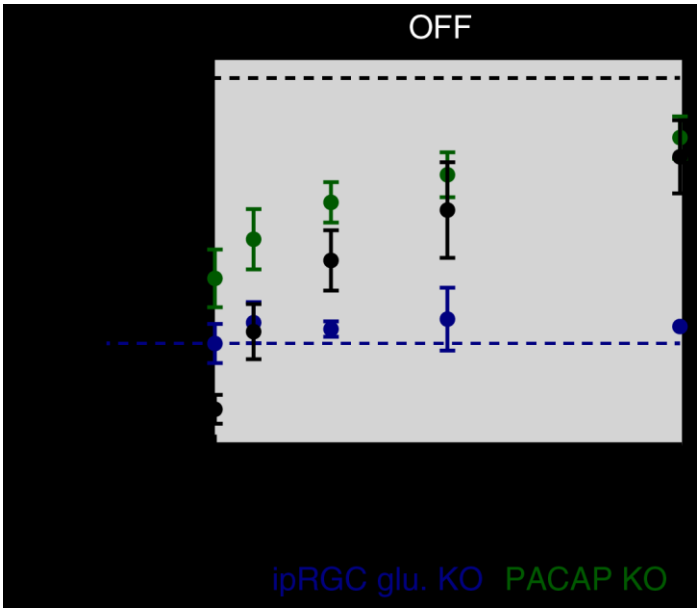

Figure 2: Dilation over longer timescales requires ipRGC glutamate.

60 minutes of 1000 lux overhead light (6500K) was followed by 60 seconds of darkness (Wildtype $n = 8$, ipRGC glu. KO: *Opn4*$^{Cre/+}$; *Slc17a6*$^{fl/fl}$ $n = 4$, ipRGC PACAP KO: *Adcyap1*$^{-/-}$ $n = 4$)(mean ± SD). The shaded region indicates darkness. Wildtype and PACAP KO mice dilate to near dark-adapted pupil size within the 60s of darkness. However, ipRGC glu.-KO mice display sustained constriction in the absence of light with no coherent dilation response.

Figure 3

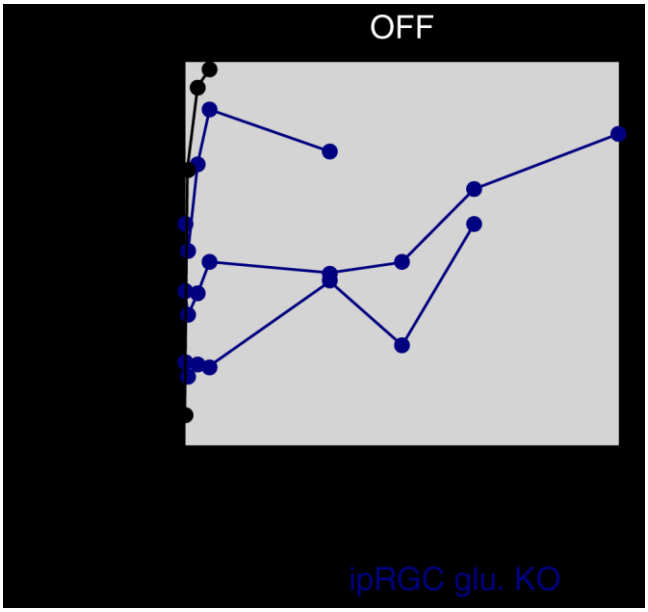

Figure 3: Long-term dilation is incoherent in the absence of glutamatergic signaling. 60 minutes of 1000 lux light (6500K) followed by 3 hours of darkness (Wildtype $n = 1$, ipRGC glu. KO: $Opn4^{Cre/+}$; $Slc17a6^{fl/fl}$ $n = 3$) (Traces show individual mice). The shaded region indicates darkness. Each data point is the result of 30 second observation of that mouse at that time. The minimum pupil size during that window was reported. Wildtype returned to pre-light pupil size within first 10 minutes of darkness. IpRGC glu. KO mice showed variable responses that were erratic during the 30 second observation windows. A trend toward dilation is observable in these mice over the course of the 3 hours of darkness, but no mice reached pre-light pupil size.

Chapter 4: Discovery and characterization of novel ipRGC neurotransmitters

This chapter is based on a manuscript in preparation:

William T Keenan, Michael Thomsen, and Samer Hattar. Discovery and Characterization of novel ipRGC neurotransmitters.

Abstract

Intrinsically photosensitive retinal ganglion cells (ipRGCs) coordinate a variety of physiological responses to light such as sleep/wake, pupil size, and mood. This small subset of retinal output neurons signal to the brain with two neurotransmitters: glutamate and PACAP. Both neurotransmitters support communicating distinct aspects of the light environment. Glutamate conveys rapid and robust responses to light dynamics while PACAP supports sustained changes over longer durations. In this chapter, we show that there is likely another neurotransmitter employed by ipRGCs and go on to characterize several candidate neurotransmitters and identify two new neuropeptides expressed by subsets of ipRGCs – Substance P (*Tac1*) and Somatostatin (*Sst*). Substance P expressing ipRGCs project to the OPN – the pupil control center of the brain making it a promising candidate for pupil regulation. Somatostatin is expressed in a small subset of ipRGCs which line the ventral periphery of the retina and may play a role in intraretinal modulation. Further work on both novel neurotransmitters is required to determine their functional role in the visual system.

Introduction

Since the initial discovery of ipRGCs, they have been thought to uniquely express two neurotransmitters: glutamate and PACAP[9,14,15]. Several studies since have shed light on the contributions of each neurotransmitter molecule to ipRGC-dependent function[42–44,46–50,92,94]. In Chapter 2, we showed that the primary difference between glutamate and PACAP is time. Glutamate is used to communicate rapid changes and fluctuations in light over milliseconds to seconds, and PACAP communicates long-term changes in the

light environment on the scale of minutes to hours. All of these studies, including our own, have been limited in their conclusions because the field has yet to demonstrate glutamate and PACAP to be the complete set of neurotransmitters used by ipRGCs.

In this study, we demonstrate the existence of novel ipRGC neurotransmission in the absence of glutamate and PACAP and begin its identification and characterization.

Results

Persistent PLR in the absence of glutamatergic and PACAPergic neurotransmission

To determine if glutamate and PACAP account for all ipRGC neurotransmission, we created a mouse lacking both – ipRGC glutamate/PACAP double knockouts (*Opn4*$^{Cre/+}$; *Vglut2*$^{fl/fl}$; *PACAP*$^{-/-}$)(See Chapter 2 for details on each allele). When we assayed rapid pupil constriction in these mice, we saw a response similar to that of the ipRGC glu. KO alone (**Figure 1**). As a negative control, we tested mice expressing Tetanus toxin in ipRGCs to silence all forms of neurotransmission indiscriminately (*Opn4Cre/+* ; TeNT)(Jax strain # 010713), and observed complete loss of pupil constriction (**Figure 1**). Together, these results suggest that glutamate and PACAP do not account for all ipRGC-elicited responses (**Figure 2**). We next endeavored to find and characterize this/these novel ipRGC neurotransmitter(s).

Several candidate ipRGC neurotransmitters have Cre lines available

A collection of works characterizing novel neurotransmitter expression in the retina[81,95–98] pointed us toward 20 candidate ipRGC transmitters (**Figure 3**). 10 of these have readily available Cre (Cck, Crh, Pdyn, Penk1, Oxt, Tac1, Sst, Avp, CART) or

transgenic reporter (NPY) lines making it simple to determine whether they label ipRGCs. To date, I have looked at Cck, Crh, Pdyn, NPY, Penk1, Tac1, Sst, and CART, but I will only cover those that are furthest along in this chapter. The approach consists of mating a neuropeptide Cre line to the Cre-dependent YFP reporter line (Jax #006148) and visualizing ipRGCs with Melanopsin antibody.

Neuropeptide Y (NPY)

NPY is a 36 amino acid peptide involved in regulation of stress, anxiety, food intake, circadian rhythms, cognition, and energy homeostasis[99]. In order to visualize cells expressing NPY in retina, I made use of a transgenic NPY reporter mouse line: tg(NPY-GFP)[100]. Observing a wholemount tg(NPY-GFP) retina revealed abundant populations of labeled cells in the ganglion cell layer (GCL) and the inner nuclear layer (INL)(**Figure 4A**). In order to differentiate ganglion cells from other cells types in the GCL, we stained reporter retinas with an RBPMS antibody (Millipore ABN1362) which labels all ganglion cells (**Figure 4B**). The vast majority NPY-positive cells were non-ganglion cells (RBPM-negative) and all strongly NPY-positive cells were non-ganglion cells. A small population of weakly reporting cells were RPBMS-positive. To test whether these ganglion cells are ipRGCs we stained tg(NPY-GFP) retinas for Melanopsin and observed no NPY-positive ipRGCs (**Figure 4C**). NPY does not appear to label any Melanopsin-antibody positive ipRGCs.

Tachykinin 1 (Tac1)

The *Tac1* locus produces 4 peptides – Substance P, NKA, NPK, and NPγ – but the locus is predominantly known for producing Substance P[101]. I made use of a Cre line

(*Tac1*$^{IRES\text{-}Cre}$)[102] available from Jax (#021877). *Tac1*^{Cre};YFP label a wide variety of cell types in the ganglion cell layer including glial cell types such as astrocytes and oligodendrocytes (identifiable by morphology)(**Figure 5A**). Both ganglion cells (RBPMS-positive) and non-ganglion cells are labeled in Tac1 reporter retina (**Figure 5A**). Of these Tac1-positive ganglion cells, some of them are also Melanopsin-antibody positive (**Figure 5B**).

YFP-positive cells are not necessarily expressing Cre in adulthood. Any cell which expressed Tac1 at any point in its life will be labeled with YFP in these lines. In order to determine whether Tac1-positive ipRGCs are expressing Tac1-Cre in adulthood as opposed to during development, I took advantage of a Cre-dependent reporter virus (AAV2-DIO-mCherry). Injecting this virus in adulthood allows for visualization of cells currently expressing Cre. Cre-dependent AAV injection reveals Tac1-positive ipRGCs actively expressing Cre (**Figure 5C**). These results reveal a novel neurotransmitter system in ipRGC: Substance P and the other Tac1 peptides. Further work will need to be done to determine the role of these peptide in ipRGC-dependent functions.

A first step toward understanding Tac1-positive ipRGCs is to determine where these cells project in the brain. For instance, if Tac1 peptides are responsible for the pupil constriction we observed in the absence of glutamate and PACAP then Tac1-ipRGCs should project to the OPN. The Cre-dependent AAV-mCherry also serves as a great way of visualizing the projections of Tac1-positive RGCs in the brain. Looking at projections, we observe strong labelling in the OPN, sparse labelling in the LGN, and little to no labeling in the SC and SCN (**Figure 6**). This provides further evidence for the possibility that Tac1 peptides are involved in PLR and may potentially be the source of our observed

residual pupil constriction. Irrespective of their role in the PLR, Tac1 labels a novel subset of ipRGCs and further characterization is critical to understanding the ipRGC system.

Somatostatin (SST)

Sst is a peptide commonly known to inhibit the release of downstream hormones and signals such as growth hormone and glucagon[103]. Sst has two critical mouse lines – a Cre knockin (Jax #013044) and a FLP knockin (Jax #028579). Sst-Cre;YFP retinas show sparse populations of cells in the GCL and INL (**Figure 7**). The majority of cells in the GCL are ganglion cells (**Figure 7A**), determined by expression of RBPMS. Additionally, a very small number of these cells are Melanopsin antibody positive ipRGCs (**Figure 7B**) revealing another novel ipRGC neurotransmitter and ipRGC subtype.

An interesting but unrelated observation in Sst-Cre;YFP retinas is the presence a small population of labeled horizontal cells (**Figure 8**). This is a particularly important observation because mice are thought to have only 1 type of horizontal cell[104]. Further investigation of these cells may reveal previously unappreciated diversity among horizontal cells.

The Sst-FLP mouse line gives us the opportunity to investigate somatostatin expressing ipRGCs with much higher sensitivity than allowed by Melanopsin antibody by coupling Sst-FLP, Melanopsin-Cre, and a dual-recombinase reporter line[105] (RC::FLTG – Jax #026932)(**Figure 9**). The RC::FLTG allele reports FLP-positive cells with tdTomato and FLP/Cre double positive cells with eGFP (**Figure 9A**). Using this system, we achieve genetic sensitivity as opposed to being limited by the sensitivity of the Melanopsin antibody. In the GCL of Sst-FLP;Opn4-Cre;RC::FLTG retinas we

observe a sparse population of FLP-only cells and an even sparser population of FLP/Cre cells (I will call these cells Sst-ipRGCs) (**Figure 9B**).

We next visualized Sst-ipRGCs within a whole retina to get an idea of their numbers and distribution (**Figure 10**). Roughly 100-150 Sst-ipRGCs populate each retina (only 1 is shown with 140 cells) which is an incredibly small subset of ipRGCs: about 3% of all ipRGCs. These Sst-ipRGCs display a clear dorsal-low to ventral-high gradient visualized by heatmap and a clear preference for the periphery of the retina (**Figure 10**). We performed the same analysis of FLP-only cells and see a similar dorsal-ventral gradient and edge preference albeit with many more cells (**Figure 11**). However, when we looked at the distribution of all ipRGCs using an Melanopsin-Cre;YFP retina, we saw no gradient or edge preference (**Figure 12**) indicating that these are features unique to Sst-ipRGCs and other Sst-RGCs. Given the small number of Sst-ipRGCs, it makes sense that you do not observe any gradient when looking at ipRGCs altogether. Significant further work is necessary to determine whether Sst-ipRGCs actively express Sst in adulthood and what functional role these cells play in the visual system

Discussion

These studies have begun an already fruitful process of characterizing the full neurotransmitter repertoire of ipRGCs. There are readily available Cre lines for promising neurotransmitter candidates Corticotropin Releasing Hormone (CRH), Cocaine and Amphetamine Responsive Transcipt (CART), Cholecystokinin (CCK), and Prodynorphin (Pdyn). Whether we will find 1, 2, or 10 more neurotransmitters employed by ipRGCs is still unclear.

Tac1 peptides are promising candidates for explaining the residual pupil constriction observed in the absence of glutamate and PACAP. However, in order to begin answering that question, we must begin characterizing mice lacking these Tac1 peptides, preferentially conditionally in ipRGCs. Unfortunately, no conditional Tac1 allele exists, but a nonconditional Tac1 knockout does (Jax #004103). Assaying PLR in these mice and in combination with glutamate and PACAP perturbations is the critical next step in understanding a potential active role for Tac1 peptides in the ipRGC system. This work is ongoing.

The potential function of Sst-ipRGCs is less clear. Determining whether Sst expression remains in adulthood and to where in the brain these cells project will be critical in uncovering function. In the work that sparked my interest in somatostatin[96], Sagar and Marshall find Sst-positive ganglion cells in human retinae and propose that these cells may equalize signal intensity along the dorsal-ventral axis. The upper portion of the visual field is often much brighter than the lower portion resulting in the ventral retina receiving higher intensity light than the dorsal retina. These cells could broadly dampen signals in the ventral retina to compensate for that fact. Melanopsin would provide this system with the ability to stably encode light intensity making this explanation particularly appealing.

Another important question to consider with Sst-ipRGCs is whether these cells are a result of sparse Sst expression in all RGCs and ipRGCs just so happen to be included. Any future study of Sst-ipRGCs will need to also investigate the function of other Sst-RGCs to see if there is any functional difference between them. If Melanopsin

plays no role in the system then it would suggest that Sst-RGC is the functional subtype and Sst-ipRGCs are simply a result of the Sst gradient expression program.

I have only investigated 4 of the 20 ipRGC neurotransmitter candidates (**Figure 3**). 2 showed either no expression in the retina generally or in ipRGCs specifically while 2 others clearly label subsets of ipRGCs. Reporter lines, preferably Cre knockin, are critical tool in this candidate approach. 6 more of the neurotransmitter candidates have existing and readily available Cre lines, but 10 have none. Given the relative ease of allele creation with CRISPR/Cas9, it may prove fruitful to create these remaining lines and characterize their expression. Even if no ipRGCs are found to express these neuropeptides, we are likely to uncover novel non-ipRGC retinal cell subtypes.

Methods

Animal husbandry

C57Bl/6 × Sv129 hybrid mice were used in all experiments except PACAP KO mice which were C57Bl/6. All mice were housed according to guidelines from the Animal Care and Use Committee of Johns Hopkins University. Male and female mice age 4-8 months were housed in plastic translucent cages with steel-lined lids in an open room. Ambient room temperature and humidity were monitored daily and tightly controlled. Food and water were available *ad libitum.* All mice were maintained in a 12hr:12hr light-dark cycle with light intensity around 100 lux for the entirety of their lives. Cre, FLP, and Cre/FLP reporter lines were obtained from Jackson Labs.

Pupillometry

All mice were dark-adapted for at least 60 minutes prior to any experiments and all PLR experiments were performed between Zeitgeber times (ZT) 2 and 10. For all

experiments, mice were unanesthetized and restrained by hand. Because stress can affect pupil size, we ensured that the mice were not stressed during these experiments. To do so, we handled the mice for several days prior to the experiments to get them accustomed to the researchers and to being scruffed. Any mice that showed signs of stress, including vocalizations and wriggling during the experiments, were not used and were subjected to more handling sessions before use in experiments.

Mice were restrained manually under a 23-Watt compact fluorescent light bulb (GE Daylight FLE10HT3/2/D or Sylvania Daylight CF13EL and CF23EL) with a color temperature of 6500 K to simulate natural sunlight. The light intensity was measured using a light meter (EXTECH Foot Candle/Lux Light Meter, 401025) at the surface on which the mouse was held. The light meter was initially calibrated by EXTECH using a Tungsten 2856 K light source; because our experiments used a fluorescent bulb of 6500 K, all measured light intensities reported here may vary by 0.92–1.12 times the actual light intensity.

Videos of the eye were taken using a Sony Handycam (DCR-HC96) mounted on a tripod a fixed distance from the mouse. Manual focus was maintained on the camera to ensure that only one focal plane existed for each mouse and that therefore variable distance from the camera should not contribute to differences in relative pupil area throughout the video. Pupil size was first recorded under dim red light and the endogenous infrared light source of the camera to capture the dark-adapted pupil size. Following at least 5 seconds of recording in dark, the pupil was continuously recorded for at least 30 seconds of a light step stimulus.

Videos were transferred from the camera to a computer as Audio Video Interleave (AVI) files and individual frames were taken using VLC media player (www.videolan.org/vlc/) and saved in portable network graphics format (PNG). Images were taken in the dark, at 5 seconds, and 30 seconds following stimulus onset. Pupil area was then quantified manually in ImageJ (http://rsbweb.nih.gov/ij/) software. The pupil area was measured in pixels using the oval tool in which the 4 cardinal points of the oval were touching their respective edges of the pupil. The relative pupil area was calculated using LibreOffice Calc or Microsoft Excel in which the area during the light stimulus was divided by the area prior to lights onset. For the transient PLR, the minimum relative pupil size after stimulus was used for all genotypes.

Viral infection

Mice were anesthetized by intraperitoneal injection of avertin (2, 2, 2-Tribromoethanol) and placed under a stereo microscope. 1 µl of AAV2-hSyn-DIO-hM3DG_q-mCherry (4.6×10^{12} viral particles/ml, Roth lab, UNC Vector Core) was placed on a piece of Parafilm and drawn into a 10-µl microcapillary tube (Sigma P0674) that had been pulled to a needle (Sutter Instruments, Model P-2000). The loaded needle was then placed in the holster of a pico-injector (Harvard Apparatus PLI-90). The needle punctured the eye posterior to the ora serrata and air pressure was used to drive the viral solution into the vitreous chamber of the eye to ensure delivery specifically to the retina. Mice recovered from surgery on a heating pad until they woke from anesthesia. All confocal imaging were done at least 3 weeks following viral injection.

Immunofluorescence and confocal microscopy

Mice were anesthetized with avertin and then euthanized using cervical dislocation. The eyes were removed and the retinas were dissected in PBS and then fixed in 4% paraformaldehyde for 1–2 hours on ice. When brain sections were necessary, mice were perfused. The retinas were then washed in PBS at least three times before mounting on a microscope slide (Fisher) in Fluoromount (Sigma). Some retinas were co-stained for melanopsin or RBPMS using rabbit anti-OPN4 (Advanced Targeting Systems, AB-N38, 1:1000) or rabbit anti-RBPMS (Millipore ABN1362) in 4% goat serum with secondary antibody Alexa Fluor 594 goat anti-rabbit (Life Technologies A11008, 1:1000). YFP signal in reporter retinas was boosted by immunostaining with chicken anti-GFP (abcam ab13970) followed by secondary Alexa Fluor 488 goat anti-chicken. Images were taken on a Zeiss LSM 710 confocal microscope using a 20X or 63X objective. For imaging of whole retinas for determining cell distributions, tilescans were performed followed by stitching with Zeiss Zen Blue software.

Retinal distribution

Cell positions were determined by a custom MATLAB script. Results of this process were cross-checked by hand to avoid gross errors. Cell distribution along the dorsal-ventral and nasal-temporal axes was again determined via custom MATLAB script and output as a heatmap (**see Figure 10, 11, 12**).

Acknowledgements

I would like to thank the entire mouse tri-lab for feedback over the course of many lab meetings. I would also like to thank my thesis committee for the useful suggestions on this project.

Figure 1

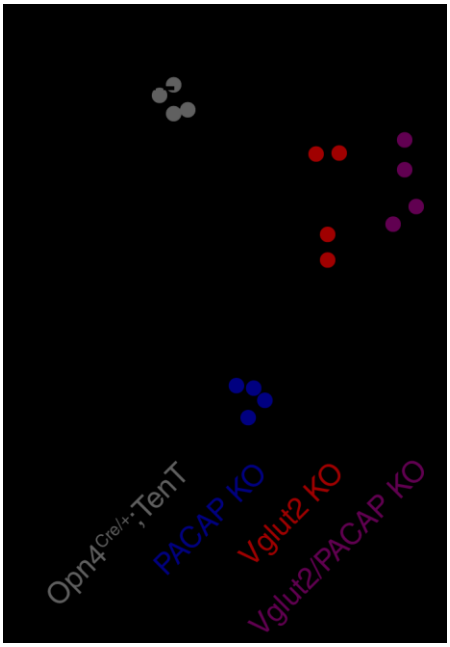

Figure 1: PLR persists in the absence of glutamate and PACAP.

Transient pupil constriction in response to high white light (1000 lux, 6500K).Y-axis is relative pupil area (pupil size in light/pupil size before light). Individual points represent separate mice and bars are the mean. *Opn4*^{Cre};*TeNT* mice possess silenced ipRGCs lacking all neurotransmission and showed no pupil constriction in response to light. PACAP KO (*Adcyap1*$^{-/-}$) and ipRGC glu.-KO (Vglut2 KO) mice display PLR thoroughly described in Chapter 2. ipRGC glutamate/PACAP double KO (*Opn4*^{Cre};*Vglut2*$^{fl/fl}$;*Adcyap1*$^{-/-}$) responses were similar to ipRGC glu. KO (P=0.95), but significantly better than mice with completely silenced ipRGCs (*Opn4*^{Cre};*TeNT*) (P=0.008).

Figure 2

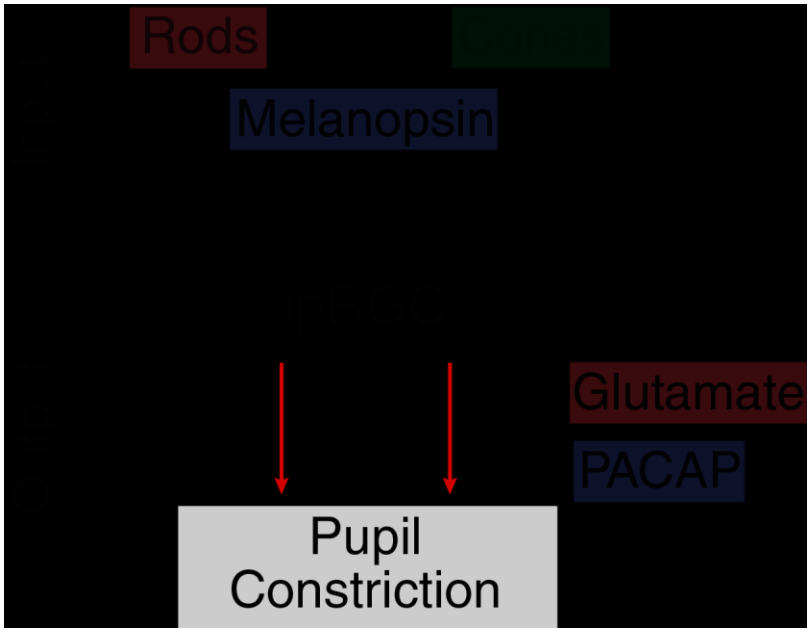

Figure 2: Schematic of inputs and outputs of the ipRGC system.

IpRGCs receive input from 3 photosensors: rods, cones, and Melanopsin (See Chapter 2 for detailed characterization of their individual contributions). Given the remaining responses in mice lacking the 2 known ipRGC outputs, glutamate and PACAP, there must be some novel signaling mechanisms.

Figure 3

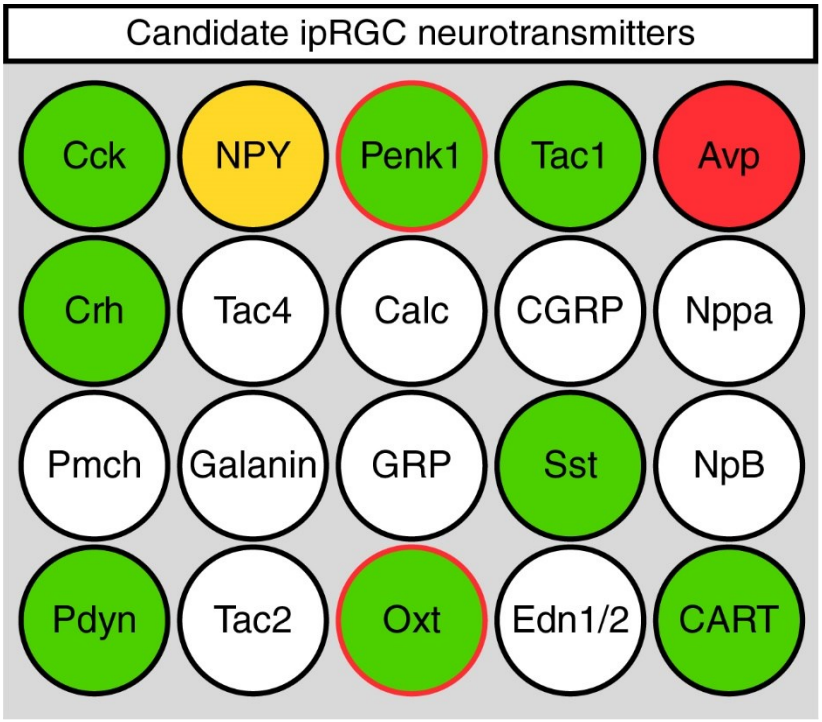

Figure 3: Candidate ipRGC neurotransmitters.

Diagram of potential novel ipRGC neurotransmitters. Twenty neurotransmitters have sufficient evidence to warrant further investigation. Of these, 9 have readily available Cre-knockin lines (Green) or transgenic reporter lines (Yellow). An Avp Cre line (Red) was briefly investigated but no signal was seen in the retina (data not shown). Of the 9 lines obtained, 2 did not produce reporter offspring (red outline: Penk1 and Oxt) and require further mating. The white peptides require the creation of new genetic tools.

Figure 4

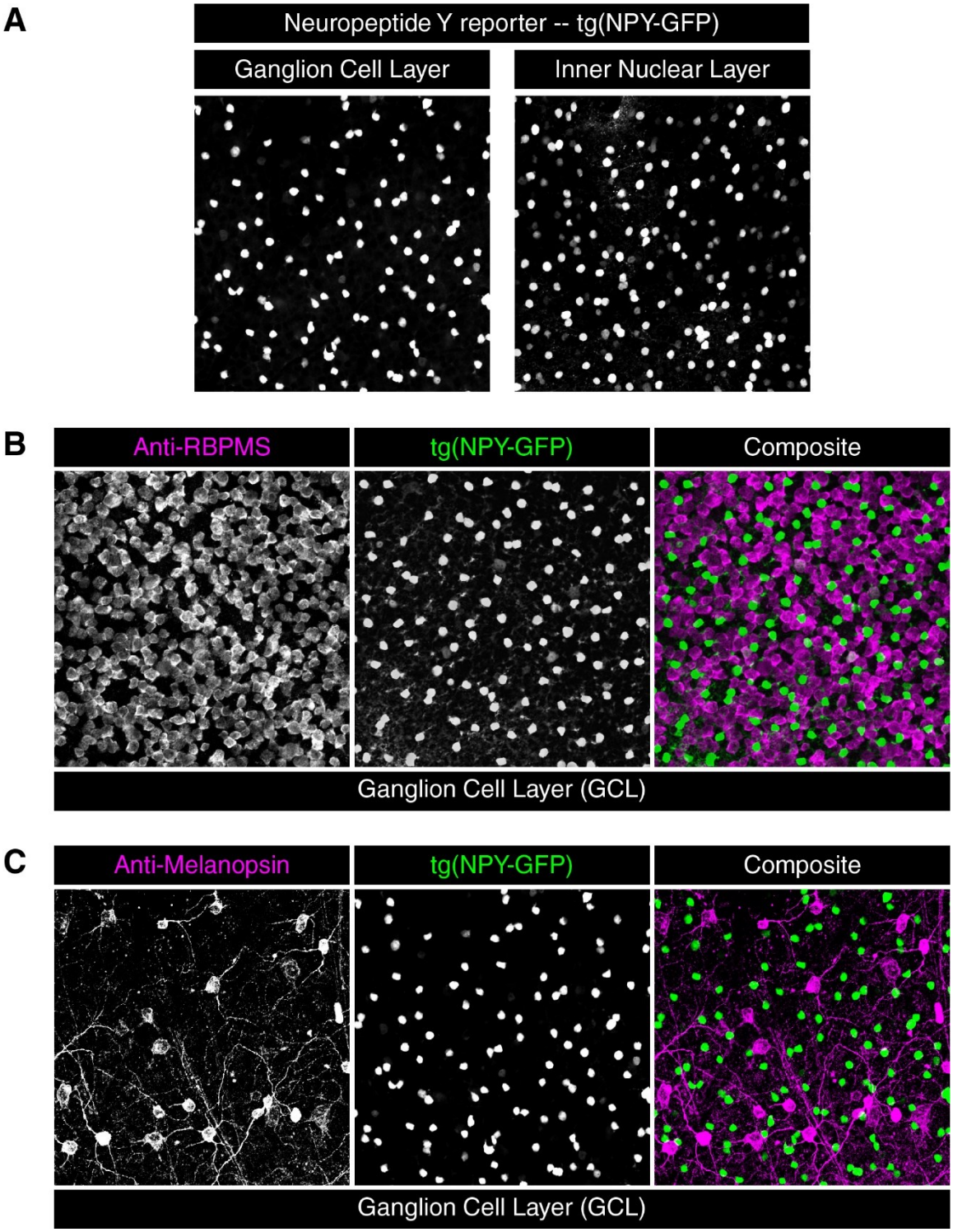
A
Neuropeptide Y reporter -- tg(NPY-GFP)
Ganglion Cell Layer
Inner Nuclear Layer
B
Anti-RBPMS
tg(NPY-GFP)
Composite
Ganglion Cell Layer (GCL)
C
Anti-Melanopsin
tg(NPY-GFP)
Composite
Ganglion Cell Layer (GCL)

Figure 4: Neuropeptide Y does not label Melanopsin antibody positive cells.

Antibody staining in NPY reporter (transgenic NPY-GFP) wholemount retina. (**A**) NPY reporter expression in the GCL and INL. Sparse cell populations in both layers. (**B**) RBPMS (labels all ganglion cells) antibody staining in a wholemount NPY reporter retina (GCL). The vast majority of NPY reporter positive cells in the GCL are not RPMS positive although a small number of weakly positive cells can be observed. (**C**) Melanopsin antibody staining in a wholemount NPY reporter retina (GCL). No colocalization was observed. (Magenta – antibody)(Green – NPY-GFP with anti-GFP antibody)

Figure 5

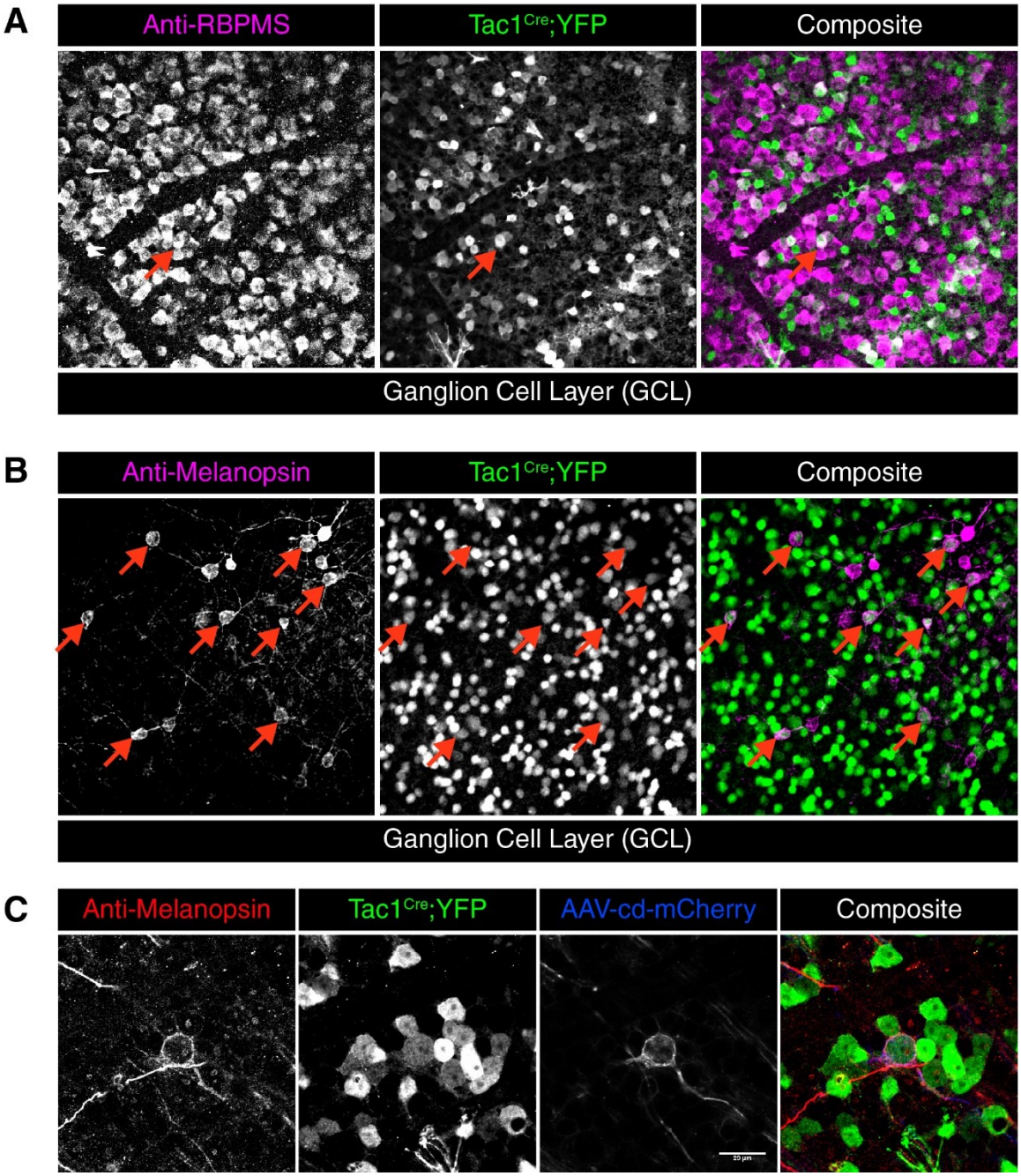
A
Anti-RBPMS
Tac1Cre;YFP
Composite
Ganglion Cell Layer (GCL)
B
Anti-Melanopsin
Tac1Cre;YFP
Composite
Ganglion Cell Layer (GCL)
C
Anti-Melanopsin
Tac1Cre;YFP
AAV-cd-mCherry
Composite

Figure 5: Tachykinin 1 reporter mice label ipRGCs and expression persists to adulthood.

Antibody staining in Tac1 reporter ($Tac1^{IRES\text{-}Cre}$) wholemount retina. (**A**) Tac1 reporter expression in the GCL and colocalization with ganglion cell marker RBPMS. Cells of nearly all types are labeled sparsely including ganglion cells. The arrow indicates a Tac1-positive RGC. (**B**) Melanopsin antibody staining in a wholemount Tac1 reporter retina (GCL). Several Melanopsin-positive cells are Tac1-positive (red arrows). (**C**) Tac1-positive ipRGCs maintain Cre expression into adulthood. High magnification image of Tac1-positive ipRGC infected with AAV2-DIO-DREADD-mCherry. (Blue – mCherry from AAV)(Magenta – antibody)(Green – $Tac1^{Cre}$;YFP with anti-GFP antibody)

Figure 6

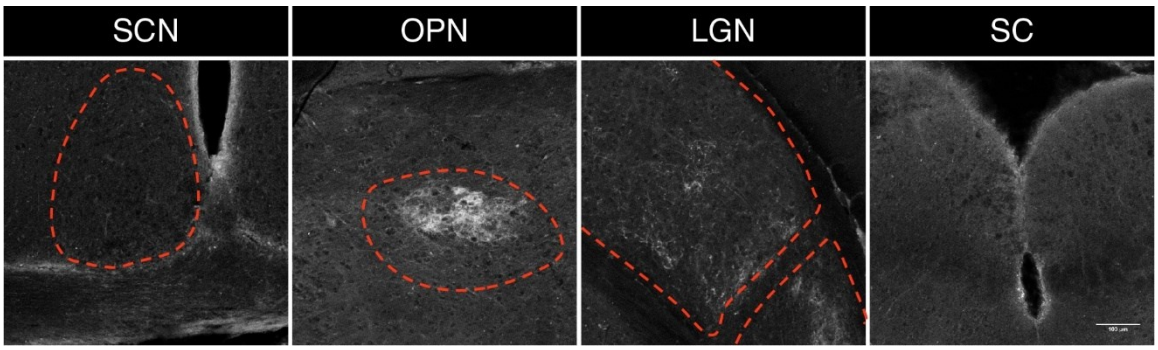

Figure 6: Tac1-positive ipRGCs project to the olivary pretectal nucleus (OPN). Tac1-positive ipRGC tracing using the mCherry signal from AAV2-DIO-DREADD-mCherry. The suprachiasmatic nucleus (SCN) and superior colliculus (SC) had no obvious innervation. The lateral geniculate nucleus (LGN) had sparse innervation and the olivary pretectal nucleus (OPN) had strong innervation. Images are in grayscale – white = mCherry.

Figure 7

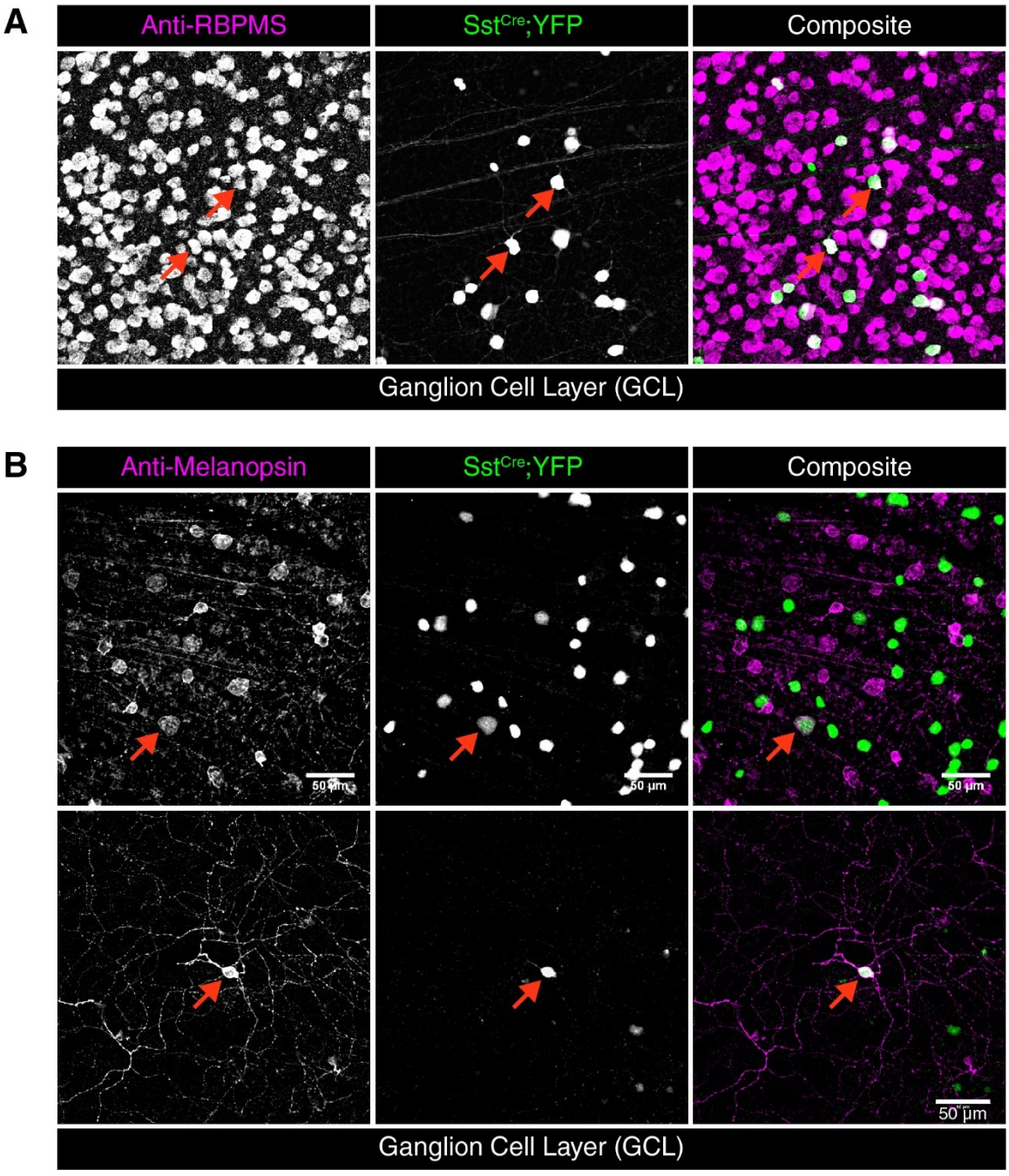
A
Anti-RBPMS
Sst^Cre;YFP
Composite
Ganglion Cell Layer (GCL)
B
Anti-Melanopsin
Sst^Cre;YFP
Composite
50 µm
Ganglion Cell Layer (GCL)

Figure 7: Somatostatin Cre reporter mice label a subset of ipRGCs.

Antibody staining in Sst reporter ($Sst^{IRES\text{-}Cre}$) wholemount retina. (**A**) Sst reporter expression in the GCL and colocalization with ganglion cell marker RBPMS. The vast majority of Sst-reporter positive cells are ganglion cells in the GCL. The arrows indicate example Sst-positive RGC. (**B**) Melanopsin antibody staining in a wholemount Sst reporter retina (GCL). (top) Rare Sst-positive ipRGCs are present (red arrow). (bottom) Another example of a Sst-positive ipRGC. (Magenta – antibody)(Green – Sst^{Cre};YFP with anti-GFP antibody)

Figure 8

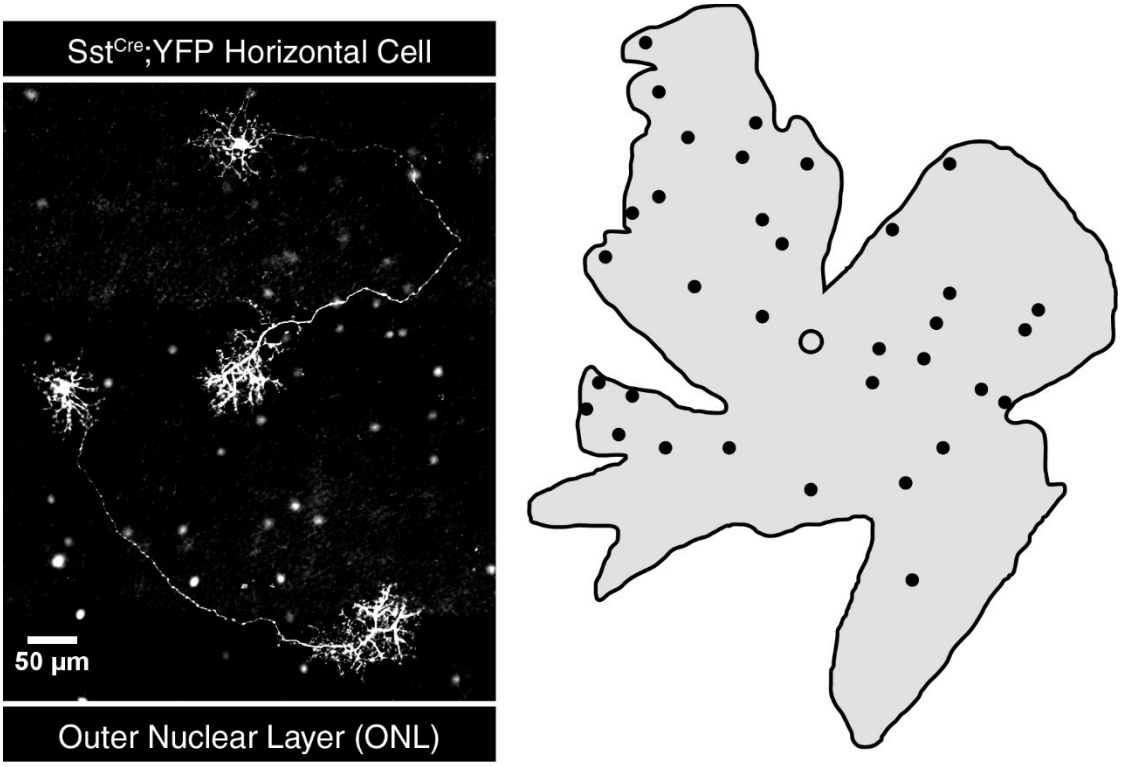

Figure 8: A small subset of horizontal cells are labeled by Somatostatin Cre.

34 labeled horizontal cells in the retina counted. (left) 2 labeled Sst-positive horizontal cells in wholemount retina. (right) Distribution of cells in a single retina.

Figure 9

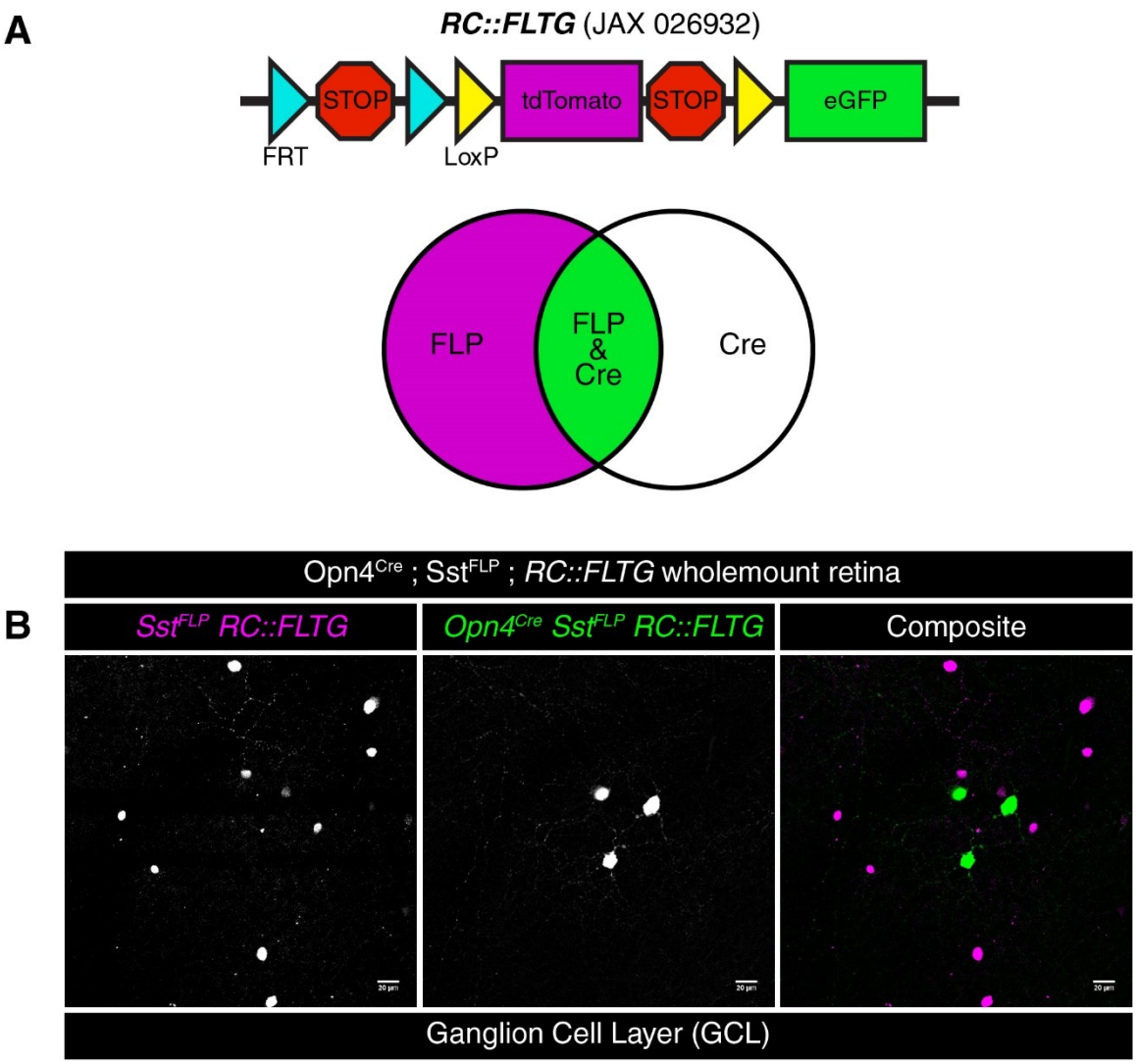

Figure 9: Intersectional approach to label Sst-ipRGCs.

(**A**) The *RC::FLTG* mouse line allows for intersectional labelling of cell subtypes using Cre and FLP systems. (top) Genetic schematic of *RC::FLTG* allele. FLP mediates excision of the FRT-flanked STOP allowing for tdTomato expression. Cre mediates excision of LoxP-flanked tdTomato-STOP. Cre and FLP lead to eGFP expression.

(bottom) Graphical description of reporter outcomes. (**B**) *Opn4^{Cre};Sst^{FLP};RC::FLTG* mice label Sst-FLP only cells (magenta) and Sst-FLP/Opn4-Cre double positive Sst-ipRGCs (green). As expected, there is no overlap between FLP-only and FLP/Cre labeled cells.

Figure 10

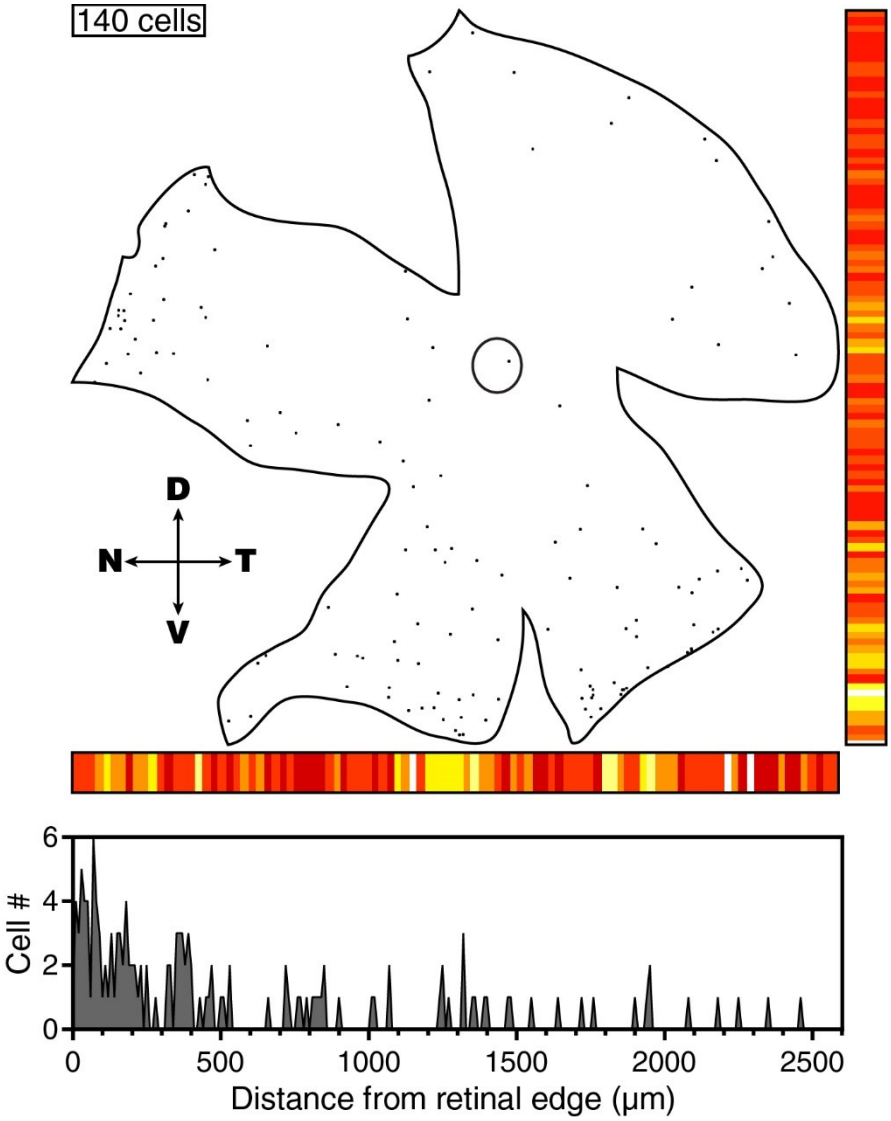

Figure 10: Sst-ipRGCs inhabit the ventral retinal edges.

Heatmap shows distribution of Sst-ipRGCs (FLP/Cre double positive) along dorsal-ventral (right) and nasal-temporal (bottom) axes. Yellow/white indicates more cells – red indicates less. For each cell, the distance to the retinal edge was calculated in microns. Sst-ipRGCs cluster close to the retinal edge.

Figure 11

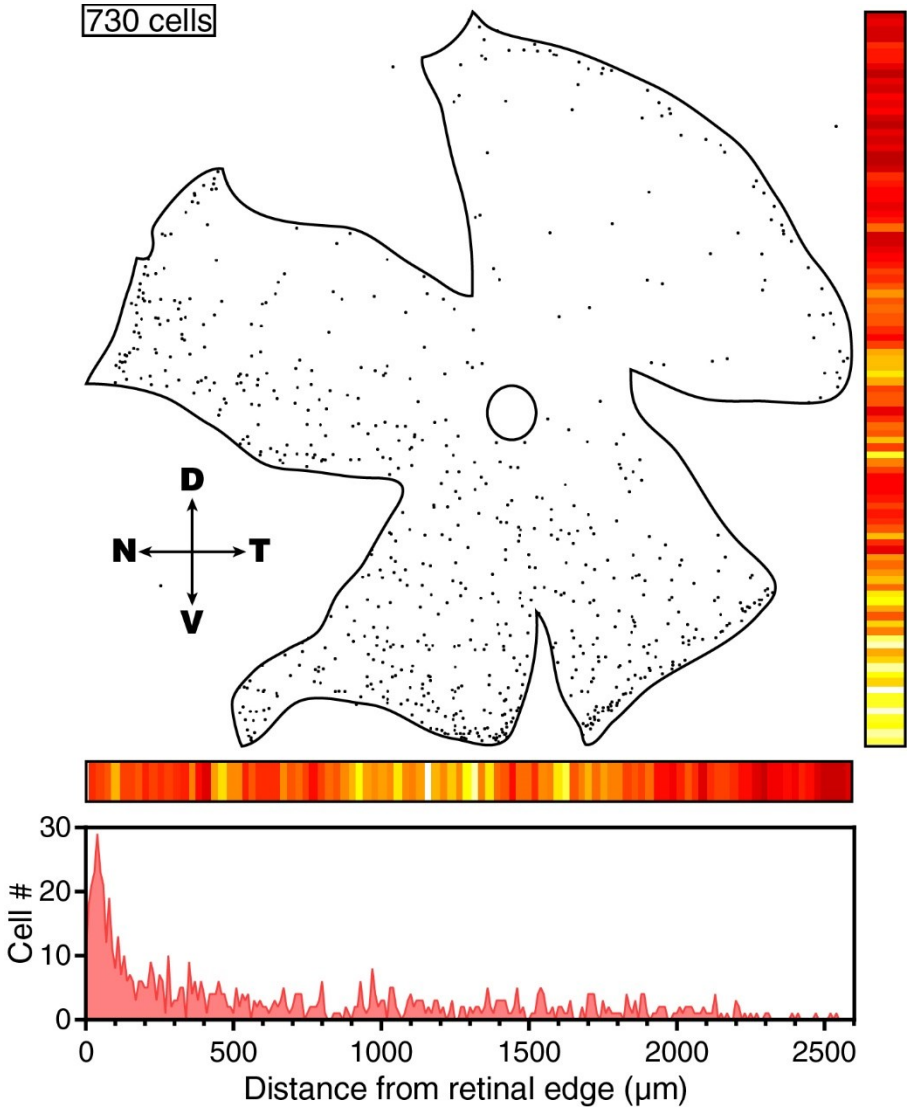

Figure 11: All Sst-positive non-ipRGCs also cluster at the edge of the ventral retina. Heatmap shows distribution of Sst-positive cells (FLP positive ONLY) along dorsal-ventral (right) and nasal-temporal (bottom) axes. Yellow/white indicates more cells – red indicates less. For each cell, the distance to the retinal edge was calculated in microns. These cells cluster at the retinal edge.

Figure 12

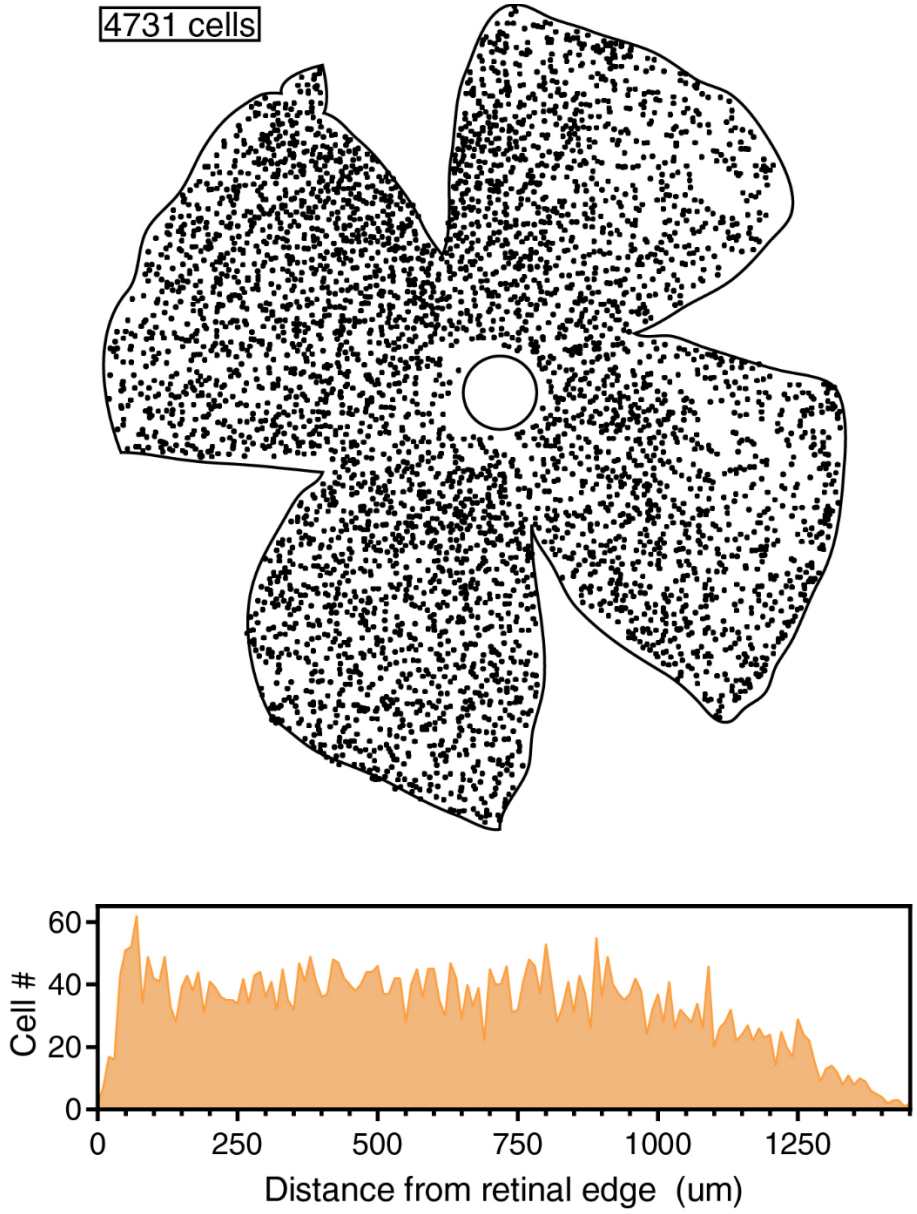

Figure 12: Total ipRGC population inhabit the whole retina with little to no preference for the retinal edge.

Heatmap shows distribution of ipRGCs (*Opn4*^{Cre} ; YFP+ cells) along dorsal-ventral (right) and nasal-temporal (bottom) axes. For each cell, the distance to the retinal edge was calculated in microns.

Chapter 6: Method—Eye-drops for activation of DREADDs

This chapter is based on a manuscript *in review*:

William T Keenan*, Diego C Fernandez, Lukas J Shumway, Haiqing Zhao, and Samer Hattar. Eye-drops for activation of DREADDs. *Frontiers in Neuroscience*

*Corresponding author

Abstract

Designer Receptors Exclusively Activated by Designer Drugs (DREADD) are an important tool for modulating and understanding neural circuits. DREADD-targeted neurons can be activated or repressed, depending on the DREADD type, *in vivo* following a dose of the DREADD agonist clozapine-n-oxide (CNO). Because DREADD experiments often involve behavioral assays, the method of CNO delivery is important. Currently, the most common delivery method is intraperitoneal (IP) injection. IP injection is both a fast and reliable technique, but it is painful and potentially stressful particularly when many injections are required. We sought an alternative CNO delivery paradigm, which would retain the speed and reliability of IP injections without being as invasive, painful or stressful. Here we show that CNO can be effectively delivered topically via eye-drops. Eye-drops robustly activated DREADD-expressing neurons in the brain and peripheral tissues and does so at the same dosages as IP injection. Eye-drops provide an easier, less invasive and less stressful method for activating DREADDs *in vivo*.

Introduction

Scientists have developed a variety of methods to modulate targeted neuronal subpopulation *in vivo* to understand the neuronal circuits underlying behavior. Two such methods have become commonplace in modern neuroscience: chemogenetics and optogenetics. Both techniques rely on engineered proteins responsive to either chemical agonists in the case of chemogenetics or photons in the case of optogenetics.

A variety of chemogenetic tools have been developed over the past two decades, and have been recently reviewed [106,107]. However, a class named Designer Receptors

Exclusively Activated by Designer Drugs or DREADDs have emerged as the primary chemogenetic tool for modulation of specific cell types[70]. The principal DREADDs used today are the activity enhancing G_q-coupled hM3Dq receptor and the G_i-coupled $hM4D_i$ receptor (G_q-DREADD and G_i-DREADD)[70]. DREADDs can be introduced virally or using an expanding collection of transgenic mice[108–112]. Both engineered receptors are activated by the chemical clozapine-n-oxide (CNO), and are being used to robustly modulate a variety of neuronal populations *in vivo* [94,113–116]. Additional CNO-responsive receptors have been engineered to activate G_s signaling[112], arrestin signaling[117], and axon specific G_i signaling[118].

The primary advantage of the DREADD approach is that it can be used in live behaving animals without any need for complex equipment—optogenetics, for instance, requires delivering intense light to a particular brain reqion which often involves surgical implantation of an optical fiber. For *in vivo* studies using DREADDs, activation only requires delivery of CNO to the subject's blood, which will eventually reach target neurons. While CNO is typically administered by IP injection, it has also been delivered in drinking water[119] and by implanted minipumps[120]. IP injection provides fine control over exact dosage and dose timing while drinking water and minipump approaches allow for chronic dosage without constant handling. However, each delivery method has disadvantages—IP injection causes both stress and pain which are undesirable when investigating animal behavior, particularly when studying aspects of behavior directly impacted by stress and pain. CNO in drinking water alleviates the confound of stress/pain but you lose control over precise dosage and dose timing. Additionally, increased costs associated with the large quantities of CNO required for dosing drinking water is also a

limitation. The implanted minipump approach retains dosage control and allows for chronic administration, however this is achieved at the cost of requiring surgery and specialized equipment.

We endeavored to find and characterize a novel method of CNO delivery which alleviates some of the difficulties of currently used techniques. An often-used method of self-administration in humans is topical administration by eye-drops and subsequent absorption into the blood. Eye-drops are a non-invasive painless way of achieving precise dosage as well as dose timing. Eye-drop drug delivery has the added benefits of being exceptionally easy to perform as well as not requiring any additional equipment such as syringes.

In this study, we first confirmed the capability of CNO eye-drops to activate DREADD-expressing neurons in the brain. Next, to investigate the feasibility of eye-drop CNO delivery *in vivo*, we utilized a subpopulation of retinal ganglion cells, intrinsically photosensitive retinal ganglion cells (ipRGCs), which drive robust and quantifiable pupil constriction when activated by light[12,13,121] or DREADDs[94,122]. *In this study, we report that CNO can be delivered by eye-drop to activate DREADDs in vivo.* Additionally, we have determined the dose-response relationship and relative bioavailability of CNO delivered via eye-drop and IP injection.

Materials and Methods

Animal husbandry

C57Bl/6 × Sv129 hybrid mice were used in all experiments. All mice were housed according to guidelines from the Animal Care and Use Committee of Johns

Hopkins University. Male and female mice age 2–8 months were housed in plastic translucent cages with steel-lined lids in an open room. Ambient room temperature and humidity were monitored daily and tightly controlled. Food and water were available *ad libitum*. All mice were maintained in a 12hr:12hr light-dark cycle with light intensity around 100 lux for the entirety of their lives.

Drug preparation

Clozapine-n-oxide (CNO, Sigma-Aldrich SKU:C0832-5MG) was dissolved in sterile 0.9% saline solution. CNO/saline solution was then diluted to achieve the dosage (mg/kg) per mouse required for the experiment.

CNO delivery

CNO was delivered either by eye-drop or intraperitoneal injection (IP). For eye-drops, CNO was diluted based on mouse weight to achieve the correct dose within a 1-2 microliter dose. 1-2 µl was then loaded into P10 micropipette followed by immobilizing the mouse via scruff. The 1-2 µl range was chosen because it is large enough to be accurately pipetted and small enough to not drip off of the eye after application. The solution in the pipette was then expelled slowly so that a stable droplet forms on the pipette tip. The droplet was then carefully touched to the cornea of the mouse eye and the mouse was released. The pipette tip never comes into contact with the mouse's eye.

Pupillometry

All mice were dark-adapted for at least 30 minutes prior to CNO delivery and subsequent pupil measurements. For all experiments, mice were unanesthetized and restrained by hand. Videos of the eye were taken using a Sony Handycam (FDR-AX33) mounted on a tripod a fixed distance from the mouse. Manual focus was maintained on the camera to ensure that only one focal plane existed for each mouse and that therefore variable distance from the camera should not contribute to differences in relative pupil area throughout the video. Pupil size was first recorded under dim red light and the endogenous infrared light source of the camera to capture the dark-adapted baseline pupil size. CNO was then delivered as an eye-drop or injection and the mouse was returned to their cage. Pupil size was monitored at intervals described in the results section. All pupil images presented in the paper were cropped to a fixed square area surrounding the eye using GNU Image Manipulation Program (GIMP). The images were made grayscale and then brightness and contrast were adjusted to enhance visibility of the pupil and exported as PNG files.

Data analysis

Videos were transferred from the camera to a computer as Audio Video Interleave (AVI) files and individual frames were taken using VLC media player (www.videolan.org/vlc/) and saved in portable network graphics format (PNG). Images were taken in the dark. Pupil area was then quantified manually in ImageJ (http://rsbweb.nih.gov/ij/) software. The pupil area was measured in pixels using the oval tool in which the 4 cardinal points of the oval were touching their respective edges of the

pupil. The relative pupil area was calculated using Microsoft Excel in which the area during the stimulus was divided by the area prior to CNO dosage.

The dose-response curve was fit using a variable slope sigmoidal dose-response curve in Graphpad Prism 6. The top and bottom of the fit were constrained to 1.0 and between 0 and 0.10, respectively.

Viral infection

For viral infection of the retina, *Opn4*^{Cre} [88] and littermate control mice were anesthetized by IP injection of avertin (2, 2, 2-Tribromoethanol) and placed under a stereo microscope. 1 µl of adeno-associated virus (AAV)2-hSyn-DIO-hM3DG_q-mCherry (4.6×10^{12} viral particles/ml, Roth lab, UNC Vector Core) was placed on a piece of Parafilm and drawn into a 10-µl microcapillary tube (Sigma P0674) that had been pulled to a needle (Sutter Instruments, Model P-2000). The loaded needle was then placed in the holster of a pico-injector (Harvard Apparatus PLI-90). The needle punctured the eye posterior to the ora serrata and air pressure was used to drive the viral solution into the vitreous chamber of the eye to ensure delivery specifically to the retina. Mice recovered from surgery on a heating pad until they woke from anesthesia. All experiments were performed 3-5 weeks following viral injection.

For viral infection of the brain, mice were deeply anesthetized by IP injection of avertin, and rAAV5-hSyn-hM3D(G_q)-mCherry (3.4×10^{12} viral particles/ml, Roth lab, UNC Vector Core) was stereotaxically delivered. All coordinates used follow the Paxinos and Franklin atlas [123]. A 10-µl microcapillary pipette was pulled and loaded with the AAV solution. A total volume of ~100 nl of AAV was injected using a microinjector

(Nanojector II, Drummond Scientific Company). A heating pad was used to maintain the body temperature at ~35◦C. Before and after the surgery, systemic analgetics (buprenorphine, 0.1 mg/kg) were administrated.

Immunofluorescence and confocal microscopy

Four weeks after brain injections, cFos induction (in AAV-infected neurons) was immunohistochemically evaluated in mice that were perfused 2 hours after application of an eye-drop of CNO (~0.5 mg/kg dose); mice were kept in constant darkness during the experiment. After perfusion, brains were post-fixed overnight, and subsequently sectioned on a cryostat (coronal sections, 40 μm). Brain sections were blocked for 2 hours in PBS containing 0.3% Triton X-100 and 3% heat-inactivated goat serum and then incubated using a mouse IgG1 α-cFos (EnCor MCA-2H2; 1:500) and a rabbit IgG α-RFP (red fluorescent protein, MBL PM005; 1:1000) overnight, at 4°C. The following secondary antibodies were used (1:200; Molecular Probes): goat anti-rabbit Alexa 546; and goat anti-mouse IgG1 Alexa 488. Finally, slides were mounted in AntiFade medium (Molecular Probes). Images were acquired using a LSM-700 confocal microscope (Zeiss). For all morphometric image processing, digitized captured TIF-images were assembled and processed with Zeiss Zen software and Adobe Photoshop (Adobe Systems).

Statistical analysis

All statistical tests were performed in Graphpad Prism 6. Specific statistical comparisons are listed in the figure captions. Because the EC50 data appears to be a

normal distribution on a log scale (log-normal distribution), all statistical tests and data analysis involving EC50 were performed on the log transformed data set.

Results

Eye-drop CNO activates DREADDs in the brain

We first sought to confirm that CNO eye-drops effectively activate DREADDs in the brain. To do so, we injected a G_q-DREADD-containing virus (AAV5-hSyn-hM3D(G_q)-mCherry) into a well-studied nucleus of the thalamus, the paraventricular nucleus (PVT) (**Figure 1A**). Four weeks following viral injection, we applied an eye-drop of CNO (~0.5 mg/kg) and evaluated neuronal activation 2 hours afterward by assaying the expression of the immediate early-gene cFos. Using the DREADD-mCherry fusion protein to identify virally infected cells, we observed robust cFos staining in neurons expressing the DREADD-mCherry reporter, indicating that the CNO eye-drop had successfully activated G_q-DREADD in those cells (**Figure 1B-D**, another example at higher magnification-**Figure 1E-G**). No cFos activation was observed when cells were infected with a virus expressing mCherry alone (data not shown). This result confirms the ability of CNO delivered by eye-drop to enter the blood and activate DREADDs in the brain. However, this approach does not allow us to quantitatively compare the effectiveness of eye-drops to IP injection *in vivo*.

Eye-drop delivery of CNO activates DREADDs in vivo

To visualize and quantify DREADD activity *in vivo*, we utilized a genetically defined subpopulation of melanopsin expressing retinal ganglion cells, intrinsically

photosensitive retinal ganglion cells ipRGCs (ipRGCs), which we and others have shown to drive pupil constriction when activated by G_q-DREADD[94,122]. This system gives us a readily observable and easily quantifiable output of DREADD activation *in vivo*. The *Opn4*^{Cre} (*Opn4* → Melanopsin) mouse[88] gives us genetic access to these cells and a Cre-dependent G_q-DREADD adeno-associated virus (AAV) allows us to specifically express G_q-DREADD in ipRGCs.

We first injected an AAV carrying a Cre-dependent G_q-DREADD construct (AAV2-hSyn-DIO-hM3DG_q-mCherry) into only the right eye of *Opn4*^{Cre} mice, leaving the left eye uninfected (**Figure 2A**). Using this system, 3 to 5 weeks after infection, we applied a 1 µl CNO (0.1 mg/kg) eye-drop to the uninfected left eye. We observed robust pupil constriction (**Figure 2B**) as has been observed previously in response to IP CNO[94,122]. This result further demonstrates that CNO delivered via eye-drop is absorbed into the blood and delivered to distant tissues at working concentrations *in vivo*.

Eye-drop and IP injection evoked responses have similar dose efficiency

After confirming the feasibility of eye-drops as a delivery method, we next compared the CNO doses required to elicit responses when using eye-drop or IP delivery (**Figure 2C,D**). To do so, we administered doses of 0.001, 0.01, 0.1, and 1.0 mg/kg CNO via eye-drop or IP injection and monitored pupil constriction (**Figure 2C**, n = 10). We observed similar dose responses for both methods, with eye-drops displaying a small but statistically significant decrease in the dose required to achieve half-maximal response (EC_{50}) (**Figure 2D**, $P = 0.0195$ by Wilcoxon matched-pairs signed rank test). This difference could be explained by changes in blood absorption efficiency or potentially by

reduced stress responses in these mice after eye-drop as opposed to IP injection. However, the magnitude of the difference is minor and essentially irrelevant when considering the practical application of either technique.

Discussion

We have shown that eye-drops are an effective way to deliver CNO and activate DREADDs for *in vivo* studies. Eye-drops offer an alternative to current CNO delivery methods: drinking water and IP injection. When chronic DREADD activation is necessary and dose timing is unimportant, drinking water still provides the best dosing method. However, in the majority of DREADD experiments in which IP injection would be used, our method provides several advantages: (1) ease of application, (2) non-invasive, (3) less pain and stress, (4) cost/waste reduction (no syringes).

We hope that the widespread use of eye-drops in the place of IP injection will further simplify performing DREADD experiments and significantly reduce the distress inflicted on test subjects during *in vivo* experimentation.

The authors declare that the research was conducted in the absence of any commercial or financial relationships that could be construed as a potential conflict of interest.

Author Contributions

WTK conceived of, designed and performed experiments, and wrote the manuscript. DCF performed experiments, contributed figures and edited the manuscript. LJS

performed experiments and edited the manuscript. HZ and SH contributed to experimental design and edited the manuscript.

Funding

This work was supported by National Institutes of Health grants GM076430 and EY024452.

Figure 1

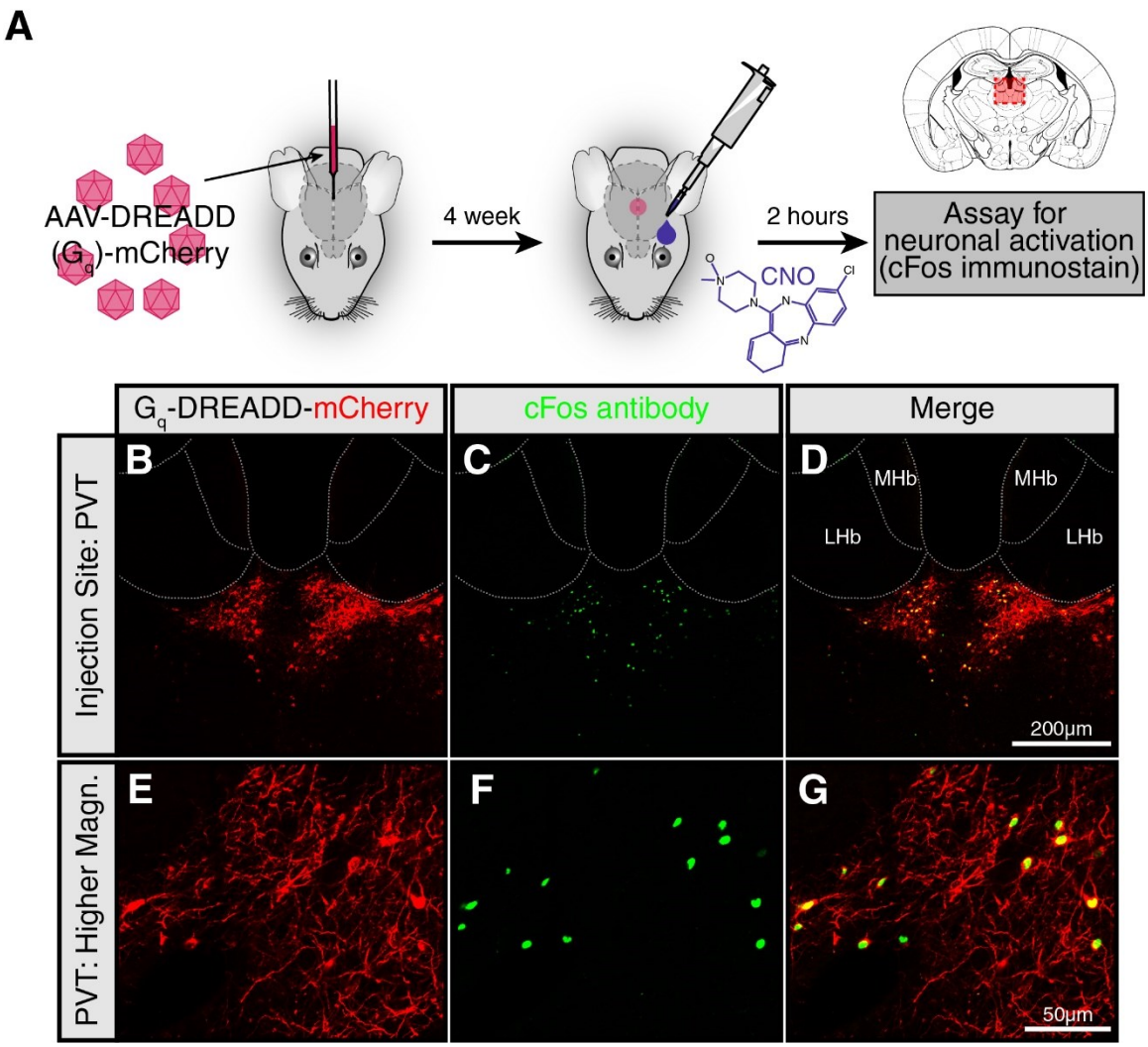

Figure 1: CNO eye-drops activate DREADDs in the brain

(A) Experimental approach. The effects of a single eye-drop of clozapine-N-oxide (CNO) were evaluated in wild-type mice stereotaxically injected in the paraventricular nucleus of the thalamus (PVT) with an AAV5-G_q-DREADD-mCherry. Four weeks after AAV injection, a single eye-drop of CNO was administrated (2 µl, 5mg CNO/ml) and 2 hours later the cFos induction was evaluated. Mouse brain schematic with AAV injection site highlighted. **(B)** mCherry expression confirms DREADD expression and cFos staining **(C)** shows cell activation in response to a CNO eye-drop. **(D)** Colocalization of mCherry

expression and cFos staining, indicating activation of infected-cells in response to CNO. **(E-G)** DREADD activation in response to a CNO eye-drop is shown at higher magnification. In all cases, a strong cFos induction was observed exclusively in infected neurons (mCherry+ cells); Scale bars: e=200μm; h= 50μm. LHb: lateral habenula; MHb: medial habenula.

Figure 2

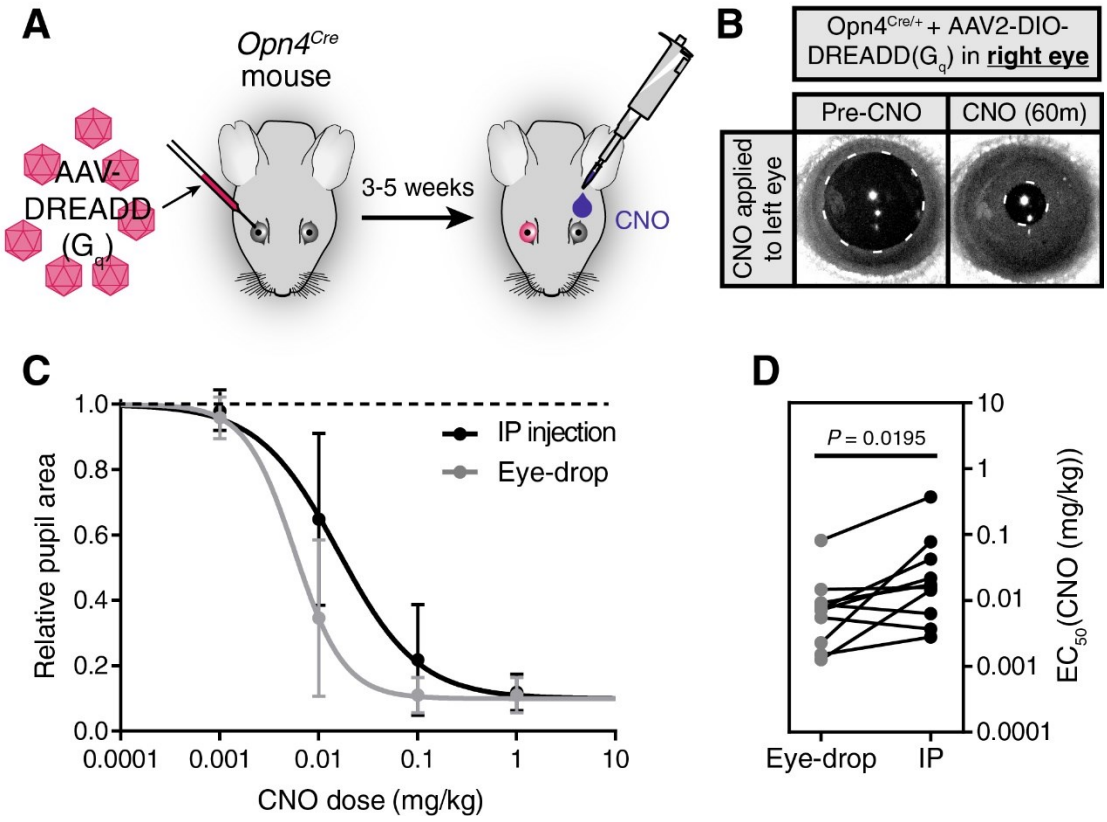

Figure 2: Eye-drop administration of CNO activates DREADDs *in vivo* similar to IP

(A) Depiction of experimental approach. An AAV carrying a Cre-dependent G_q-DREADD was injected into the right eye of mice with Cre expression in ipRGCs (*Opn4*^{Cre} mice). 3-5 weeks later, CNO was administered by eye-drop to the left eye. **(B)** DREADD activation is visualized by measuring pupil constriction in response to 1 µl CNO (1 mg/kg). (left) Baseline pupil size before CNO. (right) Pupil constriction observed in response to CNO applied directly to the left uninfected eye. **(C)** Dose-response curves for CNO applied via IP injection or eye-drop. All mice had G_q-DREADD expression only in the right eye and eye-drops were delivered to the left eye. Four doses were administered spanning the dynamic range: 0.001, 0.01, 0.1, and 1.0 mg/kg. Data fit with a sigmoidal curve (n = 10, mean ± SD). **(D)** CNO dose required for

half-maximal constriction (EC_{50}) determined for both eye-drop and IP injection. EC_{50} extracted from the sigmoidal curve fits for each mouse (points are individual mice, lines connect EC_{50} values for the same mouse). Statistical significance determined by a nonparametric Wilcoxon matched-pairs signed ranked test ($P = 0.0195$).

Chapter 7: Concluding Remarks

In the preceding chapters, I have shed light on several aspects of ipRGC sensory processing and signaling. focused on two separate but inter-dependent aspects of ipRGC sensory function: light information gathering/integration and light information communication. Using the PLR as a model behavior, I have provided evidence that the rod photoreceptor and glutamatergic neurotransmission support rapid changes to fluctuations in environmental light, while Melanopsin phototransduction and PACAPergic neurotransmission support steady state long-term signaling of ambient light intensity. I have shown that pupil dilation is an active process driven my glutamatergic neurotransmission from ipRGCs. Lastly, I have discovered two novel ipRGC neurotransmitters and identified several promising candidates for future investigation. I hope that this work will provide a strong base for future research in the Hattar lab and the field at large.

Neurotransmitters in the retina

In my view, the investigation I have begun into novel neurotransmitter systems is the most promising for future work. After a burst of work in the 80s and 90s discovering a variety of neuropeptides expressed in the retina, very little follow up has been done to characterize the role of these neurotransmitter systems. Given the tools developed since then, there are an immense amount of fairly easy questions to answer.

The idea that RGCs communicate visual information with glutamate alone is certainly an incomplete one. My work on 3 neuropeptides has revealed novel RGC populations expressing each. Further work on more neuropeptides is likely to reveal

widespread expression of neuropeptides in RGCs. Understanding the role these neuropeptides play in conveying light information to the brain is going to be critical for understanding image forming and non-image forming vision. Specific populations of RGCs are known to detect and convey unique aspects of the visual field. It is likely that the neuropeptides they express are important for conveying that information to the brain.

References

1. Sliney, D. H. What is light? The visible spectrum and beyond. *Eye* **30,** 222–229 (2016).

2. Lucas, R. J. *et al.* Measuring and using light in the melanopsin age. *Trends Neurosci.* **37,** 1–9 (2014).

3. Strauss, O., Kolb, H., Nelson, R., Graham, D. M. & Wong, K. Y. Anatomy and Physiology of the Retina. *Webvision* (2017).

4. Freedman, M. S. *et al.* Regulation of mammalian circadian behavior by non-rod, non-cone, ocular photoreceptors. *Science (80-.).* **284,** 502–4 (1999).

5. Lucas, R. J. *et al.* Identifying the photoreceptive inputs to the mammalian circadian system using transgenic and retinally degenerate mice. *Behav. Brain Res.* **125,** 97–102 (2001).

6. Lucas, R. J., Freedman, M. S., Munoz, M., Garcia-Fernandez, J. M. & Foster, R. G. Regulation of the mammalian pineal by non-rod, non-cone ocular photoreceptors. *Science (80-.).* **284,** 505–7 (1999).

7. Halford, S. *et al.* Characterization of a novel human opsin gene with wide tissue expression and identification of embedded and flanking genes on chromosome 1q43. *Genomics* **72,** 203–8 (2001).

8. Provencio, I. *et al.* A Novel Human Opsin in the Inner Retina. *J. Neurosci.* **20,** 600–605 (2000).

9. Provencio, I., Jiang, G., De Grip, W. J., Hayes, W. P. & Rollag, M. D.

Melanopsin: An opsin in melanophores, brain, and eye. *Proc. Natl. Acad. Sci. U. S. A.* **95,** 340–5 (1998).

10. Hattar, S., Liao, H. W., Takao, M., Berson, D. M. & Yau, K. W. Melanopsin-containing retinal ganglion cells: architecture, projections, and intrinsic photosensitivity. *Science* **295,** 1065–70 (2002).

11. Ruby, N. F. *et al.* Role of melanopsin in circadian responses to light. *Science* **298,** 2211–3 (2002).

12. Hatori, M. *et al.* Inducible ablation of melanopsin-expressing retinal ganglion cells reveals their central role in non-image forming visual responses. *PLoS One* **3,** e2451 (2008).

13. Güler, A. D. *et al.* Melanopsin cells are the principal conduits for rod–cone input to non-image-forming vision. *Nature* **453,** 102–5 (2008).

14. Hannibal, J., Hindersson, P., Knudsen, S. M., Georg, B. & Fahrenkrug, J. The photopigment melanopsin is exclusively present in pituitary adenylate cyclase-activating polypeptide-containing retinal ganglion cells of the retinohypothalamic tract. *J. Neurosci.* **22,** RC191 (2002).

15. Hannibal, J. *et al.* Pituitary adenylate cyclase-activating peptide (PACAP) in the retinohypothalamic tract: a potential daytime regulator of the biological clock. *J Neurosci* **17,** 2637–2644 (1997).

16. Hannibal, J., Moller, M., Ottersen, O. P. & Fahrenkrug, J. PACAP and glutamate are co-stored in the retinohypothalamic tract. *J Comp Neurol* **418,** 147–155 (2000).

17. Altimus, C. M. *et al.* Rods-cones and melanopsin detect light and dark to modulate sleep independent of image formation. *Proc. Natl. Acad. Sci. USA* **105,** 19998–20003 (2008).

18. Legates, T. A. *et al.* Aberrant light directly impairs mood and learning through melanonopsin-expression neurons. *Nature* **491,** 594–598 (2012).

19. Göz, D. *et al.* Targeted destruction of photosensitive retinal ganglion cells with a saporin conjugate alters the effects of light on mouse circadian rhythms. *PLoS One* **3,** e3153 (2008).

20. Lupi, D., Oster, H., Thompson, S. & Foster, R. G. The acute light-induction of sleep is mediated by OPN4-based photoreception. *Nat. Neurosci.* **11,** 1068–73 (2008).

21. Tsai, J. W. *et al.* Melanopsin as a sleep modulator: circadian gating of the direct effects of light on sleep and altered sleep homeostasis in Opn4-/- mice. *PLoS Biol.* **7,** e1000125 (2009).

22. Hattar, S. *et al.* Melanopsin and rod–cone photoreceptive systems account for all major accessory visual functions in mice. *Nature* **424,** 76–81 (2003).

23. Panda, S. *et al.* Melanopsin is required for non-image-forming photic responses in blind mice. *Science* **301,** 525–7 (2003).

24. Dkhissi-Benyahya, O., Gronfier, C., De Vanssay, W., Flamant, F. & Cooper, H. M. Modeling the role of mid-wavelength cones in circadian responses to light. *Neuron* **53,** 677–687 (2007).

25. Lall, G. S. *et al.* Distinct contributions of rod, cone, and melanopsin photoreceptors to encoding irradiance. *Neuron* **66,** 417–28 (2010).

26. Allen, A. E., Brown, T. M. & Lucas, R. J. A distinct contribution of short-wavelength-sensitive cones to light-evoked activity in the mouse pretectal olivary nucleus. *J. Neurosci.* **31,** 16833–16843 (2011).

27. Butler, M. P. & Silver, R. Divergent photic thresholds in the non-image-forming visual system: entrainment, masking and pupillary light reflex. *Proc. Biol. Sci.* **278,** 745–50 (2011).

28. McDougal, D. H. & Gamlin, P. D. The influence of intrinsically-photosensitive retinal ganglion cells on the spectral sensitivity and response dynamics of the human pupillary light reflex. *Vision Res.* **50,** 72–87 (2010).

29. Altimus, C. M. *et al.* Rod photoreceptors drive circadian photoentrainment across a wide range of light intensities. *Nat. Neurosci.* **13,** 1107–12 (2010).

30. Zhu, Y. *et al.* Melanopsin-dependent persistence and photopotentiation of murine pupillary light responses. *Invest. Ophthalmol. Vis. Sci.* **48,** 1268–75 (2007).

31. Gooley, J. J. *et al.* Melanopsin and rod-cone photoreceptors play different roles in mediating pupillary light responses during exposure to continuous light in humans. *J. Neurosci.* **32,** 14242–14253 (2012).

32. Mrosovsky, N. & Hattar, S. Impaired masking responses to light in melanopsin-knockout mice. *Chronobiol. Int.* **20,** 989–99 (2003).

33. Berson, D. M., Dunn, F. A. & Takao, M. Phototransduction by retinal ganglion

cells that set the circadian clock. *Science (80-.).* **295,** 1070–3 (2002).

34. Wong, K. Y. A retinal ganglion cell that can signal irradiance continuously for 10 hours. *J. Neurosci.* **32,** 11478–11485 (2012).

35. van Diepen, H. C., Ramkisoensing, A., Peirson, S. N., Foster, R. G. & Meijer, J. H. Irradiance encoding in the suprachiasmatic nuclei by rod and cone photoreceptors. *FASEB J.* **27,** 4204–12 (2013).

36. Schmidt, T. M. *et al.* A role for melanopsin in alpha retinal ganglion cells and contrast detection. *Neuron* **82,** 781–8 (2014).

37. Ruby, N. F. *et al.* Role of melanopsin in circadian responses to light. *Science (80-.).* **298,** 2211–3 (2002).

38. Panda, S. *et al.* Melanopsin (Opn4) requirement for normal light-induced circadian phase shifting. *Science (80-.).* **298,** 2213–6 (2002).

39. Lucas, R. J. *et al.* Diminished pupillary light reflex at high irradiances in melanopsin-knockout mice. *Science (80-.).* **299,** 245–7 (2003).

40. Xue, T. *et al.* Melanopsin signalling in mammalian iris and retina. *Nature* **479,** 67–73 (2011).

41. Vaaga, C. E., Borisovska, M. & Westbrook, G. L. Dual-transmitter neurons: functional implications of co-release and co-transmission. *Curr. Opin. Neurobiol.* **29,** 25–32 (2014).

42. Engelund, A., Fahrenkrug, J., Harrison, A. & Hannibal, J. Vesicular glutamate transporter 2 (VGLUT2) is co-stored with PACAP in projections from the rat

melanopsin-containing retinal ganglion cells. *Cell Tissue Res.* **340,** 243–55 (2010).

43. Gompf, H. S., Fuller, P. M., Hattar, S., Saper, C. B. & Lu, J. Impaired circadian photosensitivity in mice lacking glutamate transmission from retinal melanopsin cells. *J. Biol. Rhythm.* **30,** 35–41 (2015).

44. Purrier, N., Engeland, W. C. & Kofuji, P. Mice deficient of glutamatergic signaling from intrinsically photosensitive retinal ganglion cells exhibit abnormal circadian photoentrainment. *PLoS One* **9,** e111449 (2014).

45. Delwig, A. *et al.* Glutamatergic neurotransmission from melanopsin retinal ganglion cells is required for neonatal photoaversion but not adult pupillary light reflex. *PLoS One* **8,** e83974 (2013).

46. Engelund, A., Fahrenkrug, J., Harrison, A., Luuk, H. & Hannibal, J. Altered pupillary light reflex in PACAP receptor 1-deficient mice. *Brain Res.* **1453,** 17–25 (2012).

47. Kawaguchi, C. *et al.* PACAP-deficient mice exhibit light parameter-dependent abnormalities on nonvisual photoreception and early activity onset. *PLoS One* **5,** e9286 (2010).

48. Beaulé, C. *et al.* Temporally restricted role of retinal PACAP: Integration of the phase-advancing light signal to the SCN. *J. Biol. Rhythm.* **24,** 126–34 (2009).

49. Kawaguchi, C. *et al.* Changes in light-induced phase shift of circadian rhythm in mice lacking PACAP. *Biochem. Biophys. Res. Commun.* **310,** 169–175 (2003).

50. Colwell, C. S. *et al.* Selective deficits in the circadian light response in mice

lacking PACAP. *Am. J. Physiol. Regul. Integr. Comp. Physiol.* **287,** R1194–R1201 (2004).

51. Chen, D., Buchanan, G. F., Ding, J. M., Hannibal, J. & Gillette, M. U. Pituitary adenylyl cyclase-activating peptide: a pivotal modulator of glutamatergic regulation of the suprachiasmatic circadian clock. *Proc. Natl. Acad. Sci. USA* **96,** 13468–73 (1999).

52. Loewenfeld, I. E. The Pupil: Anatomy, Physiology, and Clinical Applications. **1,** 86–88 (1993).

53. Alam, N. M., Altimus, C. M., Douglas, R. M., Hattar, S. & Prusky, G. T. Photoreceptor regulation of spatial visual behavior. *Invest. Ophthalmol. Vis. Sci.* **56,** 1842–9 (2015).

54. Biel, M. *et al.* Selective loss of cone function in mice lacking the cyclic nucleotide-gated channel CNG3. *Proc. Natl. Acad. Sci. USA* **96,** 7553–7 (1999).

55. Cahill, H. & Nathans, J. The optokinetic reflex as a tool for quantitative analyses of nervous system function in mice: application to genetic and drug-induced variation. *PLoS One* **3,** e2055 (2008).

56. Calvert, P. D. *et al.* Phototransduction in transgenic mice after targeted deletion of the rod transducin □-subunit. *Proc. Natl. Acad. Sci. USA* **97,** 13913–8 (2000).

57. Naarendorp, F. *et al.* Dark light, rod saturation, and the absolute and incremental sensitivity of mouse cone vision. *J. Neurosci.* **30,** 12495–507 (2010).

58. Nathan, J. *et al.* Scotopic and photopic visual thresholds and spatial and temporal

discrimination evaluated by behavior of mice in a water maze. *Photochem. Photobiol.* **82,** 1489–94 (2006).

59. Zhao, X., Stafford, B. K., Godin, A. L., King, W. M. & Wong, K. Y. Photoresponse diversity among the five types of intrinsically photosensitive retinal ganglion cells. *J. Physiol.* **592,** 1619–36 (2014).

60. van Oosterhout, F. *et al.* Ultraviolet light provides a major input to non-image-forming light detection in mice. *Curr. Biol.* **22,** 1397–402 (2012).

61. Ho Mien, I. *et al.* Effects of Exposure to Intermittent versus Continuous Red Light on Human Circadian Rhythms, Melatonin Suppression, and Pupillary Constriction. *PLoS One* **9,** e96532 (2014).

62. Spitschan, M., Jain, S., Brainard, D. H. & Aguirre, G. K. Opponent melanopsin and S-cone signals in the human pupillary light response. *Proc. Natl. Acad. Sci. USA* **111,** 15568–72 (2014).

63. Kimura, E. & Young, R. S. L. Sustained pupillary constrictions mediated by an L- and M-cone opponent process. *Vis. Res.* **50,** 489–96 (2010).

64. Kimura, E. & Young, R. S. L. S-cone contribution to pupillary responses evoked by chromatic flash offset. *Vis. Res.* **39,** 1189–1197 (1999).

65. Gooley, J. J. *et al.* Spectral responses of the human circadian system depend on the irradiance and duration of exposure to light. *Sci. Transl. Med.* **2,** 31ra33 (2010).

66. Lucas, R. J., Douglas, R. H. & Foster, R. G. Characterization of an ocular photopigment capable of driving pupillary constriction in mice. *Nat. Neurosci.* **4,**

621–6 (2001).

67. Toda, A. M. A. & Huganir, R. L. Regulation of AMPA receptor phosphorylation by the neuropeptide PACAP38. *Proc. Natl. Acad. Sci.* **112,** 6712–6717 (2015).

68. Rao, S. *et al.* A direct and melanopsin-dependent fetal light response regulates mouse eye development. *Nature* **494,** 243–246 (2013).

69. Renna, J. M., Weng, S. & Berson, D. M. Light acts through melanopsin to alter retinal waves and segregation of retinogeniculate afferents. *Nat. Neurosci.* **14,** 827–829 (2011).

70. Armbruster, B. N., Li, X., Pausch, M. H., Herlitze, S. & Roth, B. L. Evolving the lock to fit the key to create a family of G protein-coupled receptors potently activated by an inert ligand. *Proc. Natl. Acad. Sci. U. S. A.* **104,** 5163–8 (2007).

71. Gompf, H. S., Fuller, P. M., Hattar, S., Saper, C. B. & Lu, J. Impaired Circadian Photosensitivity in Mice Lacking Glutamate Transmission from Retinal Melanopsin Cells. *J. Biol. Rhythms* **30,** 35–41 (2015).

72. Tikidji-Hamburyan, A. *et al.* Retinal output changes qualitatively with every change in ambient illuminance. *Nat Neurosci* **18,** 66–74 (2015).

73. Weng, S., Estevez, M. E. & Berson, D. M. Mouse Ganglion-Cell Photoreceptors Are Driven by the Most Sensitive Rod Pathway and by Both Types of Cones. *PLoS One* **8,** e66480 (2013).

74. Mrosovsky, N. & Hattar, S. Diurnal mice (Mus musculus) and other examples of temporal niche switching. *J. Comp. Physiol. A. Neuroethol. Sens. Neural. Behav.*

Physiol. **191,** 1011–1024 (2005).

75. Blakemore, C. B. & Rushton, W. A. H. The rod increment threshold during dark adaptation in normal and rod monochromat. *J. Physiol.* **181,** 629–640 (1965).

76. Wong, K. Y., Dunn, F. a & Berson, D. M. Photoreceptor adaptation in intrinsically photosensitive retinal ganglion cells. *Neuron* **48,** 1001–10 (2005).

77. Do, M. T. H. & Yau, K. Adaptation to steady light by intrinsically photosensitive retinal ganglion cells. *Proc. Natl. Acad. Sci. U. S. A.* **2013,** 1–6 (2013).

78. VanderLeest, H. T. *et al.* Seasonal encoding by the circadian pacemaker of the SCN. *Curr. Biol.* **17,** 468–73 (2007).

79. Kay, J. N. *et al.* Retinal Ganglion Cells with Distinct Directional Preferences Differ in Molecular Identity, Structure, and Central Projections. *J. Neurosci.* **31,** 7753–7762 (2011).

80. Liu, F. *et al.* Gene expression and protein distribution of orexins and orexin receptors in rat retina. *Neuroscience* **189,** 146–55 (2011).

81. Brecha, N. C. *et al.* Substance P-immunoreactive retinal ganglion cells and their central axon terminals in the rabbit. *Nature* **327,** 155–158 (1987).

82. Djeridane, Y. Immunohistochemical evidence for the presence of vasopressin in the rat Harderian gland, retina, and lacrimal gland. *Exp. Eye Res.* **59,** 117–120 (1994).

83. Krashes, M. J., Shah, B. P., Koda, S. & Lowell, B. B. Rapid versus delayed stimulation of feeding by the endogenously released agRP neuron mediators

GABA, NPY, and AgRP. *Cell Metab.* **18,** 588–595 (2013).

84. Calvert, P. D. *et al.* Phototransduction in transgenic mice after targeted deletion of the rod transducin alpha -subunit. *Proc. Natl. Acad. Sci. U. S. A.* **97,** 13913–13918 (2000).

85. Chang, B. *et al.* Cone photoreceptor function loss-3, a novel mouse model of achromatopsia due to a mutation in Gnat2. *Invest. Ophthalmol. Vis. Sci.* **47,** 5017–21 (2006).

86. Soucy, E., Wang, Y., Nirenberg, S., Nathans, J. & Meister, M. A novel signaling pathway from rod photoreceptors to ganglion cells in mammalian retina. *Neuron* **21,** 481–493 (1998).

87. Smallwood, P. M. *et al.* Genetically engineered mice with an additional class of cone photoreceptors: implications for the evolution of color vision. *Proc. Natl. Acad. Sci. U. S. A.* **100,** 11706–11711 (2003).

88. Ecker, J. L. *et al.* Melanopsin-expressing retinal ganglion-cell photoreceptors: cellular diversity and role in pattern vision. *Neuron* **67,** 49–60 (2010).

89. Hnasko, T. S. *et al.* Vesicular glutamate transport promotes dopamine storage and glutamate corelease in vivo. *Neuron* **65,** 643–56 (2010).

90. Hamelink, C. *et al.* Pituitary adenylate cyclase-activating polypeptide is a sympathoadrenal neurotransmitter involved in catecholamine regulation and glucohomeostasis. *Proc. Natl. Acad. Sci. U. S. A.* **99,** 461–6 (2002).

91. Loewenfeld, I. E. Mechanisms of reflex dilatation of the pupil. *Hist. Rev. Exp.*

Anal. (1957).

92. Delwig, A. *et al.* Glutamatergic neurotransmission from melanopsin retinal ganglion cells is required for neonatal photoaversion but not adult pupillary light reflex. *PLoS One* **8,** e83974 (2013).

93. Clarke, R. J. & Ikeda, H. Luminance and darkness detectors in the olivary and posterior pretectal nuclei and their relationship to the pupillary light reflex in the rat. *Exp Brain Res* **57,** 224–232 (1985).

94. Keenan, W. T. *et al.* A visual circuit uses complementary mechanisms to support transient and sustained pupil constriction. *Elife* **5,** (2016).

95. Akiyama, K., Nakanishi, S., Nakamura, N. H. & Naito, T. Gene expression profiling of neuropeptides in mouse cerebellum, hippocampus, and retina. *Nutrition* **24,** 918–923 (2008).

96. Sagar, S. M. & Marshall, P. E. Somatostatin-like immunoreactive material in associational ganglion cells of human retina. *Neuroscience* **27,** 507–516 (1988).

97. Cristiani, R., Petrucci, C., Monte, M. D. & Bagnoli, P. Somatostatin (SRIF) and SRIF receptors in the mouse retina. **936,** 1–14 (2002).

98. Fontanesi, G., Casini, G., Thanos, S. & Bagnoli, P. Transient somatostatin-immunoreactive ganglion cells in the developing rat retina. *Brain Res. Dev. Brain Res.* **103,** 119–125 (1997).

99. Reichmann, F. & Holzer, P. Neuropeptide Y: A stressful review. *Neuropeptides* **55,** 99–109 (2016).

100. van den Pol, A. N. *et al.* Neuromedin B and gastrin-releasing peptide excite arcuate nucleus neuropeptide Y neurons in a novel transgenic mouse expressing strong Renilla green fluorescent protein in NPY neurons. *J. Neurosci.* **29,** 4622–4639 (2009).

101. Steinhoff, M. S., von Mentzer, B., Geppetti, P., Pothoulakis, C. & Bunnett, N. W. Tachykinins and their receptors: contributions to physiological control and the mechanisms of disease. *Physiol. Rev.* **94,** 265–301 (2014).

102. Harris, J. A. *et al.* Anatomical characterization of Cre driver mice for neural circuit mapping and manipulation. *Front. Neural Circuits* **8,** 76 (2014).

103. Weckbecker, G. *et al.* Opportunities in somatostatin research: biological, chemical and therapeutic aspects. *Nat. Rev. Drug Discov.* **2,** 999–1017 (2003).

104. Peichl, L. & Gonzalez-Soriano, J. Morphological types of horizontal cell in rodent retinae: a comparison of rat, mouse, gerbil, and guinea pig. *Vis Neurosci* **11,** 501–517 (1994).

105. Plummer, N. W. *et al.* Expanding the power of recombinase-based labeling to uncover cellular diversity. *Development* **142,** 4385–4393 (2015).

106. Sternson, S. M. & Roth, B. L. Chemogenetic Tools to Interrogate Brain Functions. *Annu. Rev. Neurosci.* **37,** 387–407 (2014).

107. Roth, B. L. DREADDs for Neuroscientists. *Neuron* **89,** 683–694 (2016).

108. Zhu, H. *et al.* Cre-dependent DREADD (Designer Receptors Exclusively Activated by Designer Drugs) mice. *Genesis* **54,** 439–446 (2016).

109. Alexander, G. M. *et al.* Remote control of neuronal activity in transgenic mice expressing evolved G protein-coupled receptors. *Neuron* **63,** 27–39 (2009).

110. Zhu, H. *et al.* Chemogenetic Inactivation of Ventral Hippocampal Glutamatergic Neurons Disrupts Consolidation of Contextual Fear Memory. *Neuropsychopharmacology* **39,** 1880–1892 (2014).

111. Ray, R. S. *et al.* Impaired Respiratory and Body Temperature Control Upon Acute Serotonergic Neuron Inhibition. *Science (80-.).* **333,** 637–642 (2011).

112. Guettier, J.-M. *et al.* A chemical-genetic approach to study G protein regulation of cell function in vivo. *Proc. Natl. Acad. Sci.* **106,** 19197–19202 (2009).

113. Alexander, G. M. *et al.* Remote control of neuronal activity in transgenic mice expressing evolved G protein-coupled receptors. *Neuron* **63,** 27–39 (2009).

114. Atasoy, D., Betley, J. N., Su, H. H. & Sternson, S. M. Deconstruction of a neural circuit for hunger. *Nature* **488,** 172–177 (2012).

115. Milosavljevic, N., Allen, A. E., Cehajic-Kapetanovic, J. & Lucas, R. J. Chemogenetic activation of ipRGCs drives changes in dark-adapted (Scotopic) electroretinogram. *Investig. Ophthalmol. Vis. Sci.* **57,** 6305–6312 (2016).

116. Garner, A. R. *et al.* Generation of a Synthetic Memory Trace. *Science (80-.).* **335,** 1513–1516 (2012).

117. Nakajima, K. -i. & Wess, J. Design and Functional Characterization of a Novel, Arrestin-Biased Designer G Protein-Coupled Receptor. *Mol. Pharmacol.* **82,** 575–582 (2012).

118. Stachniak, T. J., Ghosh, A. & Sternson, S. M. Chemogenetic Synaptic Silencing of Neural Circuits Localizes a Hypothalamus→Midbrain Pathway for Feeding Behavior. *Neuron* **82,** 797–808 (2014).

119. Jain, S., Azua, I. R. De, Lu, H., White, M. F. & Guettier, J. Chronic activation of a designer G q -coupled receptor improves β -cell function. *J. Clin. Invest.* **123,** (2013).

120. Donato, F., Jacobsen, R. I., Moser, M.-B. & Moser, E. I. Stellate cells drive maturation of the entorhinal-hippocampal circuit. *Science (80-.).* **355,** eaai8178 (2017).

121. Chen, S.-K., Badea, T. C. & Hattar, S. Photoentrainment and pupillary light reflex are mediated by distinct populations of ipRGCs. *Nature* **476,** 92–95 (2011).

122. Milosavljevic, N., Cehajic-Kapetanovic, J., Procyk, C. A. & Lucas, R. J. Chemogenetic Activation of Melanopsin Retinal Ganglion Cells Induces Signatures of Arousal and/or Anxiety in Mice. *Curr. Biol.* **26,** 2358–2363 (2016).

123. K. Franklin and G. Paxinos. The Mouse Brain in Stereotaxic Coordinates. *Acad. Press* **Library of,** (1997).

William T. Keenan
Department of Biology
Johns Hopkins University
Baltimore, MD 21218
Keenanw27@gmail.com
(404) 513-7314

EDUCATION

2011-2017 Ph.D. in Biology, *in progress*
Cellular, Molecular, Developmental Biology, and Biophysics Program
Johns Hopkins University, Baltimore, MD
Advisor: Samer Hattar, Ph.D.
Thesis Defense – September 1st, 2017

2007-2011 B.S. in Biology, *Cum Laude*
University of Georgia, Athens, Georgia
Research Advisor: Sidney Kushner, Ph.D.

PUBLICATIONS

- **Keenan WT*** and Rupp AC*, Ross RA, Somasundaram P, Hiriyanna S, Wu Z, Badea TC, Robinson PR, Lowell BB, Hattar S†. (2016) A visual circuit uses complementary mechanisms to support transient and sustained pupil constriction. eLife 2016;5:e15392.
*equal contribution

- **Keenan WT**†, Fernandez DC, Shumway L, Zhao H, Hattar S. (2017) Eye-drops for activation of DREADDs. Frontiers in Neuroscience. *In review*
†Corresponding

- Chew KS* and Renna JM*, McNeill DS, Fernandez DC, **Keenan WT**, Thomsen MB, Ecker JL, Loevinsohn GS, VanDunk C, Vicarel DC, Tufford A, Weng S, Gray PA, Cayouette M, Herzog ED, Zhao H, Berson DM†, Hattar S†. (2017) A subset of ipRGCs regulates both maturation of the circadian clock and segregation of retinogeniculate projections in mice. eLife. Accepted manuscript. DOI: 10.7554/eLife22861

- **Keenan WT** and Samer Hattar. (2017) Glutamatergic signaling from ipRGCs drives rapid active dilation of the pupil in darkness. *In preparation*

- **Keenan WT**, Thomsen MB, and Samer Hattar. (2017) Novel neuropeptides define distinct ipRGC subtypes. (2017) *In preparation*

RESEARCH EXPERIENCE

2012-2017 Doctoral Research (Johns Hopkins University): I investigated the neural circuit centered on intrinsically photosensitive retinal ganglion cells (ipRGCs). I characterized the integration of sensory information from photoreceptors and the neurotransmission mechanisms necessary to communicate that information to the brain.
Advisor: Samer Hattar, Ph.D; samer.hattar@nih.gov

2011-2012 Rotation Student (Johns Hopkins University): Prior to joining my thesis lab, I worked in five distinct labs, studying the biophysical properties of the *E. coli* arabinose operon, the thermodynamic properties of repeat protein folding, the structural biophysics of nucleosome remodelers, the role of protein disorder in protein function, and the mechanisms underlying physiological responses to light.

2009-2011 Undergraduate Research (University of Georgia): I investigated the role of RNases in the post-transcriptional maturation of tRNAs in *E. coli*.
Advisor: Sydney Kushner, Ph.D; skushner@uga.edu

TEACHING EXPERIENCE

2013-2017 Research Mentor: Designed projects for and mentored six graduate rotation students and 3 undergraduate researchers while in Samer Hattar's laboratory
2017 Teaching Assistant: Introduction to the Human Brain -- Undergraduate
2016 Teaching Assistant: Biochemistry – Undergraduate
2016 Lecturer: Emerging Strategies and Applications in Biomedical Research – Graduate and Upper Level Undergraduate
2016 Teaching Assistant: Emerging Strategies and Applications in Biomedical Research – Graduate and Upper Level Undergraduate
2015 Teaching Assistant: Biochemistry (Spring and Fall) – Undergraduate
2013 Teaching Assistant: Biochemistry Lab – Undergraduate
2012 Teaching Assistant: Cell Biology Lab – Undergraduate

AWARDS AND HONORS

2014 Society for Research in Biological Rhythms – Research Merit/Travel Award
2011 Graduated *cum laude*, University of Georgia
2007-11 Hope Scholarship, University of Georgia – full tuition

PRESENTATIONS

2016 **Keenan WT**, Rupp AC, Ross RA, Somasundaram P, Hiriyanna S, Wu Z, Badea TC, Robinson PR, Lowell BB, Hattar S. A visual circuit uses complementary mechanisms to support transient and sustained pupil constriction. Society for Neuroscience, San Diego, California. **Poster**

2014 **Keenan WT** and Hattar S. ipRGC neurotransmitters, glutamate and PACAP, are distinct in their contributions to non-image forming behaviors. Society for Research in Biological Rhythms, Big Sky, Montana. **Talk – Datablitz**

Keenan WT and Hattar S. ipRGC neurotransmitters, glutamate and PACAP, are distinct in their contributions to non-image forming behaviors. Society for Research in Biological Rhythms, Big Sky, Montana. **Poster**

REFERENCES

Samer Hattar, Ph.D.	samer.hattar@nih.gov	National Institutes of Health – **(301) 435-1887**
Haiqing Zhao, Ph.D.	hzhao@jhu.edu	Johns Hopkins University – **(410) 516-7391**
Robert Johnston, Ph.D.	robertjohnston@jhu.edu	Johns Hopkins University – **(410) 516-4954**